STUTTGARTER BEITRÄGE ZUR PRODUKTIONSFORSCHUNG

LAURA COMELLA

Position Sensor and Control System for Micro Hydraulic Drives in Surgical Instruments

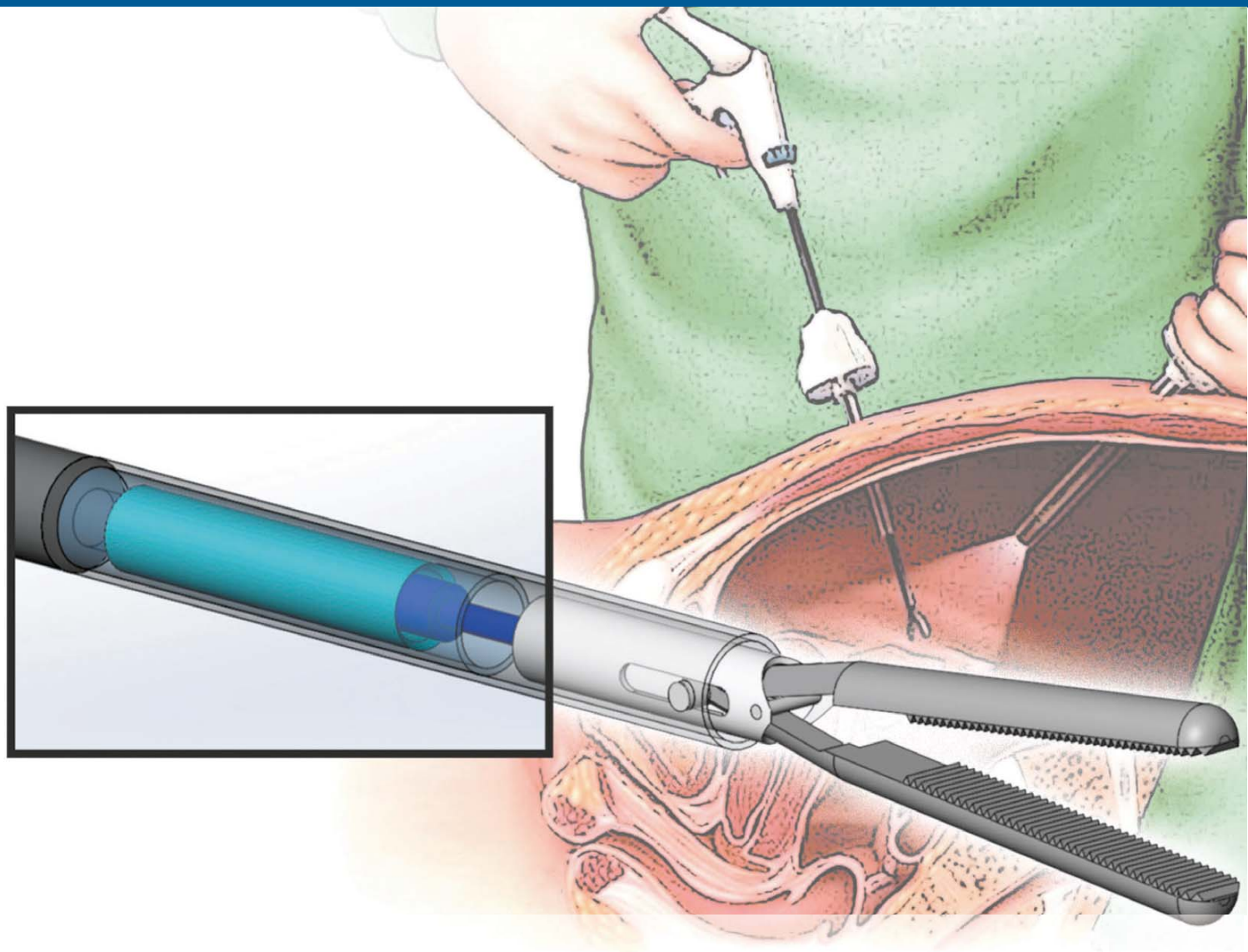

Universität Stuttgart

Fraunhofer IPA

STUTTGARTER BEITRÄGE ZUR PRODUKTIONSFORSCHUNG BAND 97

Laura Comella

Position Sensor and Control System for Micro Hydraulic Drives in Surgical Instruments

FRAUNHOFER VERLAG

Kontaktadresse:
Fraunhofer-Institut für Produktionstechnik und Automatisierung IPA, Stuttgart
Nobelstraße 12, 70569 Stuttgart
Telefon 07 11/9 70-11 01
info@ipa.fraunhofer.de; www.ipa.fraunhofer.de

STUTTGARTER BEITRÄGE ZUR PRODUKTIONSFORSCHUNG

Titelbild: © Laura Comella

Bibliografische Information der Deutschen Nationalbibliothek
Die Deutsche Nationalbibliothek verzeichnet diese Publikation in der Deutschen Nationalbibliografie; detaillierte bibliografische Daten sind im Internet über www.dnb.de abrufbar.
ISSN: 2195-2892
ISBN (Print): 978-3-8396-1550-8

D 93

Zugl.: Stuttgart, Univ., Diss., 2019

Druck: Mediendienstleistungen des Fraunhofer-Informationszentrum Raum und Bau IRB, Stuttgart
Für den Druck des Buches wurde chlor- und säurefreies Papier verwendet.

Fraunhofer-Informationszentrum Raum und Bau IRB
Postfach 80 04 69, 70504 Stuttgart
Nobelstraße 12, 70569 Stuttgart
Telefon 07 11 9 70-25 00
Telefax 07 11 9 70-25 08
E-Mail verlag@fraunhofer.de
URL http://verlag.fraunhofer.de

Position sensor and control system for micro hydraulic drives in surgical instruments

Von der Fakultät Konstruktions-, Produktions- und Fahrzeugtechnik
der Universität Stuttgart
zur Erlangung der Würde einer Doktor- Ingenieurin (Dr.-Ing.)
genehmigte Abhandlung

Vorgelegt von
M.Sc. Laura Maria Comella
aus Petralia Sottana

Hauptberichter:	Univ. -Prof. Dr.-Ing. Thomas Bauernhansl
Mitberichter:	Univ. -Prof. Dr.-Ing. Jan Stallkamp
Mitberichter:	Prof. Dr. rer. nat. habil. Peter P. Pott

Tag der mündlichen Prüfung: 18.09.2019

Institut für Industrielle Fertigung und Fabrikbetrieb der Universität Stuttgart
2019

Acknowledgment

I would like to thank Prof. Dr. Thomas Bauernhansl for the support in the formulation of the research topic, the definition of the methodology and for the useful corrections. To my department leader and main examiner Prof. Dr. Jan Stallkamp, I express my sincere gratitude for the technical discussion, the guide along the path but also the freedom he granted me to be able to work on my thesis. To the rest of my thesis committee: Prof. Dr. rer. nat. habil. Peter Pott and Prof. Dr.-Ing. Bernd Bertsche I would like to express my gratitude for the insightful comments and interesting questions at the exam. Additionally, I would like to thank the assistant of Prof. Bauernhansl Mrs. Steffi Rieck for the organizational and bureaucratic support.

A very special gratitude goes out to all my colleagues of Fraunhofer PAMB for the stimulating discussions and suggestions, the work together but also the fun we have had. I would like to single out Jonathan Schächtele for the challenging discussion about the dissertation, which motivated me to consider new ideas and to improve my work. Additionally, I would also like to thank and mention Auguste van Poelgeest, Armin Schäfer, Axel Storz, Tim Pusch, Tobias Behr, Marius Siegfarth, Flo Strobel, Lennart Karstensen and Lena Jähnert for their support along the way of my dissertation. My thanks go also to Olga Liebert, Peter Molitor, Dorothee Böhringer and all the library staff for the help with the literature and the publication procedure and to Klaus Erlach for the help in formulating the scientific question and defining the scientific method. Besides, I would like to thank the Students that have worked with me on the Project. Among them I would like to mention in particular Krasimir and Bozhidar Ayvazov.

My sincere thanks go also to Amanda Mickley-Gass, Marco Cassataro and

Jonathan Schächtele for reading the thesis and helping me to identify all the error and unclear passages

I would like to thank my family and friends, for the support and encouragement along the way, in particular Elisa Falcone for the last minute help with the graphic cover. A very special gratitude goes to my Parents Patrizia D´Amico and Vincenzo Comella for believing in me and my capability also when I was doubting them. A special thanks to my Papa´, who in a moment of tiredness motivated me to go on, giving me the energy to sprint until the end.

I would also like to express my sincere gratitude to Edith Cuntz, Karlheinz Cuntz, Elena Cuntz and Markus Kaltenbach, thank you for the support and also for the silent logistic help the day of the exam.

I very special thanks go to my partner Timo Cuntz, who has been there in every step of the way. Thank you for all the encouragement, the support on the mechanic part and the technical discussion in the creasiest time of the day and the night. Thank you for your patience!

Finally, I would like to thank Prof. Dr. Woias for supporting me and giving me the time to prepare my exam, and my actual colleagues at IMTEK for the encouragement and the insightful comments and questions very useful in preparation of the defense.

Abstract

This work is focused on the research and development of a sensor that permits the control of the movement of a hydraulically driven laparoscopic instrument tip and opens the way towards a new interpretation of surgical instruments. In the new vision the instrument is able to execute automatically preprogrammed tasks, without the constant involvement of the surgeon in the instrument control.

After an analysis on the state of the art for laparoscopic instruments and a revision of the relevant literature on sensors for displacement measurement, the coaxial cylindrical capacitive method was identified as the most suitable solution for the application analyzed. This sensor configuration can be integrated directly into the hydraulic cylinder without the need of additional parts.

The feasibility of the coaxial cylindrical capacitive sensor is theoretically analyzed, validated with FEA simulation and then characterized experimentally. Relevant is the fact that the tests are run with two different hydraulic cylinders, a mini hydraulic and a micro hydraulic cylinder, to demonstrate the scalability of the sensor and its adaptability to instruments of different size. The experimental results match the simulations and confirm the sensor´s behavior also on experimental level.

The sensor is than integrated in a closed loop system to test its suitability for controlling the position of the instrument tip in a scenario as close as possible to the real one. For this reason, a hydraulic drive, which permits the movement of the instrument tip, is designed. The full hydraulic drive system is modeled and this model is used to design a feedback control. The designed controller is initially proven through simulation. Afterwards it is tested with experiments proving the correspondence between simulated and real world behavior of the system.

Kurzfassung

Ziel dieser Arbeit ist die Erforschung und Entwicklung eines Sensors, der die Regelung der Bewegung einer hydraulisch angetriebenen laparoskopischen Instrumentenspitze ermöglicht und so den Weg für eine neue Interpretation von chirurgischen Instrumenten ebnet. In der neuen Vision ist das Instrument in der Lage, automatisch vorprogrammierte Aufgaben auszuführen, ohne die ständige Beteiligung des Chirurgen an der Instrumentensteuerung.

Nach einer Analyse des Standes der Technik für laparoskopische Instrumente und der einschlägigen Literatur zu Wegmessungssensoren wurde die koaxial-zylindrisch-kapazitive Messmethode als die geeignetste Lösung für die vorliegende Anwendung identifiziert. Diese Sensorkonfiguration kann ohne zusätzliche Bauteile direkt in den Hydraulikzylinder integriert werden. Die vorgeschlagene Lösung verwendet den Zylinder und die Kolbenstange jeweils als äußere und innere Elektrode.

Die Umsetzbarkeit des koaxiale-zylindrisch-kapazitiven Sensors wird theoretisch analysiert, mittels FEM-Simulation validiert und anschließend experimentell charakterisiert. Entscheidend ist, dass die Tests mit zwei verschiedenen Hydraulikzylindern, einem Mini- und einem Mikrohydraulikzylinder, durchgeführt werden, um die Skalierbarkeit des Sensors und damit seine Integrierbarkeit in Instrumente unterschiedlicher Größe zu demonstrieren. Die experimentellen Ergebnisse entsprechen den Simulationen und bestätigen das Verhalten des Sensors auf einer experimentellen Ebene.

Der Sensor wird anschließend in ein geregeltes System integriert, um seine Eignung für die Regelung der Position der Instrumentenspitze in einem Szenario zu testen, das der realen Anwendung so nahe wie möglich kommt. Aus diesem

Grund ist ein hydraulischer Antrieb vorgesehen, der die Bewegung der Instrumentenspitze ermöglicht. Das vollhydraulische Antriebssystem wird modelliert und dieses Modell dient zur Auslegung einer Regelung. Die entworfene Regelung wird zunächst durch eine Simulation evaluiert und zum Abschluss der Arbeit experimentell getestet um die Gültigkeit des Modells und die Übereinstimmung zwischen simuliertem und realem Verhalten des Systems zu belegen.

Index

List of figures

ALL THE FIGURES WITHOUT SOURCE ARE PRODUCED BY THE AUTHOR OF THIS THESIS

Glossary

actuator: is an element that transduces an input into an output movement in order to control a mechanism or a system

cable pull: actuation mechanism which uses cables to transmit mechanical motion. A cable core moves inside a protected conduit to cause the desired movement of the end of the cable core.

closed loop control: see feedback control

DVRT: differential variable reluctance transducer

endoscope: optical instrument used to look into the body in the minimally invasive procedures

feedback control: control method in which part of the system output is returned in input in order to adjust the system performance to meet the desired output response

hemorrhage: a profuse loss of blood caused from a ruptured blood vessel

hydraulic drive: transmission system that uses hydraulic energy to produce mechanical energy. it consists of a generator, valves, pipes and actuators.

Jaymy: surgical instrument with bendable tip controlled by electric motors from Endocontrol

Kymerax: surgical instrument with bendable tip controlled by electric motors from Terumo

LVDT: linear variable differential transducers

micromanipulators: devices or instruments used to manipulate objects without direct contact of the user. They are normally equipped with a grasp able to pick and move objects with a number of degrees of freedom.

minimally invasive procedures: surgical technique that can be performed through small incisions

NOTES: "Natural Orifice Transluminal Endoscopic Surgery". It is an operation performed through a natural orifice.

OLS: Ordinary List Squares regression analysis

open surgery: traditional type of surgery. The operation is executed through an incision which allows the visualization of the operation field and through which the instruments are inserted.

peritoneal cavity: space between the peritoneum that surrounds the abdominal wall, called parietal peritoneum, and the peritoneum that surrounds the internal organs, called visceral peritoneum

push-rod: actuation mechanism using a metal rod to transmit the motion

r2: surgical instrument with bendable tip operated by sheer hand force made by Tübingen Scientific

RMSE: Root Means Square Error

R-squared: coefficient of determination

SPL: "Single Port Laparoscopy". It is a minimally invasive surgery in which the surgeon operates through a single entry port.

sword fighting: constant collition of the used instruments between themselves or with the endoscope

telemanipulation: technique that allows to control the position of a surgical instrument from remote; a device is used to convert the movement of the user into signal to control the instrument in a different location

triangulation: operative method in which the two trocars are placed in a way that the tip of the instruments inserted forms a triangle in the operating area

trocar: instrument used as a portal for the subsequent placement of instruments in the body; it allows the quick exchange of instruments and tight the abdominal cavity when the instruments are substituted

1 Introduction

The last years have seen an increase in the efforts of surgeons and engineers to automate surgical interventions and, in particular, minimally invasive surgical procedures. The novelty of this technique is that surgery is performed through small incisions, bringing for this reason many advantages to the patient. However, because of the complexity of its execution, the enhancement of the current development phase requires instruments which are intelligent micromanipulators rather than simple manually operated scissors.

This technical revolution can be enabled by equipping the instruments with sensors, in order to control their movement in closed loop. In the short run this would improve the precision of the instruments' positioning and in the long run would give the possibility to use them in a fully automated scenario.

For a better understanding of the complexity of minimally invasive surgery, an overview of this procedure and the currently used instruments is given. Afterwards, the technology that, in the opinion of the author, represents the new frontier of laparoscopic tools is described. An introduction to the advantages and disadvantages of this technology is given and its further development, which is the subject of this thesis, is discussed. Then the scientific question is defined, followed by the description of the applied scientific method and the presentation of the structure of the thesis.

1.1 Initial situation

1.1.1 Thesis Background: minimally invasive surgery

Minimally invasive surgery has been established in the last years as the standard method in contrast to open surgery, which requires incisions of a significant size

(Tsoi et al. 1996). Minimally invasive surgery (Norton et al. 2008) refers to techniques in which the surgery is executed through incisions of small size compared to open surgery. Therefore, the interior of the body is not directly accessible and visible. Optical and medical instruments must be inserted via small cuts to see and perform surgery in the region of interest. An example of a minimally invasive surgical procedure is laparoscopy (Autorino et al. 2010), a surgery performed in the abdomen through small incisions. More advanced techniques are Single-Port-Laparoscopy (SPL) (Rané et al. 2009) and Natural Orifice Transluminal Endoscopic Surgery (NOTES) (Haber et al. 2008). SPL is a minimally invasive surgery in which the surgeon operates exclusively through a single entry port. In NOTES the operation is performed without external incisions; the endoscope and the surgical tools are inserted through natural orifices and led to the operating field through an internal incision in the stomach, vagina, bladder or colon.

The main reason for the large distribution of minimally invasive surgery is the patient's short recovery time (Robinson et al. 2003; Rosenblatt et al. 2008). Moreover, the small incisions reduce hemorrhage, the risk of infection, and the patient´s pain. This means that he can resume to normal life in a short time (Bhayani et al. 2003; Tjandra et al. 2006). However, the complexity of the procedure can present a problem for the surgeon. The scarce space of movement, for example, results in loss of dexterity and prolongation of the time required for the surgery, and, therefore, in the intensification of the surgeon´s fatigue (Berguer et al. 1999; Uhrich et al. 2002). In literature it is documented how laparoscopic procedures increase the upper extremities´ fatigue (Berguer et al. 2009) and occasionally hand injuries (Kano 1993).

1.1.2 Instrument technology

It is obvious that minimally invasive procedures imply other difficulties with respect to open surgery. The operative field is small and only indirectly visible via a camera. This complicates the surgeon's space perception and compromises eye-hand coordination (Breedveld 1997; Breedveld et al. 2009).

The classical instruments used for laparoscopic surgery are shown in Figure 1.1(a) and (b)

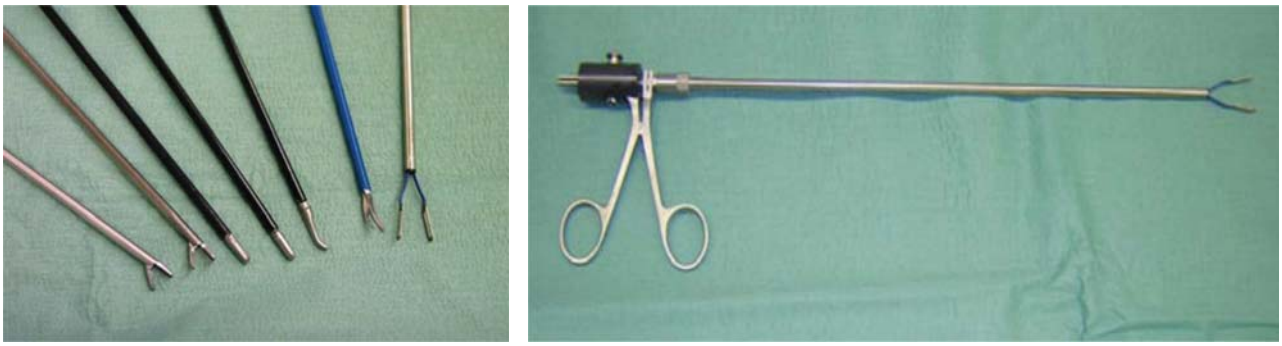

(a) **(b)**

Figure 1.1: (a) Instruments for laparoscopic surgery (Rosenblatt et al. 2008) (b) Bipolar grasper (Rosenblatt et al. 2008)

However, because of the incontestable advantage that this technique brings to the patient, research activity on the improvement of the instruments has increased in the last years (Miniati et al. 2014; Zdichavsky et al. 2015; Bensignor et al. 2016; Cuntz 2016). Given the requirements of minimally invasive surgery, various efforts have been taken to reduce the complexity and the difficulties that this technique represents for the surgeon. The success of the EndoWrist, produced by the company Intuitive, proved that multiple degrees of freedom of the instrument tip and an automated interface are an answer to the dexterity issues of minimally invasive procedures. These two important features for the next generation of minimally invasive tools led to the development of other instruments, with the

design based on the Endowrist concept. Examples are Kymerax by Terumo in Figure 1.2, Jaymy by Endocontrol in Figure 1.3, and r2 drive by Tübingen Scientific in Figure 1.4. All of them have the advantage of increasing the degrees of freedom of the grasper by a bending mechanism for the tip of the instrument. For the bending movement they use either push-rod or cable pull mechanisms. In both cases, the actuator force must be applied from the instrument's handhold and has to be mechanically transmitted along the instrument's shaft. For this reason, both mechanisms are characterized by a low transmission efficiency caused by elasticities in the system and friction, the latter especially in the case of a cable pull working in bended position.

Figure 1.2: Kymerax by Terumo

Figure 1.3: Jaymy by Endocontrol

Figure 1.4: r2 drive by Tübingen Scientific

r2 drive is the only instrument among these examples that is operated by sheer hand force, which makes it difficult to maneuver using one hand only.

Jaymy and Kymerax have motor drives, making it easier for the user to actuate the instrument's tip. However, since the motors are mounted on the instrument, they make it heavy to hold especially during long surgical procedures.

In all the cases mentioned above, the used drives make the operation of the instruments too difficult to be accepted by the surgeon. In this respect, the use of an alternative drive could permit a widespread use of the discussed instrument´s concept. Such a drive should have lower weight than the previously discussed systems and should be able to actuate with a comparable force. An alternative drive´s method is proposed in (Cuntz et al. 2013): Laparoscopic instruments with hydraulic power´s transmission.

Hydraulically driven instruments offer significantly improved performance over the established minimally invasive surgical instruments. Equipped with hydraulic drives, the instruments can be handled more precisely and apply greater forces (Volder et al. 2010; Cuntz et al. 2013). They are lightweight, because the power generator, the pump, does not have to be placed in the instrument. Moreover, due to the small dimensions and the lightness of the hydraulic cylinder, it can be integrated right into the tip of the instrument, increasing the efficiency of the generated force without compromising the manageability.

As already discussed, an automated interface is the second relevant feature to permit the establishment of automated instruments among specialists. The following work is focused on this aspect and, in particular, on bringing forward the concept of automation for hydraulically driven laparoscopic instruments.
The concept of automation, which this work is aiming for, goes beyond the classical hand control of the instrument with a joystick in open loop control. It is designed to make the accomplishment of preprogrammed tasks possible. Difficult operations like stitching (Giddings 2013) or cutting complex geometries could then be automatically executed by pressing one button and letting the tip move automatically along a trajectory. However, automation in complex environments such as the human body demands a closed loop control, which can only be implemented with a sensor directly integrated at the tip of the instrument to detect its movement.
The integration of a sensor with the ability to observe the instrument tip also opens the scenario of guided operations, in which a proximity sensor can be used to locate a target and the position sensor is used to drive the instrument tip on the desired position. Moreover, hydraulics is influenced by trapped air, leakage, compressibility of the medium, and elasticity of the tubes in the hydraulic circuit. Therefore, their use in systems that must fulfill safety standards for medical application requires the integration of a measurement technology that gives feedback about their movement, guaranteeing no harm for the patients.

1.2 Scientific question

The main objective of this work is the investigation and research of a sensing method to measure the position in hydraulic drives with sufficient accuracy to control the tip position of a laparoscopic instrument.

Given the instrument's and cylinder´s size, it is not possible to incorporate an off-the-shelf sensor, as the standard sensors available on the market are too big for the given application (Hodges 1993; Krivts et al. 2006). They would not fit in the limited space at the tip of the instrument which is already occupied by the hydraulic cylinder and the transmission mechanism. More information about the available space at the tip of the instrument will follow in chapter 2. Moreover, as the development of hydraulic instruments is in a research stage, no specific sensor has been developed by the medical industry yet. Therefore, it is necessary to identify a sensor concept that is scalable for the intended application.

The scalability of the sensing principle must be studied, since in literature there is no investigation on the feasibility of the sensing concept, which is chosen and discussed in chapter 4, for the required dimension-scale.

Thus, the main objective of this work is to find an answer to the scientific question: ***"How can a sensor system concept for measuring the tip position of a laparoscopic instrument be designed in order to be accurate enough for the application and compact enough to be integrated in the laparoscopic instrument without substantially changing the existing instrument's mechanical design?"***

1.3 Scientific method

This thesis work fits in the context of engineering science. The definition of engineering as a science has its roots in the work of Johann Beckmann, who, in his work Anleitung zur Technologie (Beckmann 1777), defines technology as the science that teaches the processing of natural goods and the knowledge of crafts. Unlike in workshops, where the goods' fabrication follows only the directions of the master, technology gives, in a systematic order, in depth instructions on how

to find ways to achieve the final purpose of a good´s fabrication through true principles and reliable experience. It gives directives on how the phenomena occurring during the processing can be explained and used accordingly. According to this definition, technology is characterized by a methodical approach. Its knowledge comes from empirical findings and always pursues a purpose.

Today, the Ingenieurwissenschaften@BW2025´s commission defines engineering as a science that serves society by recognizing and designing technical capabilities using specific methods. Engineering sciences are institutionalized in constantly changing independent disciplines (MWK-BaWü 2015). As in Beckmann's work, this definition also implies that technology must be purposeful and its main goal is the acquisition of knowledge and the development of new systems. However, in addition to Beckmann´s definition it is claimed that all achievements of the engineering science must fulfill social needs.

This work, the purpose of which is the development of a sensor concept for the precise measurement of a laparoscopic instrument tip position, fulfills all the parameters to be addressed as an example of scientific engineering according to the definition of the Ingenieurwissenschaften@BW2025´s commission. The work has the precise purpose of developing an innovative sensing method which, by improving laparoscopic tools, contributes to the further development of the corresponding surgical technique. As already mentioned, laparoscopic surgery brings numerous advantages to the patient in comparison to open surgery. This means that the technical knowledge produced to permit its development generates benefits to our society.

Being an example of scientific engineering, this work follows the scientific empirical method, according to which knowledge is gained by means of direct

observation of empirical evidence. The research work starts with the formulation of a hypothesis. In order to prove it, experiments are planned and predictions about their results are made. Finally, the predictions are tested with suitable experiments (Galilei 1974).

In this work, the hypothesis is formulated in accordance to Popper´s definition of science. Popper asserts that all empirical scientific sentences must be arbitrable: They must have such a form that their verification as well as their falsification is logically possible (Gadenne et al. 1999). This means that the hypothesis must be formulated in a way that conditions can be deduced from which the erroneousness of the hypothesis can be proved.

In order to formulate the hypothesis, the deductive method is used. The deductive method starts with a general statement and examines the possibilities to reach a specific logical conclusion (Herr 2011). Therefore, the hypothesis is formulated starting from the premise that when a sensor concept is miniaturized its function typically does not change. There are measurement systems that can measure displacement in the hydraulic drive for large scale industrial applications. The logical conclusion follows that a sensing method, miniaturized and adapted to the specific case of the laparoscopic instrument, can be identified.

In the next chapters, the following scientific approach to validate the defined hypothesis will be used. Research on sensing systems for the position of hydraulic drives will be executed, a concept that fulfills the requirements will be identified, and its adaptability to small size devices will be proved. The suitability of the concept will be verified, in the first place, through analytic methods and FEA simulations. Afterwards, an experimental set-up will be designed and the concept will be validated on an experimental level to test its performance. The theoretical and experimental results will be compared for an overall understanding of the

measuring principle. The work is concluded with the design of a hydraulic circuit that allows the movement of the hydraulic cylinder and of a closed loop controller to test the suitability of the sensor when used to control the movement of a laparoscopic instrument tip.

1.4 Structure of this thesis

This thesis consists of seven chapters, which are listed and described below.

Chapter 1 contains a brief introduction to minimally invasive surgical procedures, the advantages that they bring to the patient, and the challenges that they pose to the surgeon. In this chapter, an overview of the instruments used for this surgical procedure and their evolution is given. The analysis of the strengths and weaknesses of the available technology leads to the conclusion that hydraulically driven instruments have the potential to improve the performance of surgeons during laparoscopic surgeries. However, the integration of a displacement-sensing technology is required to enable feedback control and tele-manipulation. Given the laparoscopic instrument's and the hydraulic cylinder's small size, a sensor concept must be identified which is accurate and compact enough to be integrated into the instrument, and requires the least changes to the existing mechanical design. The chapter concludes with the presentation of the scientific question, the description of the used scientific method, and the presentation of the structure of the thesis.

Chapter 2 describes the classical and the hydraulically driven minimally invasive tools. Their working principle is explained, their sizes and the available space for the sensor integration is reported. This overview leads to the definition of the requirements that the sensor concept must fulfill.

Chapter 3 contains a review of the relevant literature on sensors for displacement measurement. The special focus of this research is to find a sensor concept which can be integrated directly into the drives of the minimally invasive surgical tools. The result of the literature research is the identification of the capacitive principle as most suitable for this application, since the integral structure of the hydraulic cylinder can be used as a sensor without any additional element.

In **Chapter 4** the most suitable capacitive sensor concept for the analyzed problem is identified and presented. In the beginning, two types of capacitive sensing methods are taken into consideration. Their principle of operation is discussed and their characteristics are analyzed using a simplified model. This analysis will lead to the conclusion that among the possible sensor configurations the coaxial cylindrical capacitor is the most suitable for the analyzed application. It follows an FEA (Finite Element Analysis) simulation to prove the validity of the concept on a sensor model. Furthermore, the model behavior in the presence of mechanical tolerances will be analyzed to verify their influence on the sensor´s performance.

Chapter 5 describes the experimental tests executed to prove the sensing concept elaborated in chapter 4. The chapter describes the hardware and software set-up for the experiments. It gives details about the approach used to run the experiments and the statistical method to analyze them. The tests results are used to validate the simulation model.

The aim in **Chapter 6** is to integrate the sensor into a closed loop control and to run tests in order to check the suitability of the sensor for the control of the instrument's position. In this chapter, the chosen closed loop control method will be discussed, its parameters tuned, and a hydraulic drive designed to permit the movement of the cylinder presented. The designed controller is initially proven

through simulations. Afterwards, it is tested in the real system and the experimental data obtained are compared with the simulation results.

Chapter 7 contains a critical review of the results and discusses which aspects are still open and belong to future work.

Chapter 8 contains the summary of the thesis and **chapter 9** the literature.

2 Analysis

This chapter contains the analysis of the classical minimally invasive surgical instruments and of the newly developed hydraulically driven laparoscopic instruments, which are not yet on the market. In the following, their working principle will be discussed and the space available for the sensor integration identified. Out of this analysis, the requirements for the sensor concept will be derived.

2.1 Currently used instruments in minimally invasive surgery

2.1.1 Laparoscopic instruments

The equipment required for the classic laparoscopy can be grouped into three categories: imaging, peritoneal access devices and instrumentation.

The procedure starts with creating an access to the peritoneal cavity. Once the first access has been set, the cavity is insufflated with CO_2 in order to lift the abdominal wall into a dome to increase the operative field. A camera port for the laparoscope is then inserted. Under direct visualization of the cavity, two other trocars are placed, through which two instruments are inserted.

The access points are arranged in a triangular shape in order to have the laparoscope and the two instruments, inserted through the trocars, pointing towards the operative site in the same direction. The triangulation is necessary to avoid interaction or "sword fighting" (Norton et al. 2008). If the instruments´ positions are not following this rule, in fact, they are prone to collide.

Trocars exist in various sizes. They are available in 5 mm, 10 mm, 12 mm, and 15 mm diameter (Rosenblatt et al. 2008). The biggest ones are used for the laparoscope, whereas the smaller ones for the instruments.

Because of the size constraints set by the trocar, laparoscopic instruments are available in 3 mm, 5 mm, 10 mm and 12 mm diameter (Karl Storz 2015; Aesculap 2017). Laparoscopic instruments are rigid and, as shown in Figure 2.1, are composed of handle, shaft and pincers, which can have different shapes according to the instrument´s purpose. The length of the shaft can vary between 300 mm and 350 mm (Carus 2010).

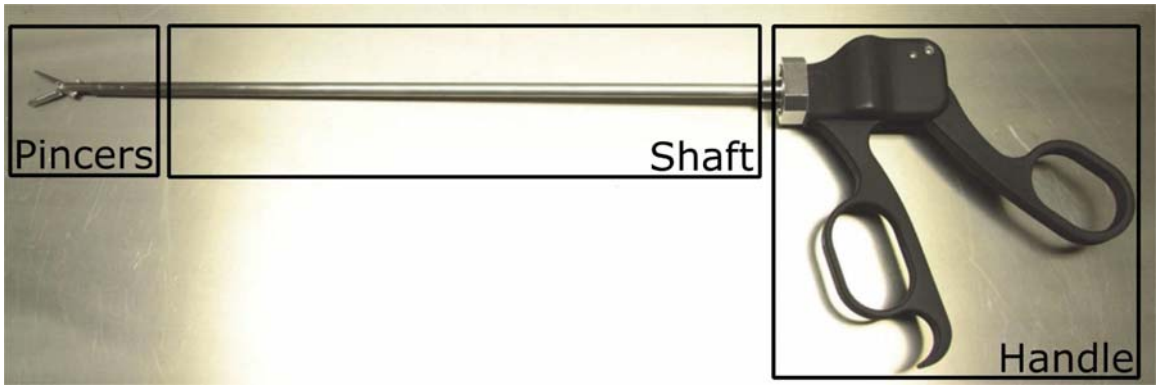

Figure 2.1: Example of a laparoscopic instrument and definition of the parts of which it is composed

The most common types of laparoscopic instruments are: dissectors, graspers, scissors, needle holders and coagulation instruments. Every type of instrument presents a different type of pincer, the design of which depends on the type of task for which it is meant (Pappas et al. 2008).

Dissectors have thin and bended pliers as shown in Figure 2.2. The tissue can be dissected by placing the instrument tip on it and opening the branches. If

Figure 2.2: Pliers of laparoscopic dissector (Carus 2010)

necessary, the pliers can also be used to grasp and pull parts of tissue. A mechanism on the handle allows 360° rotation of the tip (Feußner et al. 2009).

Graspers are used for holding and moving tissues or organs. They are characterized by two pliers with an internal spline perpendicular to the pliers' length. There are different types of grasper pliers, the geometry of which changes according to the necessary force and rigidity (Carus 2010). Pliers large and thin, like the one in Figure 2.3, with no deep spline are used as an atraumatic grasper.

Figure 2.3: Pliers of atraumatic grasper (Carus 2010)

Stronger grasping can be achieved using a deep spline like the one in Figure 2.4. This instrument can cause trauma to the tissue, for this reason sensitive tissues should never be grasped with it.

Figure 2.4: Pliers of aggressive grasper (Carus 2010)

More aggressive graspers are also available on the market. Their spline also has teeth. These graspers are used only on tissues that must be cut (Rosenblatt et al. 2008).

Scissors are very similar to the dissectors, but they have sharp edges to cut tissues. An example of a scissors tip is shown in Figure 2.5.

Figure 2.5: Pliers of laparoscopic scissor (Carus 2010)

Needle holders have the tip specifically designed for holding needles, see Figure 2.6. In order to simplify the suture procedure, the instrument is normally equipped with a lock mechanism, so that no force must be applied by the operator to hold the needle (Nakada et al. 2009).

Figure 2.6: Pliers of needle holder (Carus 2010)

Coagulation instruments are used to trigger the process of coagulation, through which the blood changes from liquid to gel form. During operations, this phenomenon is used to stop loss of blood. Coagulation instruments apply a radio frequency (RF) alternating current to the tissues to heat them. The applied RF signal induces the oscillation of ionized molecules in the cells and consequently the intracellular increase of the temperature. At a temperature between 60-99 ˚C coagulation occurs (Feldman et al. 2012). The tip of the instrument is generally a grasper or a dissector. An example of the instrument tip is shown in Figure 2.7.

Figure 2.7: Tip of coagulation instrument

To conclude the overview of laparoscopic instruments, it was estimated that the maximum frequency for the tip movement when actuated by hand is 2 Hz, a value that was measured by moving the instrument tip at the fastest speed allowed by hand´s movement in an interval of 1 minute.

2.1.2 EndoWrist Manipulator

EndoWrist manipulators are designed for laparoscopy by the surgical company Intuitive. Two examples are shown in Figure 2.8. They are characterized by multiple degrees of freedom at the tip, which allow a wrist-like movement (Sung et al. 2001).

Figure 2.8: EndoWrist Needle holder on the left and grasper on the right

For the bending movement they use the cable pull mechanism. The instrument is mounted at the tip of the arm of the Da Vinci robot, a robotic surgical system used for performing minimal invasive surgery. It is constituted by a visual console, three robot arms, and a console. The movements of the arms are controlled in open loop by the doctor with two joysticks mounted on the console (Palep 2009).

2.1.3 SPL instruments

The SPL is a minimally invasive surgery in which the surgeon operates exclusively through a single entry port, typically the navel.

For this surgery, a special type of trocar is used that allows an endoscope and instruments to enter through one single incision (Canes et al. 2008).

As the instruments are inserted through one opening, the triangulation between the instruments´ positions, typical of laparoscopic surgery, cannot be reproduced. That is why instruments with a curved shaft are used (Haber et al. 2010).

2.1.4 NOTES instruments

NOTES operations are performed without external incisions. The endoscope and the surgical tools are inserted through natural orifices of the body and led to the operating field through an internal incision in the stomach, vagina, bladder or colon (Haber et al. 2008).

Until now, there are no instruments on the market specifically designed for this type of surgery. Mostly flexible biopsy forceps, like the one shown in Figure 2.9, are used and guided in place using a flexible endoscope (Santos et al. 2011).

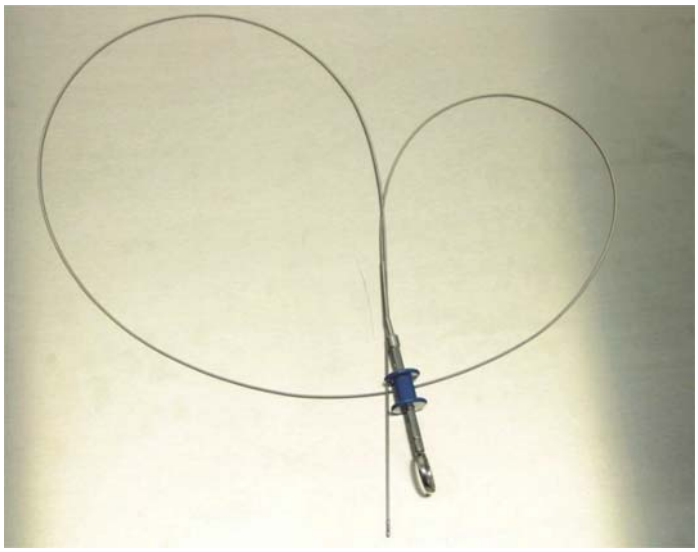

Figure 2.9: Flexible biopsy forceps

Flexible biopsy forceps are available on the market in diameters between 1.7 mm and 3 mm. They are composed of a handle, forceps and flexible shaft (Aesculap 2012; Karl Storz 2015).

2.2 Hydraulically driven minimally invasive instruments

Hydraulic cylinders are a category of micro actuators (Bell D. J. et al. 2005) which is becoming increasingly popular for medical applications (Lazeroms et al. 1996; Peirs et al. 1998; Cuntz et al. 2013; Cuntz et al. 2015) due to the increased force and power density provided when compared with electrostatic, thermal or piezo-electric actuators (Volder 2008).

Hydraulic drives have been successfully integrated into minimally invasive surgical tools in (Cuntz et al. 2013; Spindler et al. 2013).

The working principle of the hydraulic instruments is shown in Figure 2.10.

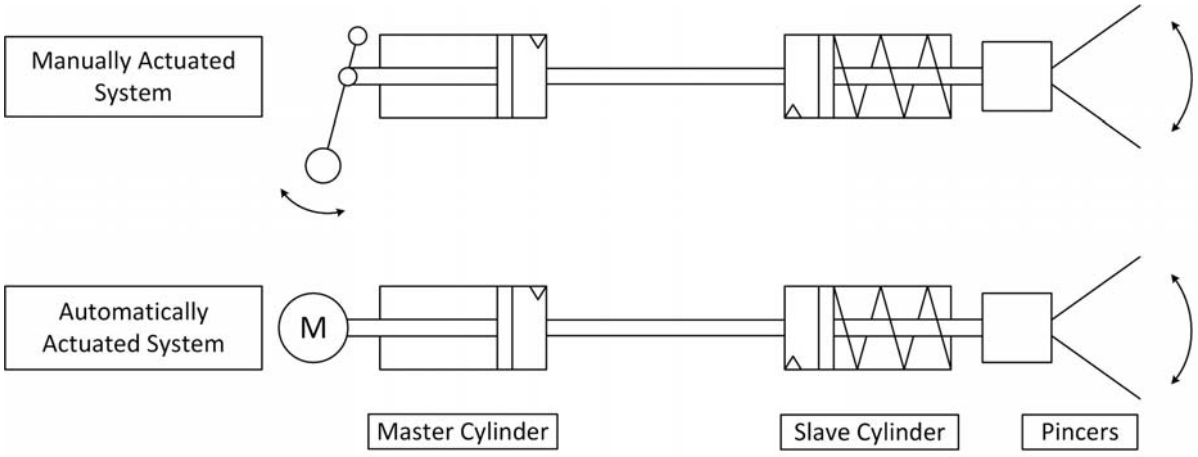

Figure 2.10: Drawing of the hydraulic system concept. Actuation obtained with force transmitted to a single actuation cylinder (Cuntz 2016).

For closing the pliers, a force is applied either manually or automated, through a motor (M), and the master cylinder is moved. The applied hydraulic pressure causes a linear movement of the rod of the slave cylinder. A scissor kinematic transduces the linear movement into the rotating movement of the pliers. For

opening the pliers, the force applied to the master cylinder is counterbalanced by a spring, in order to prevent the system from reaching a status of vacuum.
Based on this concept, both fixed shaft instruments for laparoscopic surgery and flexible shaft instruments for endoscopic surgery, shown in Figure 2.11 and in Figure 2.12 respectively, were built. Their sizes follow the standard of the surgical instruments on the market previously discussed (Carus 2010; Karl Storz 2015; Aesculap 2017).

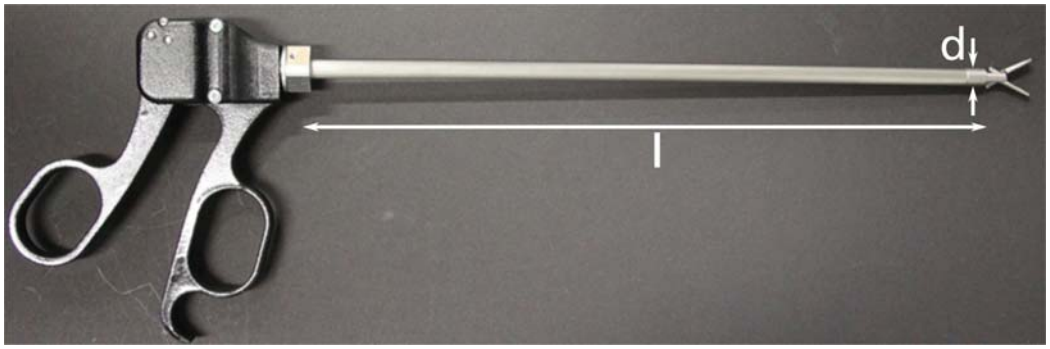

Figure 2.11: Fixed shaft instrument (Cuntz et al. 2013)

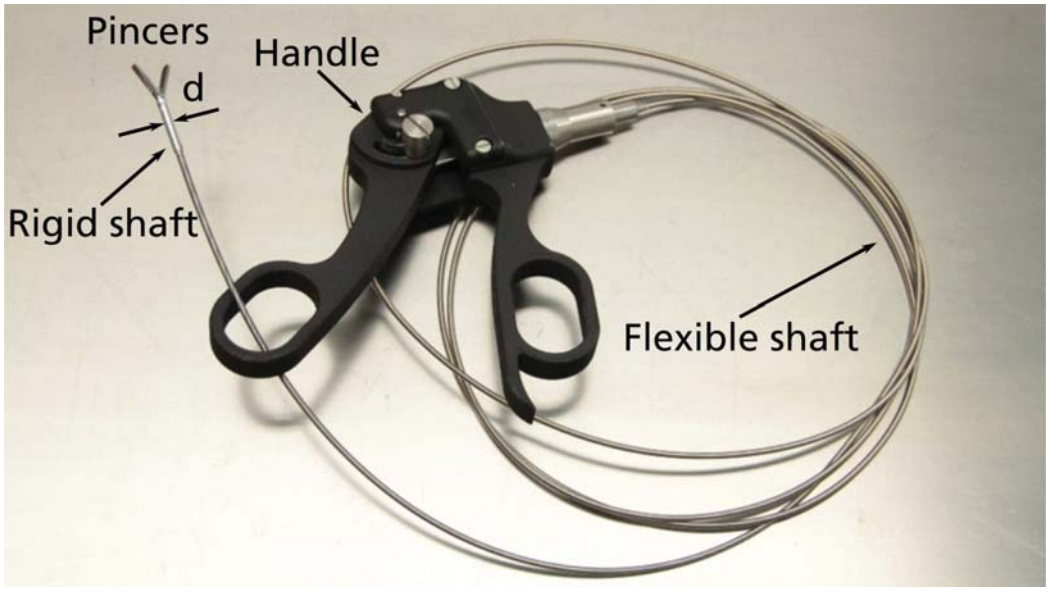

Figure 2.12: Flexible shaft instrument (Cuntz 2016)

The **fixed shaft instrument** has a shaft external diameter of d = 8 mm and a length of l = 320 mm. Both the master and the slave hydraulic cylinder have a

diameter of 7 mm and the hydraulic power transmission is possible through a rigid tube of 7 mm diameter (Cuntz 2016).

The **flexible shaft instrument** is composed of a handle, a hollow flexible shaft, and a rigid shaft hosting the slave cylinder connected to the pincers.

The rigid shaft has a diameter of d = 2.9 mm. Like in the previous case, both the slave and the master cylinder have the same sizes and their diameter is 2.4 mm. The hydraulic power is transmitted through a flexible steel pipe (Cuntz 2016).

2.3 User interface of laparoscopic instruments

The handle of classical laparoscopic instruments uses a simple scissor mechanism and allows the manual control of the opening and closing of the tip. The complexity of the handle mechanism grows together with the complexity of the tip. Instruments like Kymerax, Jaymy and r2 with multiple degrees of freedom of the tip are equipped with a handle able to control all of them separately. In the r2, the handle´s movement is mechanically connected with the instrument tip. In Kymerax and Jaymy, a sensor measures the entity of the movement on the handheld and a corresponding adjustment of the instrument tip is triggered using motor drives (Zahraee et al. 2010; Sieber et al. 2017).

The same mechanism is used in the da Vinci system, in which the instrument tip is moved using two joysticks. The entity of the movement is also in this case measured on the handheld and the tip position is adjusted controlling the robot drives (Sung et al. 2001).

A different concept of handheld is shown in (Stoianovici 2000), where the user hand is clamped and the finger´s articulation is used to control the tip of the laparoscopic instrument shown in Figure 2.13.

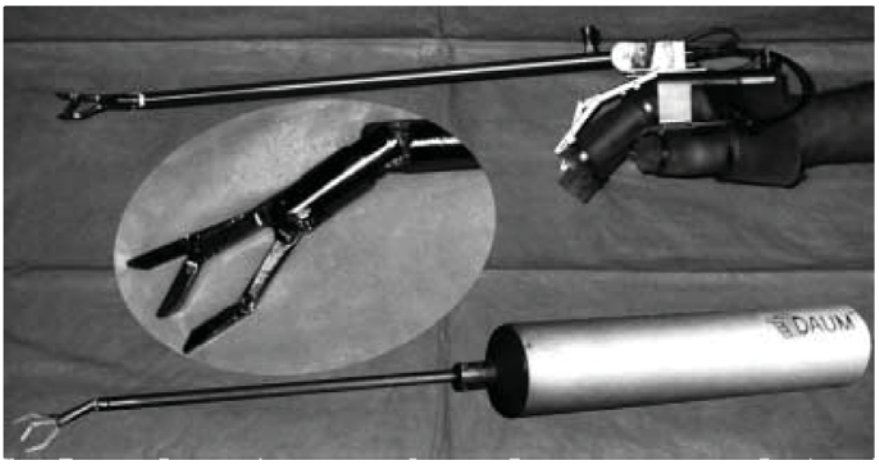

Figure 2.13: DAUM Endohand to control a laparoscopic instrument tip (Stoianovici 2000)

All these systems have in common that the surgeon dictates the movement of the instrument using only his personal perception and the instrument tip moves consequently.

The laparoscopic procedure can be made easier if, instead of the open loop control, the instrument would work in closed loop as already discussed in chapter 1.1.2. In this case the tip would be able to follow pre-programmed trajectories accomplishing autonomously the execution of complex tasks like stitching or cutting. Such a system would allow more accurate movements and would reduce surgeon fatigue. The surgeon, in fact, would only have to keep the instrument in place and start the automatic procedure.

The precondition for the establishment of this new concept is the development of a sensor that can be integrated at the instrument tip to control its position, and this will be the core of this thesis work.

Of course, a specific handle interface must be developed for this new type of instrument which is not on the market yet. This is an aspect that will not be discussed in this thesis and will be the subject of following works.

2.4 Hygiene requirements

For safety reasons, medical instruments must be sterilized and disinfected before each use. There are two possible approaches to fulfill this requirement. In the first case scenario the instrument is disposable, i.e. it can only be used one time and is then thrown away. In the second case scenario the instrument can be used several times, hence it must be cleaned, disinfected and sterilized after every surgical procedure. The instruments´ cleaning procedure is strictly regulated and must follow established national and international standards.

In the following, the relevant hygienic themes for the analysis of the thesis and for setting the sensor specifications are summarized.

The first step of the cleaning process starts in the operating room, directly after the surgical procedure. Big residues must be removed immediately. At this point the real cleaning/disinfecting procedure starts and it can be either manual or automatic (AKI Aufbereitung 2009).

During the manual procedure, the instruments are cleaned using a solution containing active non-protein-fixing process chemicals. For the disinfection, the manufacturer´s instructions about detergent, concentration, and time of exposure must be followed. It is important to be sure that during the cleaning/disinfecting process all the instrument´s surfaces are in contact with the solution. The manual process is normally concluded with rinsing and drying (AKI Aufbereitung 2009).

Alternatively, it is possible to use cleaning/disinfecting machines. Devices exist which perform automated cleaning with thermal disinfection or with chemo-thermal disinfection. The thermal disinfection is performed in fully demineralized water at temperatures between 20 and 90 °C (AKI Aufbereitung 2009). An automated cleaning process with thermal disinfection normally goes through the

following phases: pre-wash, cleaning, intermediate rinse, thermal disinfection, and drying. In every cleaning phase the instrument is placed in a specific solution and treated for a defined amount of time at a specified temperature. The automated cleaning process with chemo-thermal disinfection is characterized by the same cleaning phases as the previously described procedure, with the difference that the disinfecting phase is performed before the intermediate rinse, using a chemical disinfectant and at a temperature lower than 65 ˚C. This is the maximum temperature that will be achieved in this kind of procedure (AKI Aufbereitung 2009).

In addition to one of the cleaning/disinfecting procedures discussed, the ultrasonic cleaning method can be utilized. It uses ultrasounds to gently remove encrustations in places difficult to reach otherwise (AKI Aufbereitung 2009).

Sterilization is normally achieved with saturated steam and performed at 134 ˚C. When such a high temperature is a problem for the instrument, sterilization can be performed using a chemical agent, with temperatures lower than 75 ˚C (AKI Aufbereitung 2009).

2.5 Sensor requirements

From the information about the laparoscopic instruments and the hygienic standards collected in the previous subchapters, it is possible to identify the requirements that the sensor concept must fulfill.

Sensor size specifications

- As already discussed in chapter 1, the goal of this work is the integration of a sensor on minimally invasive instruments to allow the accomplishment of preprogramed tasks or guided operations. The two concepts are adaptable to every kind of surgery and all the instruments discussed in chapter 2.1 are

candidates for the sensor integration. Scissors and needle holders, if equipped with a position sensor, would allow the automatic execution of preprogramed tasks like stitching or cutting complex geometries. Graspers, dissectors, coagulation instruments, SPL and NOTES instruments could be used in guided operations. Cameras or proximity sensors would be responsible for the environment´s mapping, whereas the sensor would be used to drive the instrument tip in the desired position. As the laparoscopic instruments exist in different dimensions (Rosenblatt et al. 2008) as already discussed in chapter 2.1, the developed sensor should be integrable on all of them to guarantee the potential use of the new automated approach in as many surgical procedures as possible. Moreover, it should be able to be integrated in instruments with multiple degrees of freedom. However, for the first development and the proof of concept, it was chosen to design it for the measurement of the opening and closing of the pliers in classical laparoscopic instruments. The developed concept can be later readapted for instruments with multiple degrees of freedom.

- Given the advantages of hydraulically driven instruments, the sensor will be developed to be integrated on these kind of drives. Hydraulically driven instruments do not exist in all the forms of classical instruments. Figure 2.11 and Figure 2.12 show two examples of developed hydraulic instruments. They prove the concept of hydraulically driven instruments for minimally invasive surgery, opening the door to the integration of these drives in all minimally invasive instruments. In order to develop a sensor for instruments of different dimensions, it must be proved that its integration in the smallest hydraulic instrument currently available is possible. Hence, for the sensor development the dimensions of the instrument in Figure 2.12 will be taken

into consideration. This means that the sensor must be miniaturized to fit in a shaft with 2.9 mm diameter.

- The integration of the sensing system should not substantially alter the existing mechanical design of the cylinder in order to avoid complications in the manufacturing process. Moreover, it must not change the instrument´s design which is standardized to fit the tools used for body access in laparoscopy and endoscopy.
- To continuously monitor the position of the instrument tip, the sensor must be able to measure the position of the slave cylinder. Hence, it must be integrated at the tip of the instrument. This function also allows for the detection of malfunctioning of the hydraulic connection between the slave and the master cylinder.
- To guarantee a good transmission of the sensor signal to the acquisition interface, the analogue to digital conversion of the sensor output should also be performed at the tip of the instrument and the digital signal should be transferred with cables towards the handhold.

Sensor characteristics

- The sensor´s precision is defined using the angular resolution of the eyes which permits to calculate the minimum distance between two points in order for them to be distinguishable. It is experimentally defined that the angular resolution of the human eye is $2 \cdot 10^{-4}$ rad (Wimmer-Schweingruber 2017). This means that when an object is placed 25 cm from the eyes, two points must be placed at a distance not smaller than 50 µm to be distinguished. This would be the sensor resolution required if the surgeon would directly watch the operative field. However, in the case of

laparoscopy, the operative field is watched through a monitor that is normally 2.5 m away from the surgeon (Supe et al. 2010). At a distance of 2.5 m from the object, the minimum distance between two points that the eyes can perceive is 500 µm. If we, however, take into account that the image in a laparoscopic surgery can be zoomed between 5 and 10 times (Urologie Leipzig 2010), it is possible to conclude that the minimum distance that can be sensed by the eyes is again 50 µm, and that this is the precision of the sensor that must be guaranteed.

- The sensor must be able to measure linearly a stroke of 20 mm, which is required for the actuation of the pincers.
- The sensor must be electrically isolated from the environment, so that no external disturbances can affect its performance. The electrical insulation must also guarantee patient protection from eventual electric energy loss.
- As the maximum frequency estimated for the tip movement is 2 Hz, the minimum bandwidth of the sensor must be ≥2 Hz.

Control specifications:

- The sensor must be able to control the instrument tip in closed loop. As discussed in chapter 2.3, the closed loop control allows the instrument to perform movements more accurately and to execute pre-programmed tasks autonomously.

Hygiene specifications

- As the sensor is integrated inside the instrument, disinfection and sterilization must be possible. This means that the sensor should survive the sterilization process in which 135 ˚C are reached and should be ready to be immersed in liquid without being subjected to damages.

As an alternative, the instrument in which the sensor is integrated must be designed as disposable.

Material specifications

- As the sensor is directly integrated in the instrument which enters the patient´s body, it must be manufactured with biocompatible materials.

Table 1: Sensor specifications

Specification	**Limit definition**
Sensor miniaturization and adaptability to different kinds of instruments	Sensor integration possible in instruments having 3 mm, 5 mm, 10 mm and 12 mm diameter
Sensor diameter	<2.9 mm
The sensor integration must not alter the cylinder´s and the instrument´s design	
The sensor must directly measure the slave cylinder position	
Sensor output digitalization at the instrument tip	
Sensor precision	≥50 µm
Stroke linearly measured	≤20 mm
Electrical isolation of the sensor from the environment	
Sensor bandwidth	≥2 Hz
Type of control for the instrument tip	Closed loop
The sensor must be: liquid resistant	
disinfectable	At temperatures between 20 and 90˚C
sterilizable	At a temperature of 134˚C;
Sensor material	Biocompatible

3 State of the Art

Displacement sensors are an established technology and several kinds are offered on the market. A general overview of displacement sensors can be found in (Webster 1999), but only some of the listed technology is suitable for the measurement of displacement in hydraulic or pneumatic cylinders. Standard displacement sensors for hydraulics (Jelali et al. 2003) and pneumatics (Krivts et al. 2006) are: resistive, inductive, magnetostrictive and capacitive sensors, optical and magnetic encoders.

Resistive displacement sensors or potentiometers are electromechanical devices composed of a fixed resistive element and a wiper contact which slides on the resistor. See Figure 3.1(a) for the component schematic.

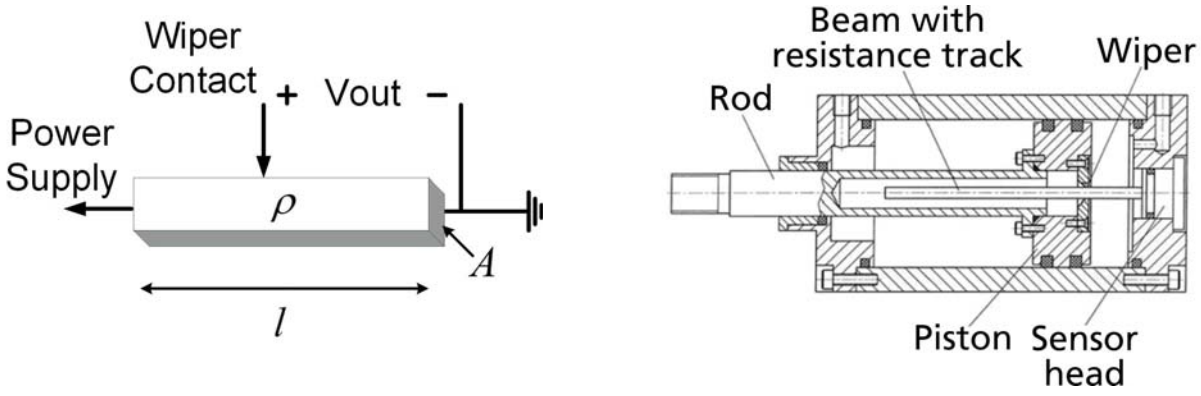

Figure 3.1: (a) Potentiometer schematic (b) Potentiometer integrated in pneumatic cylinder (Krivts et al. 2006)

Its working principle is based on the fact that the resistance of a conductor is proportional to its length according to the formula

$$R = \frac{\rho\, l}{A}, \qquad (1)$$

where ρ is the resistivity, l the conductor's length and A the cross section area. This means that if a moving object controls the movement of the wiper, hence

the conductor's length, a displacement can be measured in terms of resistance variation. In practical applications, the measurement of the resistance's change is realized through the measurement of a voltage drop between wiper contact and ground (Fraden 2016).

Potentiometric displacement sensors can be internally or externally mounted at large size pneumatic or hydraulic cylinders (Krivts et al. 2006). In both cases, the wiper would be mounted on the moving part (rod or piston), whereas the resistive element can be either externally or internally mounted. Figure 3.1(b) shows an internally mounted potentiometer.

This kind of sensor is commonly used in large scale applications because of its low costs, but it has several disadvantages. It increases the friction of the mechanical system as the wiper has to be in mechanical contact with the resistor to allow the current to flow. This also leads to a limited lifespan due to mechanical wear. Moreover, it has a poor repeatability as its measurements are subject to hysteresis (Mraz 2004).

The flexible technology allows for potentiometers with a resistor thickness in the range of hundreds of micrometers. However, the miniaturization of the wiper is not equally simple and its size is usually in the range of the 3 to 5 mm (Hoffmann+Krippner 2017).

Inductive displacement sensors use a magnetic field to detect position. In particular, the relative movement of a ferromagnetic core and a magnetic field can be measured, where the core is normally connected to a moving element.

There are several techniques that can be used, but differential variable reluctance transducers (DVRT) and linear variable differential transducers (LVDT) are the most common. Both systems convert a linear displacement into a linear electrical output signal (LORD Corporation 2014).

The DVRT is composed of two coils in series (LORD Corporation 2014), as in Figure 3.2(a). The working principle of this method is based on the fact that the movement of a core changes the reluctance of the coil, hence its inductance. The reluctance is the magnetic equivalent of the resistance in an electric circuit. Just as an electric field makes the current prefer the path with the smallest resistance, the magnetic field makes the flux follow the path with the smallest reluctance. Equivalent to the resistance, reluctance depends on the core material and its geometry. It is related to inductance according to the formula

$$L = \frac{n^2}{R}, \qquad (2)$$

where L is the inductance, n^2 the number of turns of the coil, and R the reluctance. The movement of the core causes the change of the reluctance as by moving, the geometry and the material experienced by the flux along its path change. The variation of the reluctance causes an inductance change according to formula (2). It follows that the displacement of the core can be obtained from the variation of the inductance (Webster 1999).

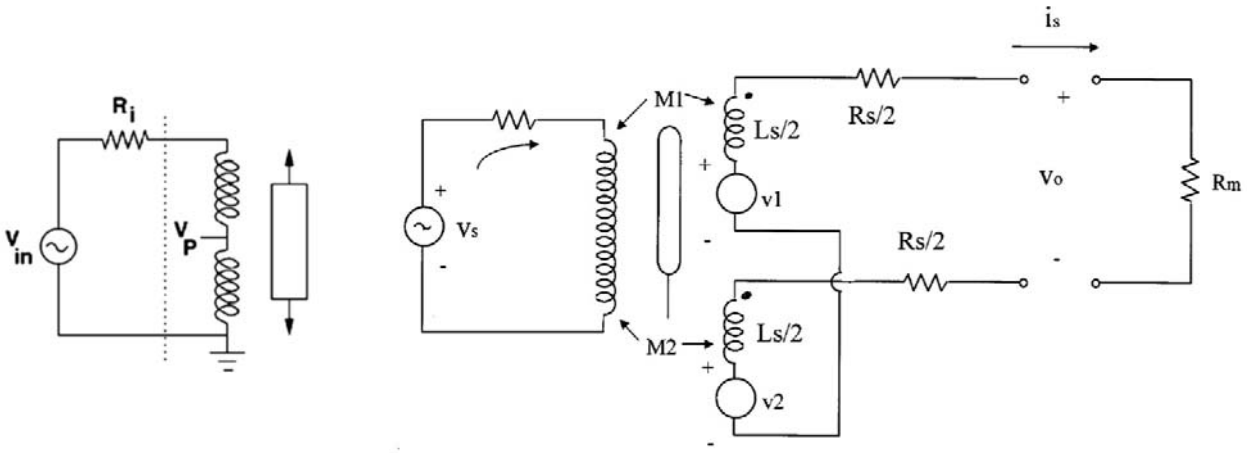

(a) **(b)**

Figure 3.2: (a) Circuit design of DVRT sensing system (Webster 1999) (b) Circuit design of LVDT sensing system (Webster 1999)

The working principle of the LVDT sensor system is based on the fact that if electric current passes through a coil which is situated in close proximity to another coil, according to Faraday's law, an electromotive force on the charge carriers in the second coil will appear, resulting in a voltage V_2

$$V_2 = M_{21} \frac{di_1}{dt}, \tag{3}$$

where M_{21} is the mutual inductance between the two coils, proportional to the magnetic permeability of the coupling material and its geometry. i_1 is the current passing through the first coil (Webster 1999).

When a ferromagnetic core or plunger is moved between the coils, their mutual inductance is altered together with the induced electromotive force, which can be used to measure displacement (Hodges 1993).

The standard LVDT sensing system is composed of a primary coil and two secondary coils, which are identical, having the same mechanical and electrical characteristics. They are connected in series, so that the voltages induced by the primary coil's field are oriented in opposite directions. See Figure 3.2(b) for the circuit design. When the core is in the middle of the stroke, the coupling between the primary coil and both the secondary coils is the same, hence the output voltage V_o is zero. In correspondence to the core displacement the magnitude of the output signal V_o is different than 0 and proportional to the core movement, whereas its phase is dependent on the movement direction (Fraden 2016).

Both methodologies are frequently used because of their linearity and high resolution, and also because they allow contactless measurement. However, they are not an optimal solution in applications where size is a critical parameter, as the stroke to length ratio is small. In fact the actuator stroke is limited to less than half of the sensor length (Krivts et al. 2006).

The two described techniques have been adapted respectively in Sumali et al. 2003 and Volder et al. 2008 for the measurement of displacement in hydraulic cylinders. Both use a single ended variant of the two methodologies in order to reduce the size of the sensor.

In Sumali et al. 2003 only one coil is mounted around the cylinder barrel, and the rod made of ferromagnetic material causes variation in the coil´s inductance. The method has been tested on a larger cylinder than the one taken into consideration in this work: a cylinder of 38.1 mm diameter with a stroke of 203.2 mm. The accuracy of the position sensor is 25.4 mm.

In Volder et al. 2008, as shown in Figure 3.3, two coils are evenly spread on the cylinder barrel. One of them is supplied with a voltage and generates the magnetic field.

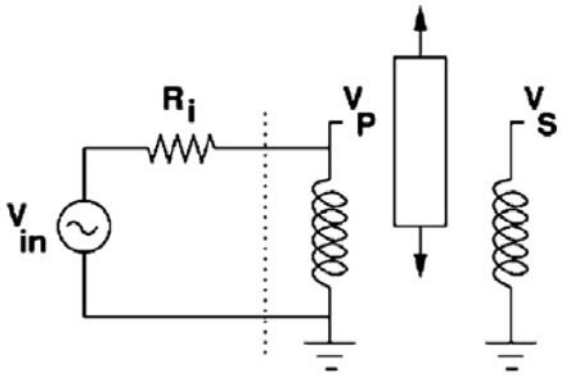

Figure 3.3: Circuit schematic of the single ended LVDT inductive sensing system (Volder et al. 2008)

Depending on the ferromagnetic rod position the coupling between the first and the second coil changes and thus the output voltage measured on the second coil. The system has been tested for a cylinder of 1.3 mm diameter, 15 mm length and a stroke of 12 mm. The sensor accuracy is ±30 µm.

Magnetostrictive sensors are another type of displacement measurement systems which are used in large scale applications (Hodges 1993). Their function

is based on electromagnetic fields and their interaction with ferromagnetic materials.

They are composed of a ferromagnetic waveguide which remains stationary and a permanent magnet which can move along the guide as shown in Figure 3.4 without touching it and the position of which can be measured (Fraden 2016).

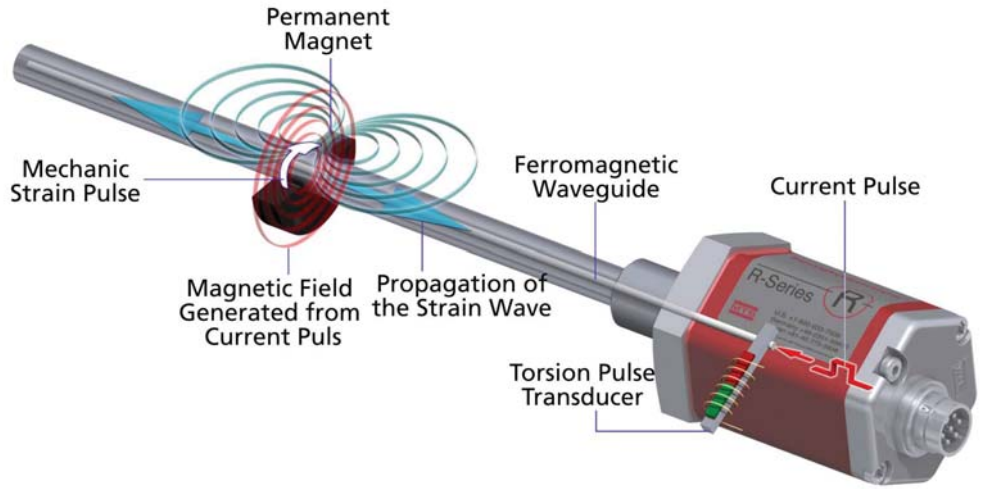

Figure 3.4: Schematic diagram of a magnetostrictive sensor (Hankinson et al. 2015)

When a measurement is required, a current interrogation pulse is sent and a circular magnetic field is generated around the ferromagnetic waveguide. At the place where the magnetic field generated by the permanent magnet and the one generated by the current flowing meet, a torsional strain pulse is produced. The strain pulse spreads out from the permanent magnet at the speed of sound, moving along the waveguide in both directions. When the pulse reaches the torsion pulse transducer at the detector head, the time of its arrival is registered. The elapsed time between the moment in which the interrogation pulse was sent and the arrival of the stain pulse represents the distance between the sensor head and the permanent magnet. Magnetostrictive sensors are widely used in pneumatic cylinder applications (Krivts et al. 2006). An example of this sensor integrated into a pneumatic cylinder is shown in Figure 3.5.

The head of the sensor is mounted on the base of the cylinder and the ferromagnetic waveguide extends from the head within the rod. The permanent magnet is mounted on the moving part: the piston. An external application of the sensor is also possible, but less compact.

This sensing method has the advantage of not being affected by shock and vibration. The disadvantage is its large size, which makes the integration difficult in the case of compact systems.

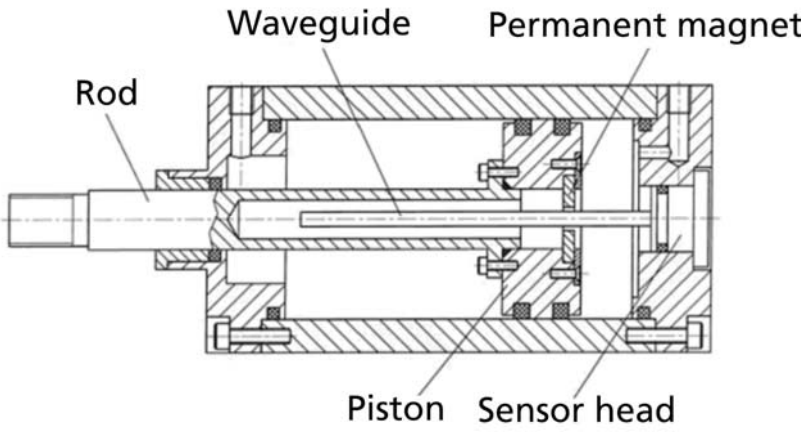

Figure 3.5: Magnetostrictive sensor embedded into a pneumatic cylinder (Krivts et al. 2006)

Encoders are non-contact displacement sensors that convert linear displacement into an analogue or digital signal. They consist of a head that moves along a pattern. Based on the pattern readings, the sensor´s head is able to determine its position (Krivts et al. 2006).

According to the technology used for the sensing head and the pattern, encoders can be divided into two categories: optical and magnetic (iC-Haus GmbH 2012).

Optical encoders are composed of a marked scale that can be engraved on different kinds of materials like glass, metal or plastic. The sensor´s head is equipped with a light source and a detector and reads the scale through reflected light as shown in the schematic in Figure 3.6(a) (Webster 1999).

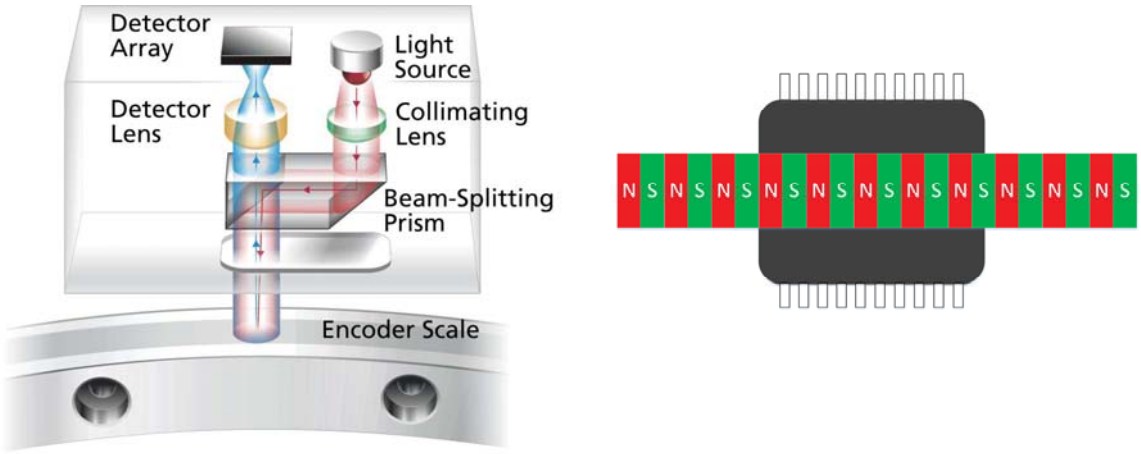

(a) **(b)**

Figure 3.6: (a) Schematic diagram of optical encoder (Renishaw 2016) (b) Schematic diagram of magnetic encoder

In the magnetic encoders, the stripe consists of alternating magnetic north and south poles, as shown in Figure 3.6(b). The sensor can detect the alternating magnetic field, transducing this information into displacement (ams AG 2013). Both magnetic and optical encoders offer high sensitivity. Optical encoders are sensitive to contaminants such as dust, dirt, and liquids, as they affect the light reflected from the pattern. Magnetic encoders are more robust, as these contaminations do not affect the measurement. However, it is very important for their correct functioning to keep the air gap between sensor and pattern in a specified range (Krivts et al. 2006; iC-Haus GmbH 2012; ams AG 2013).

Capacitive sensors (Terzic et al. 2012) are composed of two electrodes with a surface area A, separated by a distance d. A dielectric medium or material is placed between them, the relative permittivity of which is ε_r. See Figure 3.7 for its schematic structure. When the capacitor is supplied with a constant voltage, it will accumulate charge on the two plates until the differential potential on the capacitor matches the one of the power source. The capacitance C is an electrical property of the capacitor and is a measure for the amount of charge stored in

relation to the applied voltage. This value is dependent on the capacitor's geometry and the dielectric´s characteristic $C = f(A, d, \varepsilon_r)$ (Webster 1999).

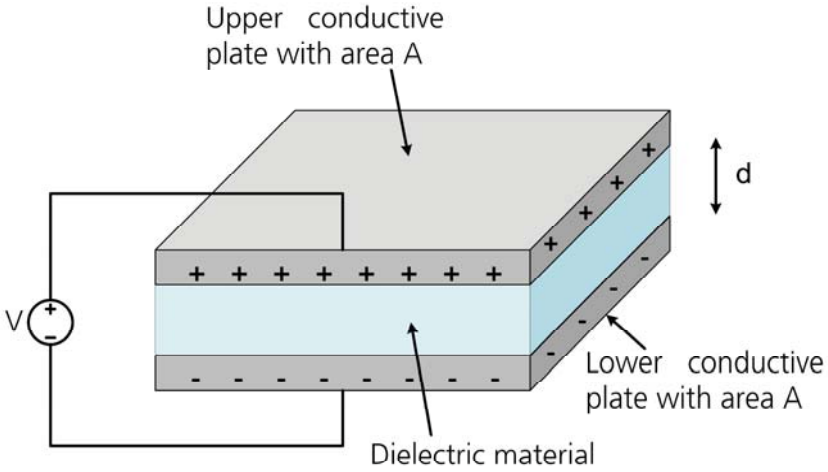

Figure 3.7: Schematic diagram of a parallel plate capacitor

Given the relationship between capacitance, geometry and dielectric characteristics, the working principle of the sensor is based on the fact that the variation of one of these parameters under an external influence can be measured in terms of capacitance (Webster 1999).

Parallel plate capacitive sensors for example, (Webster 1999; Bentley 2005) are used to measure displacement, pressure or humidity. If a moving part is connected to one of the electrodes, causing a variation of either d or A, its displacement can be measured as a variation of capacitance. If in the environment humidity changes, the relative permittivity will be altered, which also changes the capacitance. Pressure can be measured if one of the plates of the capacitance is a diaphragm of a pressure sensor. Its bending will cause a variation of the effective distance d between the plates, hence the capacitance can be correlated to the pressure applied.

Capacitive transducers have a simple construction and thus are easy to fabricate. They can be easily integrated and do not need complex electronics. Additionally,

they typically have a bandwidth of up to 1 kHz, which fulfills the requirement on the sensor dynamics. Their drawback is that their performance is normally affected by external interferences like radiated and conducted noise from other components or close electrical devices, noise in supply voltage, change in temperature or humidity (Krivts et al. 2006).

All the previously mentioned sensors are summarized in Table 2 and rated according to the specifications defined in Table 1. Magnetostrictive sensors, optical and magnetic encoders have the highest performance in terms of precision and linearity. However, they are not available off the shelf to fit in the available space (Krivts et al. 2006; Fraden 2016).

Table 2: Table of displacement sensor with rated specification

Sensors	**Precision**	**Linearity**	**Sensor miniaturization**	**Complexity of signal acquisition front end**	**Temp. tolerance**	**Contact**
Potentiometer	+	++	+	low	+	yes
LVDT/DVRT	+++	++	++	moderate	++	no
Magnetostrictive	++++	+++	-	high	++	no
Capacitive	+++	++	+++	low	++	no
Magnetic encoder	++++	+++	+	low	++	no
Optical encoder	++++	+++	-	high	++++	no
Legend: ++++Excellent; +++ Very Good; ++ Good; +Fair; Poor						

Magnetostrictive sensors should be integrated, as shown in Figure 3.5, with the ferromagnetic waveguide aligned with the axis of the cylinder and the sensor´s head in the base. This means that the integration of such a sensor is possible only by moving the position of the liquid inlet to the side, which contradicts the requirement that substantial changes in the design have to be avoided. Moreover, the solution cannot be taken into consideration as there is not enough space to

move the liquid inlet on the side of the cylinder in the laparoscopic instrument.
The integration of an optical encoder would be equally complicated. Its sensor´s head is composed of a light source, a detector and optical lenses, which cannot easily be compacted in a size range of less than 2 mm.
The magnetic encoders available on the market are already more compact than the optical encoders and the magnetostrictive sensors. Nevertheless, they are still far from the desired dimensions. The smallest magnetic encoder chip available has the dimensions 7 x 6 x 1.2 mm (ams AG 2013), which are too big to be integrated at the instrument's tip.
The LVDT and the DVRT show a similar sensing performance as the capacitive sensor. Moreover, the LVDT was already miniaturized and integrated into a cylinder of 2.5 mm diameter (Volder et al. 2008). However, this method has been excluded in this work, as its use requires the integration of an additional element, the coil, into the hydraulic cylinder. This would make the manufacturing process of the cylinder complex and substantially change its design.
The potentiometer was also excluded, since, despite its low price and ease of use, it has a poor repeatability, large hysteresis, the output worsens overtime and it is not available on the market in the necessary dimensions (Mraz 2004). Its miniaturization is complex and it requires an external additional element to be integrated in the small available space.
Among the discussed sensing methods, the capacitive measurement system is the one that best fulfills the requirements. It is the easiest sensor to miniaturize and integrate, as for the realization of the two electrodes the integral structure of the hydraulic cylinder can be used without the need of additional elements. Moreover, the sensor also shows good sensing performance, precision and linearity.

4 Sensor solution concept

This chapter analyzes the capacitive sensor designs suitable for hydraulic cylinders. First, their principle of operation is discussed and their characteristics are analyzed using a simplified model in chapter 4.1. Afterwards, the hypotheses stated in this first phase are proved using FEA (Finite Element Analysis) simulation.

The software tool used for FEA simulation is Ansys Maxwell. It is a program that, given the boundary conditions, uses finite element analysis to solve electromagnetic field problems by finding a solution for the Maxwell equations in the static case for a discretized form of the analyzed model. This calculation takes into account the materials used for the manufacturing and the fringing effect at the sensor´s boundary, which are difficult to handle analytically.

The FEA tool was chosen because it permits to prove the validity of the sensor concept without experimental tests, hence without the costs and the time necessary for prototyping. Moreover, this tool allows for a better understanding of the system, helping to define the sensor geometry most suitable for the application and later the design of the experimental tests. Of the FEA simulation tools available on the market, ANSYS and COMSOL are the two widest spread ones. As ANSYS was already in use in the research team and both tools allow to use finite element analysis to solve electromagnetic field problems with the same performances (Ansys 2018; COMSOL® 2018), it was chosen to work with ANSYS.

4.1 Preliminary concept analysis

There are several configurations of capacitive sensor, which differ in geometry of the electrodes, configuration of the electric field and capacitance.

The sensing electrodes can be cylindrical rods, flat parallel plates, coaxial

cylindrical tubes, interdigitated electrodes, and helixical wires (Terzic et al. 2012). Among them, the flat parallel plate and the coaxial cylindrical capacitive sensor are the only two configurations that can be adapted and integrated in the geometrical structure of the hydraulic cylinder, without additional elements. Both configurations will be analyzed in the following and the most suitable will be identified. The hydraulic cylinder developed in this work will be able to drive an instrument and measure its displacement.

The *flat parallel plate capacitor,* as shown in Figure 4.1, is composed of two parallel electrodes of surface A, separated by a distance d.

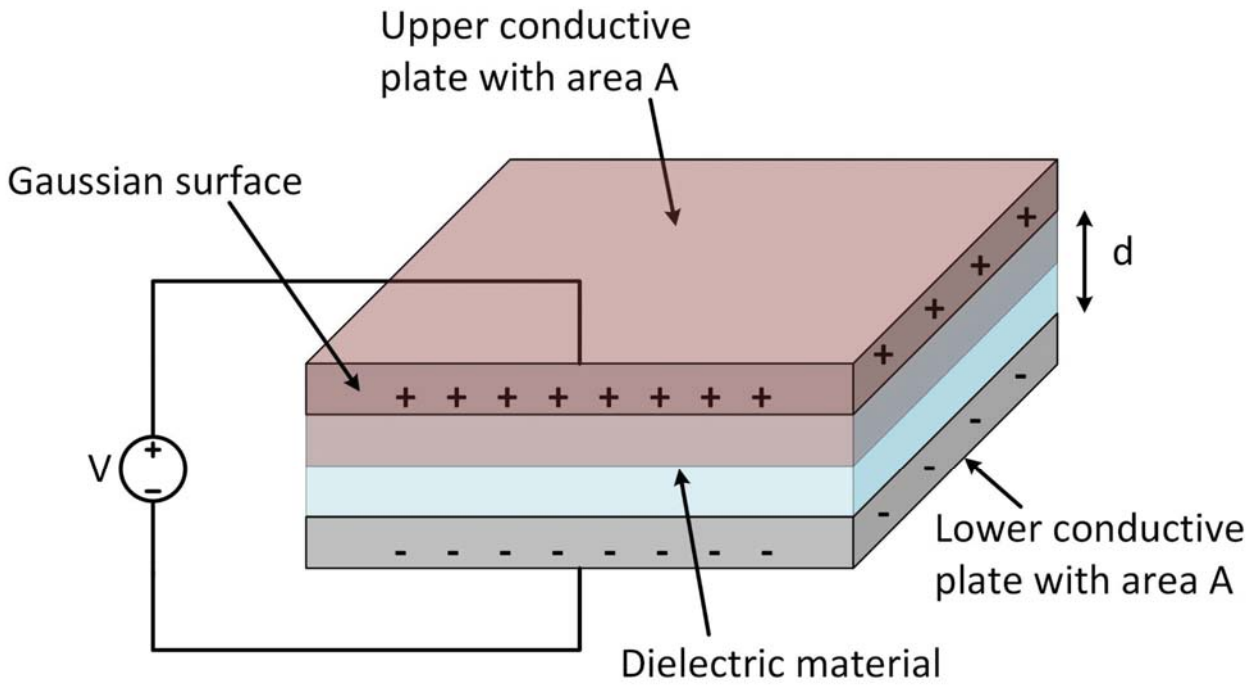

Figure 4.1: Schematic diagram of parallel plate capacitor

A simplified formula of the capacitance C can be calculated by using the relationship $Q = CV$, where Q is the charge accumulated on the electrodes and V the voltage applied. Q can be calculated by using Gauss´s Law (Colwell 2016) with the formula

$$\oint \vec{E} \cdot d\vec{A} = \frac{Q_{enc}}{\varepsilon_0 \varepsilon_r}, \tag{4}$$

where $\vec{E}$ is the electric field between the plates, $d\vec{A}$ is the differential surface vector, Q_{enc} the electric charge enclosed in the Gaussian surface, ε_r the relative permittivity of the dielectric and ε_0 the dielectric constant.

To solve the integral, the red box shown in Figure 4.1 is used as a Gaussian surface. The top surface of the box corresponds to the top electrode and, since in electrostatic conditions there is no field within a conductor, the integral on this surface is 0. Moreover, the vectors $\vec{E}$ and $d\vec{A}$ are perpendicular on all the other planes of the Gaussian surface, aside from the bottom surface. Therefore, the integral on the Gaussian surface can be reduce to the integral on the bottom surface:

$$\oint \vec{E} \cdot d\vec{A} = EA = \frac{Q_{enc}}{\varepsilon_0 \varepsilon_r}. \tag{5}$$

This solution of the integral is an approximation obtained under the assumption of a homogeneous electric field and negligible fringing effects at the boundary. The fringing effect occurs due to the electric field that extends over the edges of the plates. There, the density of the electric field is lower than between the electrodes but still present and it can affect the accuracy of the sensor.

As Q_{enc} in the Gaussian region is the electric charge on the electrode, $Q_{enc} = Q$ and from equation (5) it is possible to calculate Q as

$$Q = E\ A\ \varepsilon_r \varepsilon_0. \tag{6}$$

The voltage between the plates can be calculated from Figure 4.1 by applying Kirchhoff's law

$$V = V_B - V_A = \int_0^d E\, dr, \tag{7}$$

where V is the source voltage, E the electric field between the plates, V_A and V_B the voltages applied respectively to the upper and the lower electrode.

Assuming that V_B is the reference potential and is equal to zero, it follows that

$$V = Ed. \tag{8}$$

By substituting (6) and (8) in the formula $Q = CV$, the capacitance can be expressed as

$$C = \frac{\varepsilon_0 \varepsilon_r A}{d}, \tag{9}$$

where ε_r is the relative permittivity of the dielectric, ε_0 the dielectric constant, A the surface of the electrodes and d the distance between the electrodes.

As already mentioned, formula (9) is an approximated solution of equation (4). A more accurate analysis of the sensor behavior will be done in chapter 4.2. Nevertheless, for the purposes of this subchapter formula (9) is a good approximation, in order to analyze advantages and disadvantages of the flat parallel plate configuration.

As already discussed in the previous chapter, one of the main reasons for choosing the capacitive method is the fact that the sensor can be built using the mechanical parts of the hydraulic cylinder. Therefore, the flat parallel plate sensing configuration can be integrated into the cylinder by using the barrel base and the piston surface as electrodes. Once the two plates are powered, charge is accumulated on them and an electric field is generated in the piston chamber, as shown in Figure 4.2.

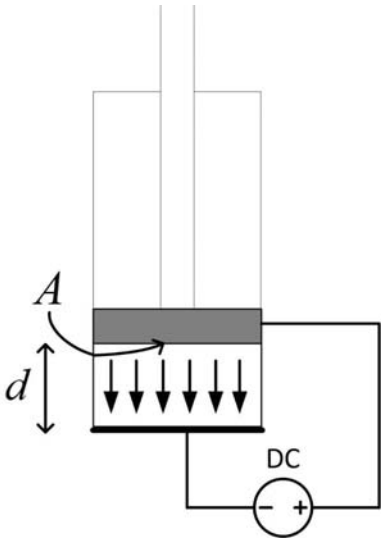

Figure 4.2: Schematic of a parallel plate capacitor integrated into a hydraulic cylinder using its parts as electrodes

According to formula (9), when the cylinder expands, the distance d between the electrodes increases and the capacitance C decreases, whereas during the cylinder retraction d decreases and C increases. Therefore, the measurement of the capacitance C can be transduced into the cylinder displacement.

A drawback of this configuration is that for values of d bigger than the cylinder diameter, the electric field between the plates cannot be considered uniform, making the relationship between capacitance and displacement non-linear and strongly reducing the sensor's sensitivity. Moreover, the scaling of the cylinder´s dimensions can be critical for the performance of the sensor. The radial miniaturization of the cylinder entails the reduction of the electrodes´ size which is proportional to the capacitive value. This means that the miniaturization of the sensor causes the worsening of the signal to noise ratio (Dyer 2004).

The *coaxial cylindrical capacitor* is composed of two coaxially aligned cylindrically shaped electrodes. A simplified formula of the capacitance can be calculated by following a procedure similar to the one used for the parallel plate capacitance (Colwell 2016). In this case, a cylinder is chosen as Gaussian surface, which lies

between the two electrodes. Figure 4.3 shows the structure of a coaxial cylindrical capacitor.

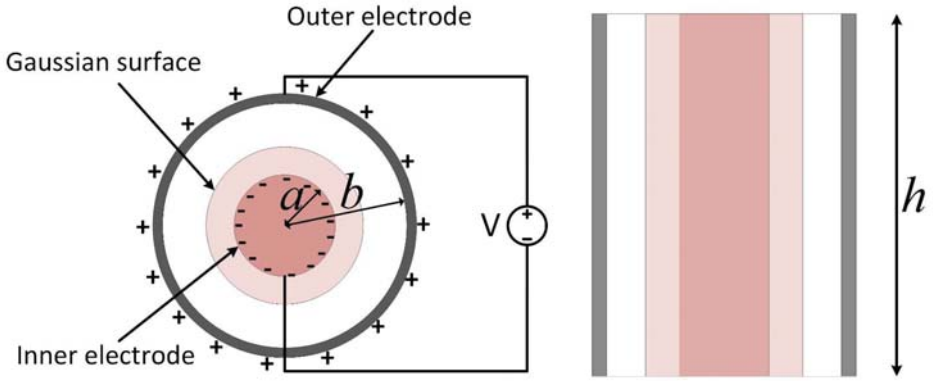

Figure 4.3: Schematic diagram of a coaxial cylindrical capacitor

By solving the Gaussian law in equation (4), the following solution for the electric field is obtained

$$E = \frac{Q}{2\pi r h \varepsilon_0 \varepsilon_r}, \tag{10}$$

where E is the electric field between the electrodes, Q is the charge on the electrodes, r is the radius of the Gaussian cylinder, h is the height of the Gaussian cylinder, ε_r is the relative permittivity of the dielectric, and ε_0 the dielectric constant.

The potential difference between the plates is

$$V_{out} - V_{in} = -\int_a^b E\, dr = \frac{Q}{2\pi h \varepsilon_0 \varepsilon_r} \ln\left(\frac{b}{a}\right), \tag{11}$$

where b is the radius of the external electrode, a the radius of the internal electrode, and V_{out} and V_{in} the potential applied respectively to the outer and the inner electrode. The remaining parameters were already defined for formula (10).

Substituting (10) and (11) in the formula $Q = CV$, the resulting capacitance is

$$C = \frac{2\,\pi\,\varepsilon_0 \varepsilon_r h}{ln\frac{b}{a}}, \tag{12}$$

where h is the length of the overlap between the electrodes, b is the radius of the outer electrode, a is the radius of the inner electrode, ε_r the relative permittivity of the material between the plates and ε_0 the dielectric constant.

This sensor configuration can be integrated into the hydraulic cylinder by choosing the barrel and the rod as the outer and the inner electrode respectively. When a voltage is applied to the electrodes, the accumulation of charge on the plates generates an electric field, which radially extends from the barrel to the rod as shown in Figure 4.4.

The functional principle of the sensor is based on the fact that, when the cylinder expands, the inner electrode moves out of the barrel. This causes a reduction of the overlap length h between the electrodes and consequently of the capacitance C. On the other hand, when the cylinder retracts, the overlap length increases together with the capacitance. Therefore, like in the previous case, the capacitance C can be transduced into displacement.

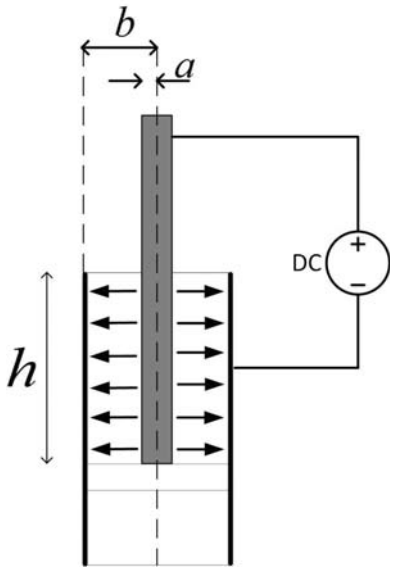

Figure 4.4: Schematic of the coaxial cylindrical capacitor integrated in a hydraulic cylinder using its parts as electrodes. The barrel and the rod are the outer and the inner electrode respectively.

The coaxial cylindrical configuration has several advantages in comparison to the flat parallel plate configuration. One benefit is the linear relationship between capacitance and displacement. Another advantage comes from the fact that the sensor sensitivity S in formula (13), derived from equation (12), is a function of the ratio between the two electrodes diameters:

$$S = \frac{\pi \varepsilon_0 \varepsilon_r}{ln\frac{b}{a}}. \tag{13}$$

From equation (13) it follows that the sensitivity can be maximized by making the ratio of the radii as close as possible to 1, hence by maximizing the radius of the inner cylinder in the design. Moreover, other than for the flat parallel plate capacitor, a radial rescaling of the cylinder does not affect the performance of the sensor as long as the ratio of outer and inner electrode diameter remains constant. This offers the possibility to adapt the size of the cylinder to the application without changing the sensitivity of the sensor. Such a sensor-actuator is adaptable to different kinds of laparoscopic instruments as, like already discussed in chapter 2.1, they exist in several dimensions.

For the reasons above, the coaxial cylindrical capacitive sensor system has been identified to be the most suitable for the purpose of this work and hence will be in the focus of the rest of this thesis.

4.2 Detailed concept analysis supported by FEA simulation

In the previous subchapter, simplified formulas were used for a preliminary analysis of the sensing method. In the following, in order to verify the behavior of the sensor concept, a precise calculation of the capacitance and definition of the electric field distribution of the coaxial cylindrical capacitive sensor is made. With the help of a FEA simulation tool, the already discussed themes will be verified:

- The relationship between capacitance and displacement is linear.
- The sensitivity increases with size ratio of rod and barrel approaching value 1.
- The sensitivity is not affected by rescaling the cylinder as long as the ratio between inner and outer diameter of the electrodes remains constant.

Moreover, the eventual influence of mechanical tolerances and of the fringing effect on the behavior of the sensor will be discussed.
The simulation´s results presented in this chapter have been published in (Comella et al. 2017).

4.2.1 Model

To run the FEA simulation, a model of the cylinder is necessary. The assembled model used for the Ansys Maxwell software is shown in Figure 4.5. It is investigated for three different designs, whose parameters are shown in Table 3. Stainless steel is used for the electrodes and the thermoplastic PEEK (Polyether ether ketone) for the remaining parts, to isolate electrically the electrodes from the rest of the mechanics. The choice has fallen on these two materials because they are mechanically stable, chemical resistant and biocompatible. Stainless steel is a good conductor for the electrodes. Moreover, it is the only alloy that withstands the temperatures necessary for the reprocessing procedures of the instrument without special treatments. PEEK is a good isolator. It also retains its properties during disinfection and sterilization and it can be machined with tolerances more precise than any other plastic.

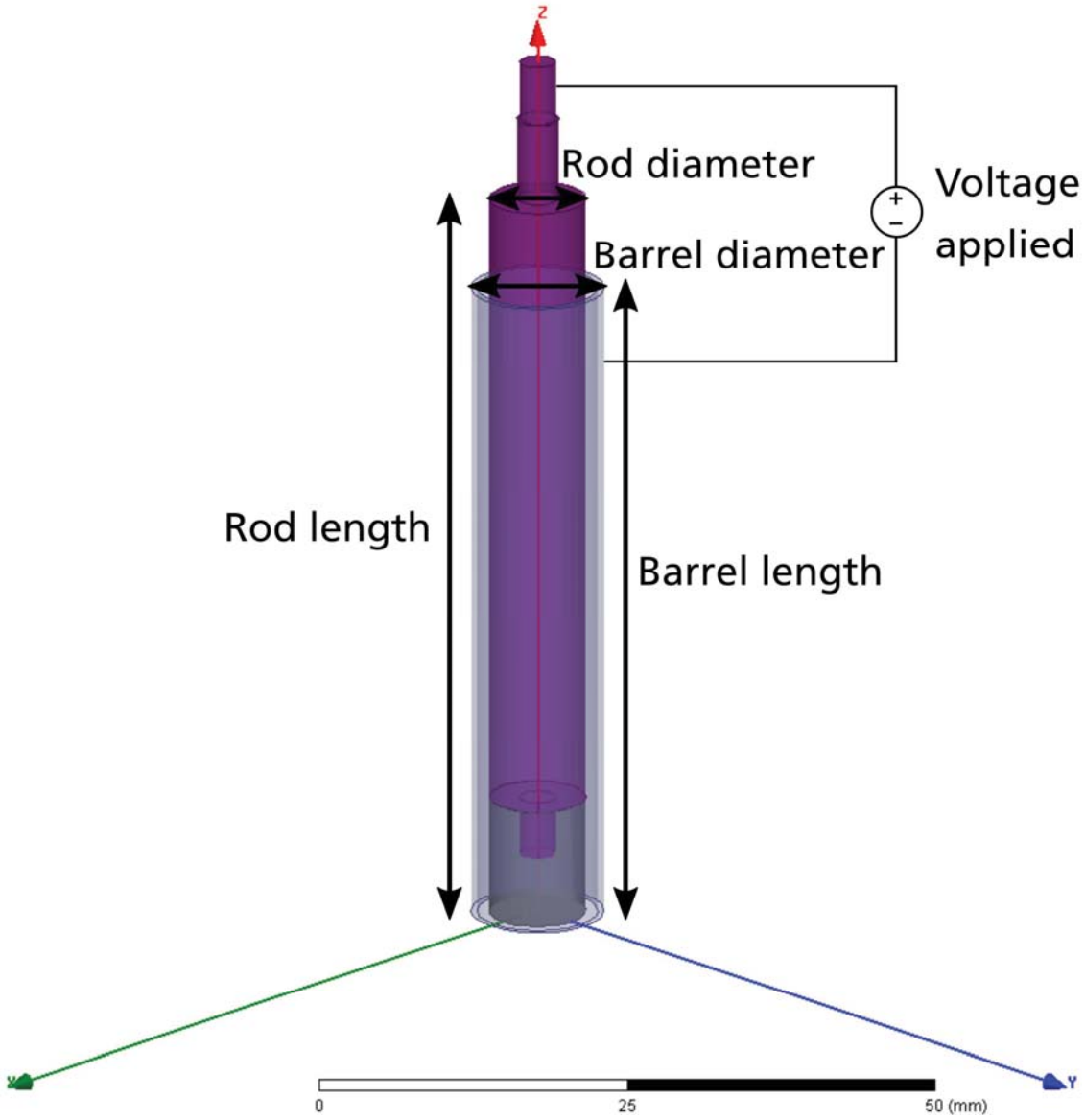

Figure 4.5: The cylinder´s assembly used for the FEA simulation

Table 3: Dimensions of the simulated models and applied voltage

Design	Barrel diameter (mm)	Barrel length (mm)	Rod diameter (mm)	Rod length (mm)	Voltage applied (V)
A	10	55	8	70	5
B	10	55	3	70	5
C	2.5	13.8	2	25	5

Design A and B, with a barrel diameter of 10 mm, belong to the mini hydraulic cylinder´s category. Design C, with its diameter of 2.5 mm, is a micro hydraulic cylinder. The sizes of the three models were chosen to investigate the behavior of the sensor on its extreme dimensions. Design A and B, with their diameter of 10mm, allow to test the behavior of a sensor fitting in laparoscopic instruments with the maximum diameter in use (see specification in Table 1). They also permit to simulate the electric field when the rod diameter change between its two extreme sizes. Design C is to test the sensor miniaturization to the minimum size of instruments, also specified in Table 1. Both the mini and the micro cylinder designs are used to analyze, how miniaturization affects the behavior of the sensor. Moreover, as the manufacturing costs of the mini hydraulic cylinder are lower in comparison to the micro hydraulic cylinder, the sensor concept will be first proved on the mini hydraulic cylinder and, if successful, tested on the micro hydraulic cylinder. Therefore, simulations with cylinders of both dimensions are necessary for comparison with the experimental results.
In the rest of this work, the mini hydraulic cylinder will also be addressed as design A and the micro hydraulic cylinder as design C.

4.2.2 Results and discussion

On the following pages, the results of the conducted simulations will be presented and discussed. The results will be sorted by the different objectives of the simulations.

4.2.2.1 Dependence of sensor linearity and sensitivity on sensor geometry

Figure 4.6 and Figure 4.7 show the distribution of the electric field for designs A and B respectively, when a voltage of 5 V is applied between the inner and the outer electrode.

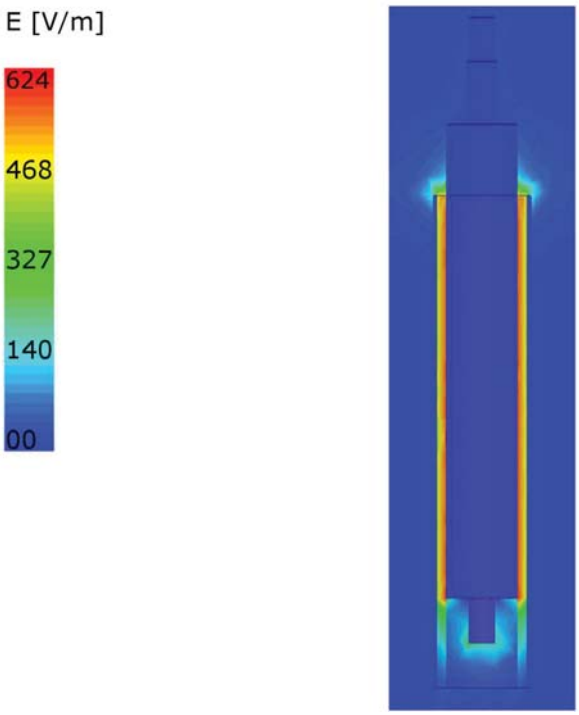

Figure 4.6: Electric field distribution of design A in the longitudinal cross-section calculated using the FEA software Ansys Maxwell

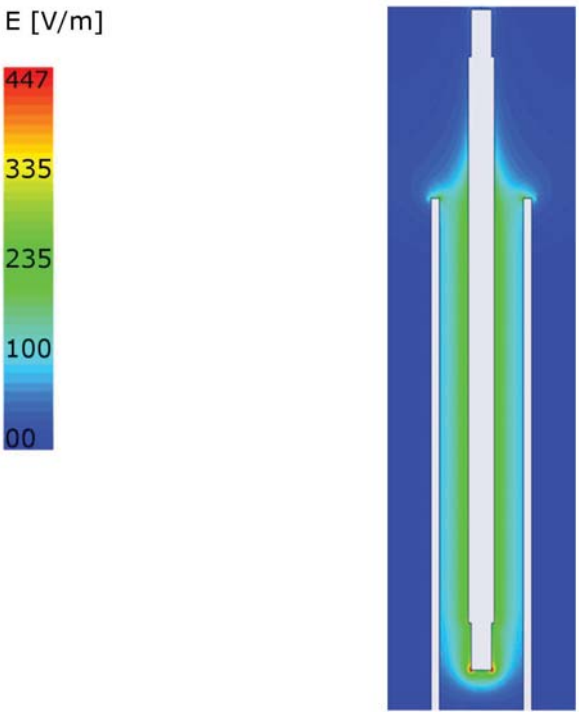

Figure 4.7: Electric field distribution of design B in the longitudinal cross-section calculated using the simulation FEA software Ansys Maxwell

The supplied voltage generates an electric field between the plates which is most intense where the distance between the electrodes is the lowest. For this reason, in model A the field intensity is bigger than in model B. Moreover, a fringing effect can be seen in both cases: There are field lines, though less dense at the edge of the barrel.

Figure 4.8 shows the plots of the capacitance against displacement calculated with Ansys Maxwell. The dependency is highly linear. Moreover, it can be observed that the slope of the capacitance against displacement for model A is bigger than for model B. The capacitance against displacement curve´s slope corresponds to the sensor sensitivity and, as already discussed in chapter 4.1, it is bigger in model A than in model B, because in A the ratio between the outer and the inner electrode diameter is closer to 1. This means that Figure 4.8 confirms the statement that in order to maximize the sensor sensitivity the size of the rod´s diameter must be as close as possible to that of the barrel diameter.

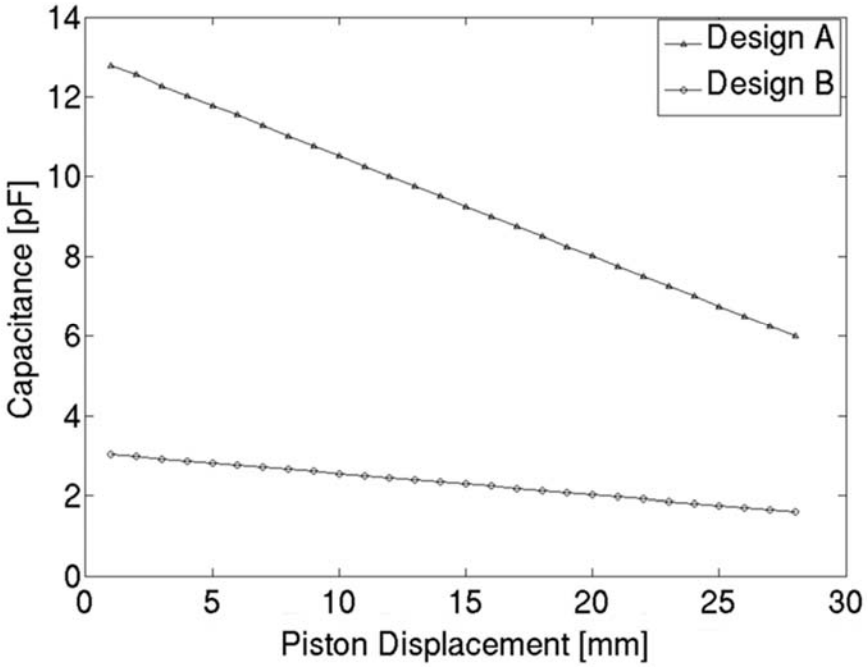

Figure 4.8: Plot of capacitance against displacement for design A and B calculated using the FEA software Ansys Maxwell

4.2.2.2 Verification of the behavior of sensitivity with sensor miniaturization

Figure 4.9 shows the electric field distribution for design C. As in the previous cases, a radial electric field is generated by applying a voltage of 5 V to the electrodes. Figure 4.10 shows the corresponding capacitance against displacement plot. The figure makes it possible to compare the characteristic curve of design A and C and shows that both curves have the same slope, hence the same sensitivity. This is due to the fact that, although the two models have different sizes, they have the same ratio of the outer and the inner electrode's diameter. The following assertion is, therefore, verified: the sensitivity of the sensor will not be affected, if the piston's dimensions are scaled, as long as the ratio of the rod and the barrel´s diameter remains constant. The different capacitance range of designs A and C is due to the different stroke length of the two designs.

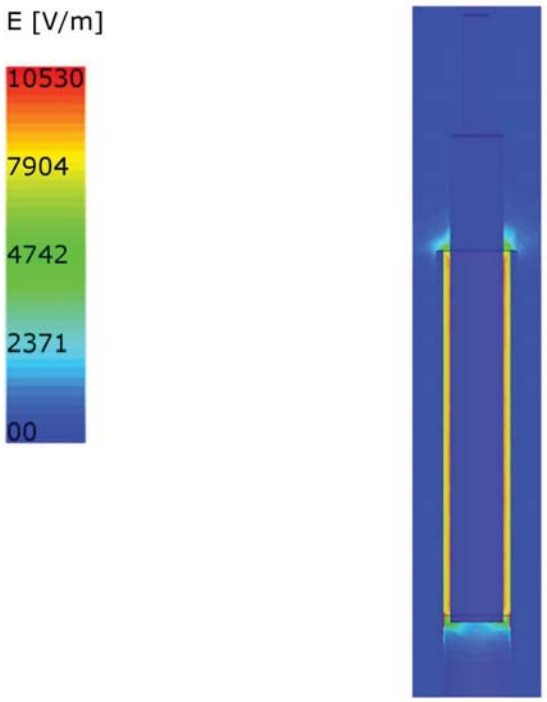

Figure 4.9: Electric field distribution of design C in the longitudinal cross-section calculated using the FEA software Ansys Maxwell

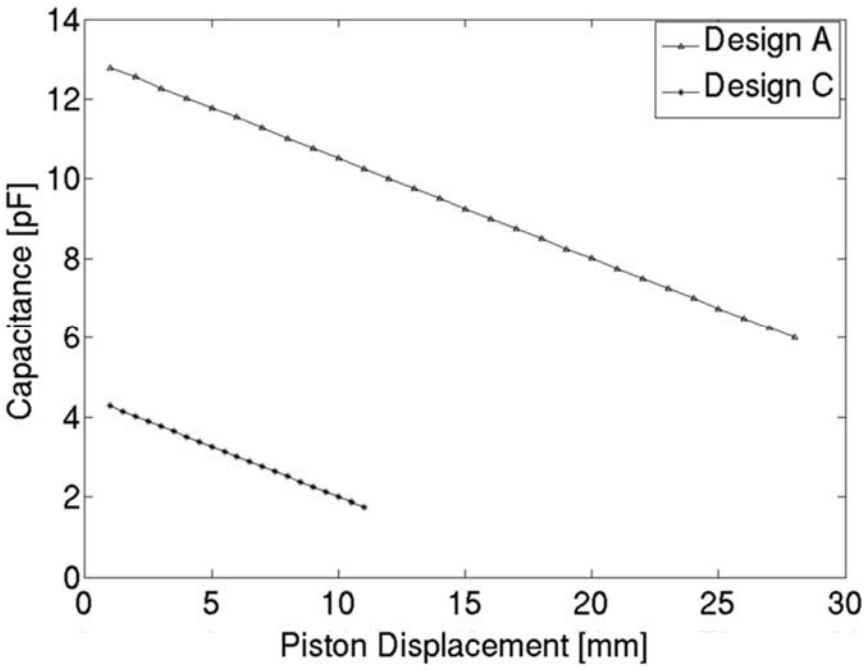

Figure 4.10: Plot of capacitance against displacement for design A and C calculated using the FEA software Ansys Maxwell

4.2.2.3 Investigation of the influence of mechanical tolerances

In order to better understand the behavior of the real system, possible mechanical reasons that can cause a deviation of the behavior of the sensing system from the ideal case have been investigated. Typical mechanical tolerances that can affect the hydraulic cylinder´s performance are: an eccentric position of the rod and its misalignment with respect to the longitudinal axis of the barrel.

Both cases have been investigated by FEA simulations, in order to observe the change in the electric field distribution and in the characteristic of the sensor.

Figure 4.11 shows design A with an eccentricity of the rod of 0.2 mm, which is the maximum manufacturing tolerance set for the designed prototype. Unlike in Figure 4.6 the radial distribution of the electric field is not homogeneous. The electric field is stronger in the parts where the gap between the inner and outer electrode is smaller.

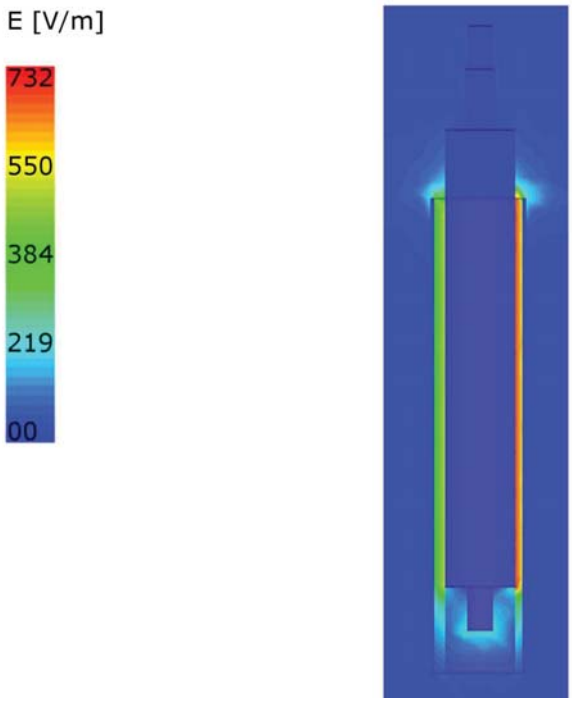

Figure 4.11: Electric field distribution of design A in the longitudinal cross-section, where the rod is eccentric; calculated using the FEA software Ansys Maxwell

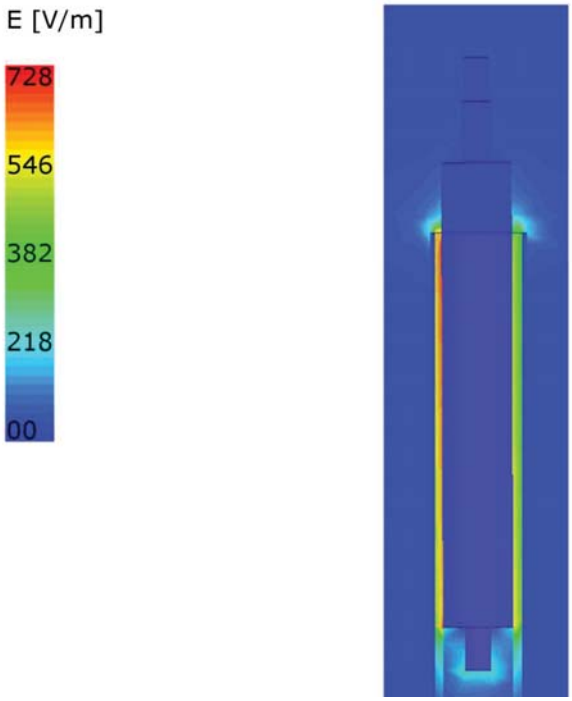

Figure 4.12: Electric field distribution of design A in the longitudinal cross-section, where the rod is inclined respect to the barrel longitudinal axis; calculated with Ansys Maxwell

A similar behavior of the electric field can be observed in Figure 4.12, which shows the asymmetric electric field distribution of a cylinder in which the rod is misaligned with respect to the longitudinal axis of the barrel. The rod in the model has been tilted 0.2 degrees, which is the tolerance of the designed prototype.
Figure 4.13 shows the capacitance against displacement characteristic calculated for the ideal case, the eccentric rod and the inclined rod case. The graph shows that the characteristic of the eccentric rod remains linear, even though its slope changes in comparison to the ideal case.

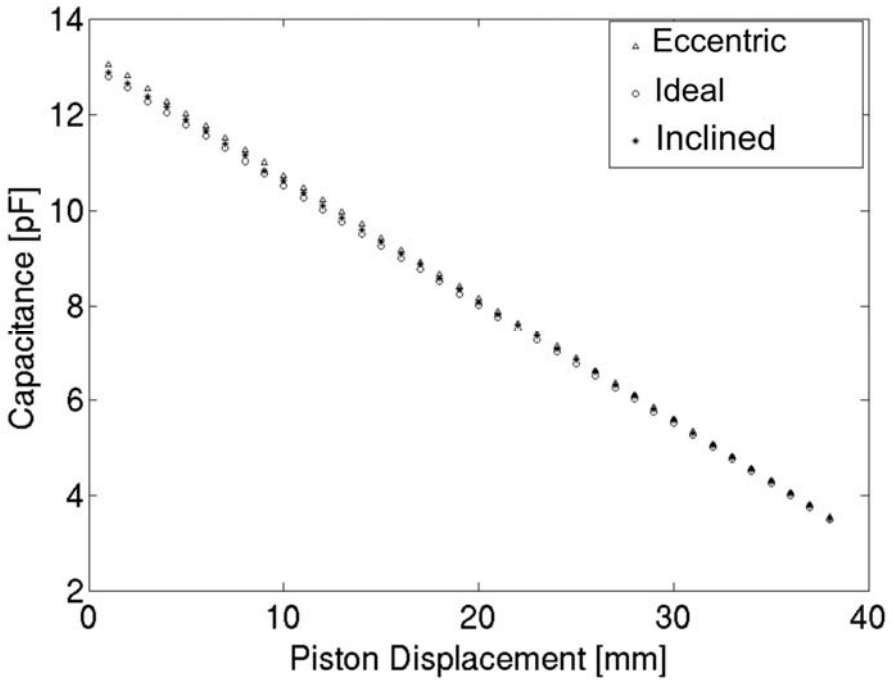

Figure 4.13: Capacitance against displacement for design A, in the ideal, eccentric, and in the inclined case; calculated using the FEA software Ansys Maxwell

When the rod is inclined with respect to the longitudinal axis of the barrel, a non-linear characteristic is expected. In fact, the extension and retraction movement of the rod cause a continuous change of the effective distance between the rod and the barrel, whereas for the eccentric rod case the movement of the rod does not change this distance. However, only a variation of the slope can be observed,

while the characteristic remains linear. This is because the rod´s tilt is so small that the non-linearity is negligible.

The simulation shows that neither the eccentricity nor the inclined rod have a severe influence on the sensor's usability. In both cases only the curve slope changes, while the characteristic remains linear. However, it was shown that the two effects influence the sensor´s performance and, therefore, their reduction is desirable. Additionally, the simulation proves that the sensor´s performance is not severely affected by the fringing effect over the simulated stroke.

The results of the FEA simulation in this chapter confirm the validity of the chosen sensor´s concept for the measurement of displacement in a micro and a mini hydraulic cylinder. As the linearity and the sensitivity are not affected by the rescaling and parts of the hydraulic cylinder can be used as sensor themselves, this sensor´s concept is a suitable choice for the control of the position of the laparoscopic instruments´ tip.

5 Sensor characterization and model validation

Given the positive results of the FEA simulation in chapter 4, the validity of the sensor concept in this chapter will be proved experimentally.

Tests will be run with two different hydraulic cylinders: one with the dimensions of design A and the other with the dimensions of design C (see Table 3 in chapter 4.2.1 for the cylinder sizes). The results of the sensor´s characterizations will be compared with the data from the simulation to check their correspondence.

For both designs it will be experimentally proven that non-linearity due to fringing effect is negligible along the stroke of interest, as shown in the simulations. Moreover, the precision of the sensors will be determined and the impact of tolerances in the mechanical design on the sensor´s characteristics will be analyzed.

Design A and C have different dimensions but the same ratio between the diameters of the outer and the inner electrode. Therefore, by characterizing both of them, it will be analyzed if the sensitivity is affected by the radial rescaling of the cylinder.

The experimental results presented in this chapter have already been published in (Comella et al. 2017).

5.1 Experimental hardware and software setup

Figure 5.1 shows the test setup for the characterization of the coaxial cylindrical capacitive sensor. For a better understanding of the connection between the elements of the test setup, Figure 5.2 displays its schematic.

The test setup is composed of the neMESYS pump, the hydraulic cylinder, whose barrel and rod are used for the coaxial cylindrical capacitive sensor, an optical

encoder, a PC, the FDC1004 and the electronics for the data acquisition.
The LabVIEW software running on the PC controls the movement of the neMESYS mid pressure syringe pump from Cetoni. The Pump produces a hydraulic pressure that moves the piston of the hydraulic cylinder. The FDC1004 by Texas Instruments acquires the signal from the coaxial cylindrical capacitive sensor and converts it into digital information, which is sent to the computer via an Arduino DUE microcontroller board. An optical linear encoder is used to calibrate the coaxial cylindrical capacitive sensor and, as a reference, to double-check the measurements of the newly developed sensor.

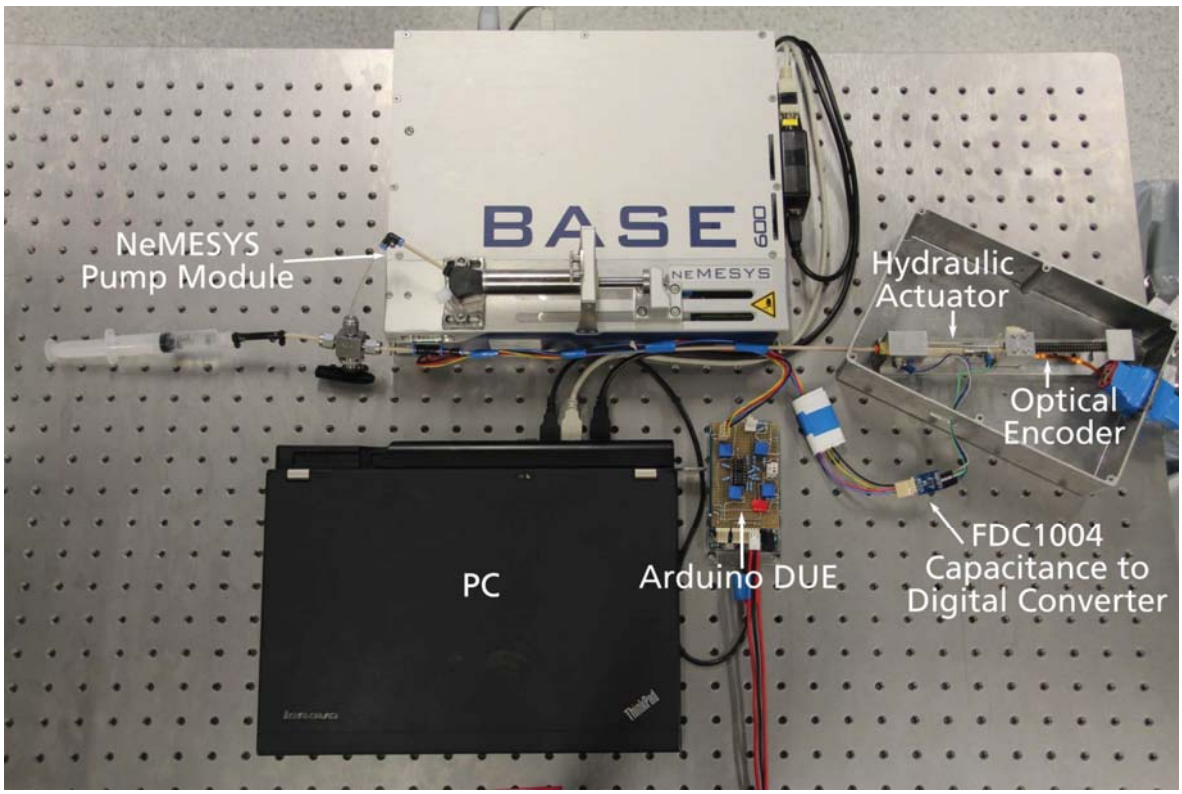

Figure 5.1: Picture of the experimental setup for the sensor characterization

The elements of the test setup are described in the following bullet list in detail, to make the experimental tests understandable, repeatable and to allow the estimation of the precision with which the hydraulic cylinder can move and the coaxial cylindrical capacitive sensor can measure its displacement.

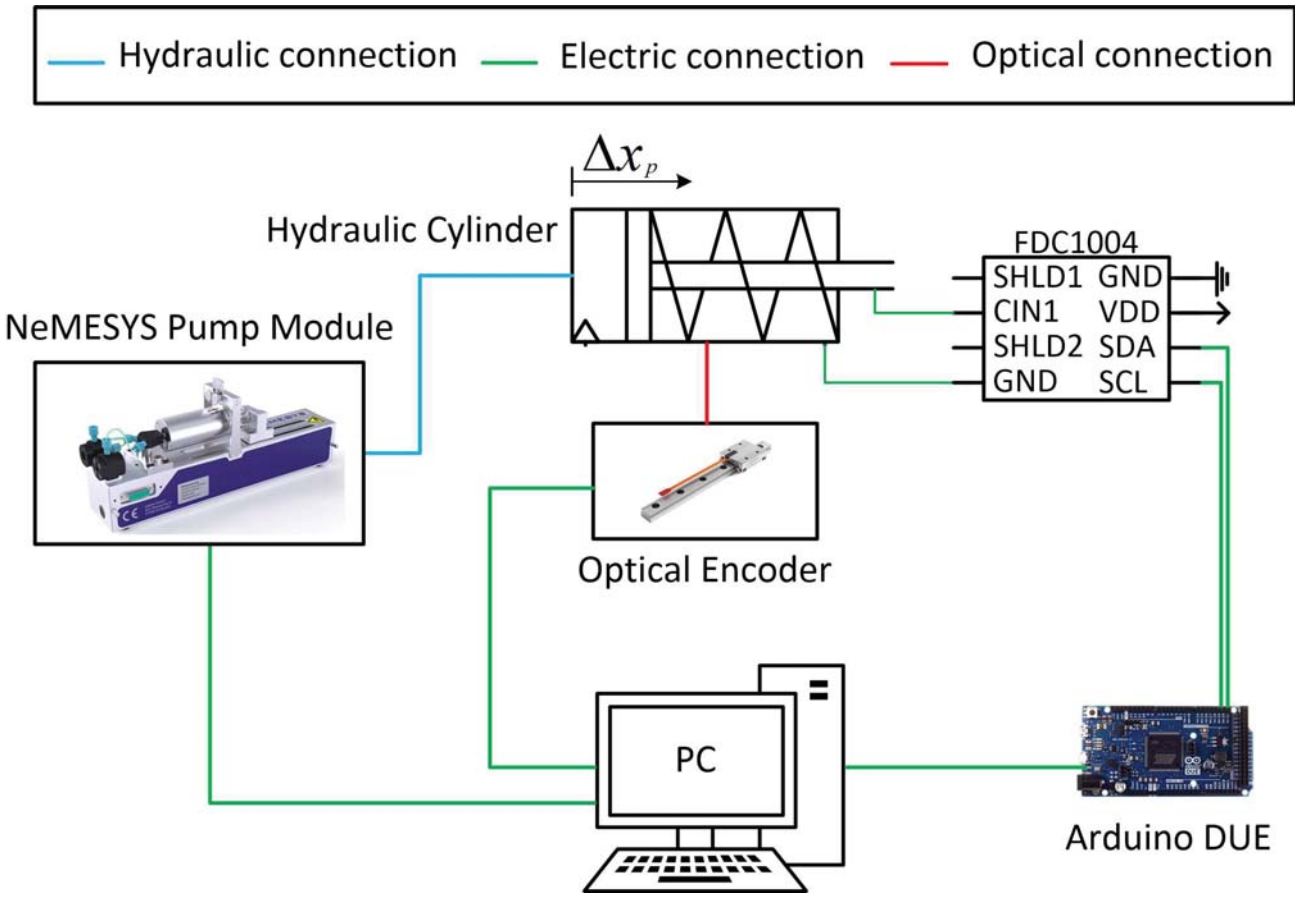

Figure 5.2: Schematic of the test setup for the sensor´s characterization

- The **neMESYS pump** is a syringe pump of Cetoni. For the experiment, a stainless steel syringe of 2.5 ml, 7.976 mm internal diameter and 50 mm maximum stroke is used. The combination of the drive unit of the pump and of the chosen syringe ensures an accuracy of 3.4 nl/min.
- The **FDC1004** (Texas Instruments 2015) is a low power, low cost and high resolution capacitance to digital converter. It has a full scale range of +/-15 pF with a resolution of 0.5 fF.

  The FDC1004 allows a sampling frequency of 100 Hz which covers the required bandwidth for the sensor dynamics. In non-operative condition the chip tolerates temperatures up to 150 ˚C. This enables its disinfection and sterilization. As previously discussed, the cleaning procedures imply the use

of liquid. Therefore, not only the electronics but also the sensing system must be encapsulated into a hermetic packaging.

This chip was also chosen, because it includes shield drivers for sensor shields, which reduce electromagnetic field interferences and enhance the accuracy of the measurements. The chip measures the capacitance between the input pin CIN and ground. Therefore, any parasitic capacitance on the signal path would also be measured. The SHLD pin is an output driven by the same potential and has the same waveform as the CIN pin. Therefore, the conductors attached to the pins CIN and SHLD have the same potential and there is no electric field between them. Any capacitance between them does not affect the measurements. That is why the SHLD signal, as shown in Figure 5.3, is used to shield the wires and for the faraday cage in which the sensor is placed. Moreover, Figure 5.3 shows the electrical connections between the hydraulic cylinder, the FDC1004 and the Arduino DUE microcontroller board, used to transmit the data to the computer interface.

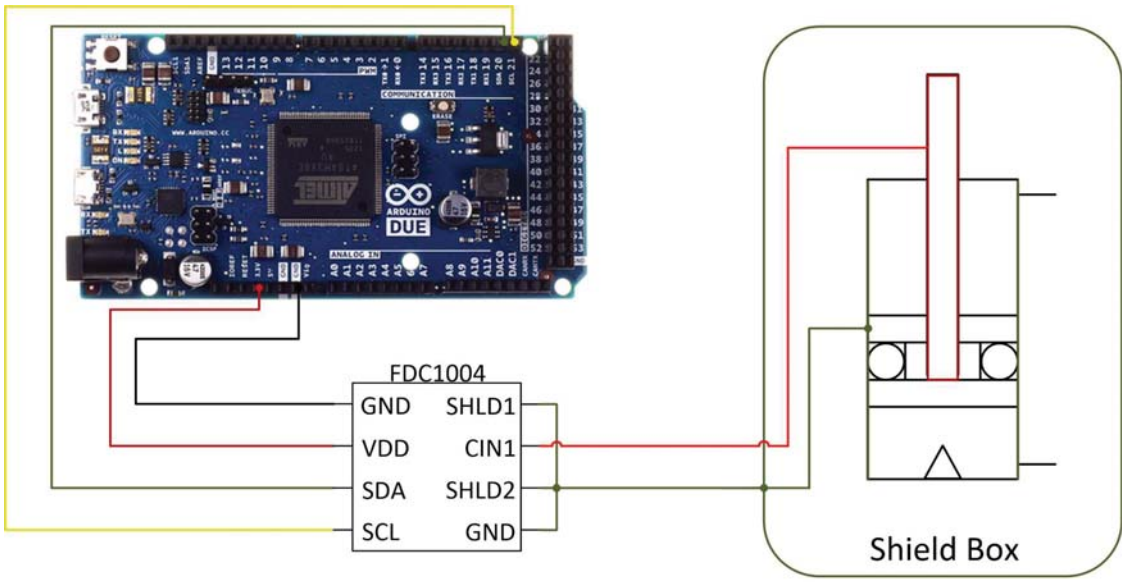

Figure 5.3: Schematic of the electrical connections between the microcontroller board, the Texas instrument´s chip, and the hydraulic cylinder

- The **optical encoder** MINISCALE PLUS of Schneeberger, shown in Figure 5.4, is a displacement sensor selected for its high precision of +/-5 µm. As this sensor is used as a reference for the measurements obtained and to calibrate the cylindrical capacitor, it must have a higher precision than the newly developed sensor. The encoder output signal is processed by the USB-counter 026 of Heilig and Schwab and sent to the computer.

Figure 5.4: Optical encoder MINISCALE PLUS from Schneeberger

- The hydraulic cylinder is shown in Figure 5.5.

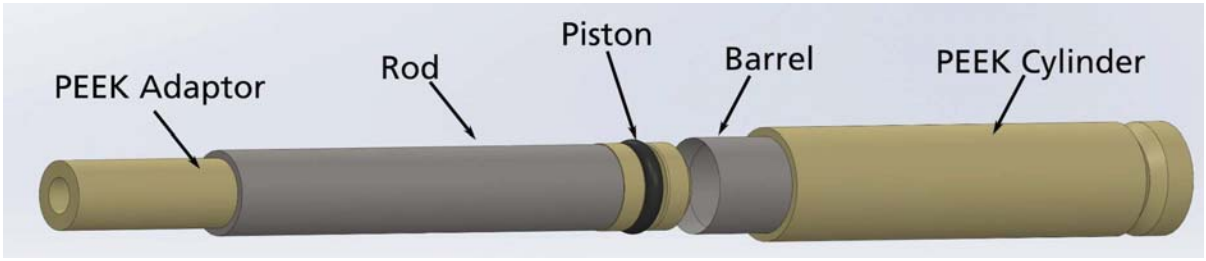

Figure 5.5: Hydraulic cylinder used for the sensor´s tests. Conductive parts are in grey; non-conductive material are in beige

The figure shows its geometry and gives additional information about the material used to build the cylinder: The conductive parts manufactured in stainless steel are colored in gray, the isolating parts made of the synthetic material PEEK are in beige. The only two conductive parts of the cylinder are the rod and the barrel, whereas the piston and the barrel base are made

of PEEK. This guarantees the electrical isolation between the inner and the outer electrode of the coaxial cylindrical capacitive sensor.

The hydraulic cylinder is mounted on a test rig to hold it. Figure 5.6 shows the rig built for the mini hydraulic cylinder (design A), and Figure 5.7 shows the rig for the micro hydraulic cylinder (design C). The design of both hydraulic cylinders is the same.

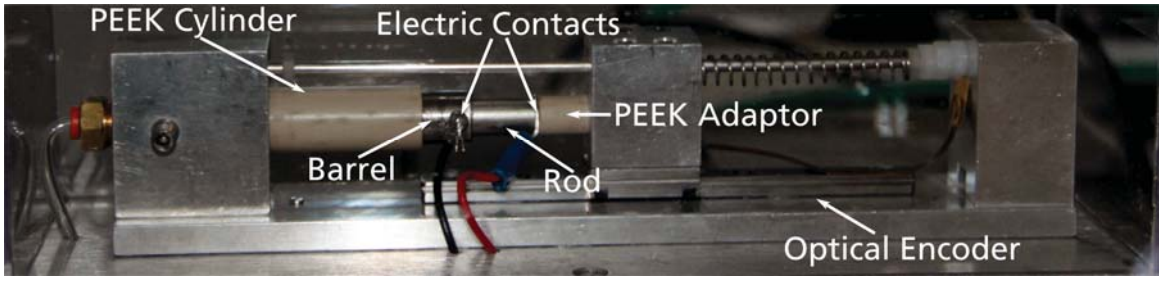

Figure 5.6: Test rig used for experiments on the mini hydraulic cylinder

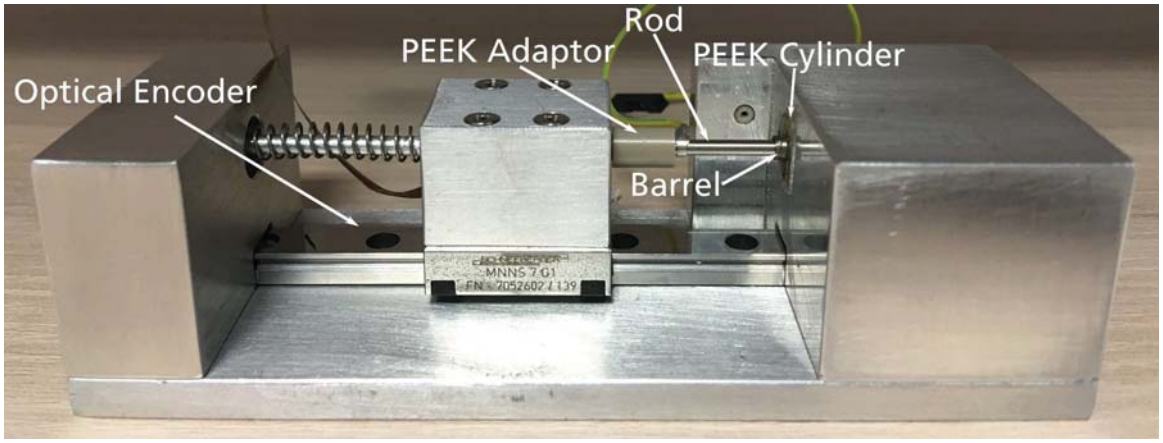

Figure 5.7: Test rig used for experiments on the micro hydraulic cylinder

The test rigs are built of stainless steel, because this material offers mechanical stability and smaller tolerances on the part´s dimensions than a rig made entirely of plastic. This means that the electrical isolation between the electrodes and the rig must be guaranteed. Therefore, as seen in Figure 5.5, the outer electrode is surrounded by a PEEK cylinder and the rod is connected to the test rig via a PEEK adaptor.

One of the challenges of the rig design was to find a suitable method to attach the electrical contacts onto the electrodes. The electrical contacts should be strong enough to withstand the constant movement of the cylinder and not generate noise that would interfere with the circuit used for the measurement of the capacitance.

It was found that repeatable and precise measurements are obtained when soldering the wire to the barrel and using a mechanical contact for the rod. The wire was connected to a crimping plug like the one shown in Figure 5.8(b). The electrical connection was obtained pressing the crimping plug between the rod and the PEEK adaptor, used to mount the rod on the rig as shown in Figure 5.8(a).

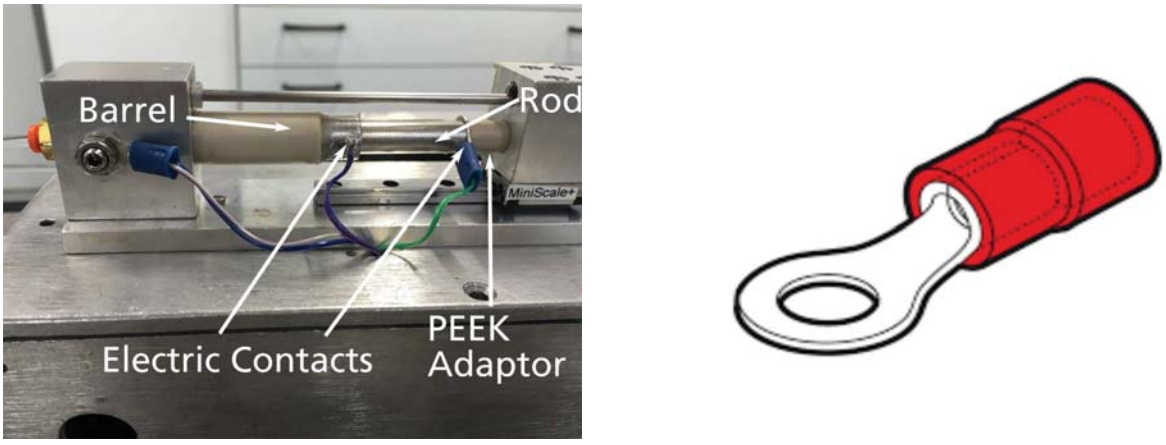

(a) **(b)**

Figure 5.8: (a) Electrical contacts shown on the test rig (b) Crimping plug used for contacting the rod

The soldered contact is an acceptable solution for the barrel, as it is a static element. On the contrary, the rod is a dynamic element, which moves back and forward in accordance with the liquid being pumped in and out of the piston. That is why a mechanical contact is to be preferred to a soldered one which can easily break due to the movement.

5.2 Method

Measurement tests were planned to characterize the sensor integrated on the mini and the micro hydraulic cylinder, in order to prove that the sensor concept is suitable for the measurement of the position of the laparoscopic instruments´ tip on an experimental level and fulfills the requirements given in chapter 2.5.

5.2.1 Characterization of the sensor-actuator system

In order to characterize the coaxial cylindrical capacitive **sensor, integrated on the mini hydraulic cylinder**, four measurement series were carried out. In every series the measurement setup shown in Figure 5.2 was programmed to obtain increments of the syringe´s volume corresponding to a theoretical hydraulic cylinder displacement Δx_p of 1 mm, 0.5 mm, 0.05 mm, and 0.025 mm. For the direction of Δx_p see Figure 5.2. The step of 0.05 mm was chosen to test the sensor in the range of the precision specified in Table 1. The smaller step of 0.025 mm was chosen to check if the sensor performance can be guaranteed also for values smaller than the specification. The step of 1 mm and 0.5 mm were chosen to prove the behavior of the sensor for bigger steps; which are more likely to be used during real application of the instrument. Conducting the experiments for decreasing step sizes, permitted the identification of the minimum measurable displacement.

No mechanical stop was used for the piston to characterize the sensor, other than in Sumali et al. 2003 and Volder et al. 2008, as later there will be no space for it in the laparoscopic instrument. This allowed the observation of the sensor´s performance in conditions close to real use. However, this meant a difference between the experiments´ starting positions.

A measurement range of circa 30 mm was chosen for increments of Δx_p= 1 mm

and Δx_p= 0.5 mm, a range of 10 mm for Δx_p= 0.05 mm and Δx_p= 0.025 mm. Every measurement series was repeated for ten motion cycles to test their repeatability. Every cycle consisted of an extension and a retraction movement of the cylinder. During those cycles, the capacitance measurements were sampled at every step and recorded together with the corresponding displacement measurements from the optical encoder.

To prove the performance of the coaxial cylindrical capacitive **sensor, integrated in the micro hydraulic cylinder**, 500 measurement samples were taken, moving the piston for 30 motion cycles. Every cycle consisted of an extension and a retraction movement of the cylinder. During those cycles, the capacitance measurements were sampled every step and recorded together with the corresponding displacement measurements by the optical encoder. For these measurements the setup in Figure 5.2 was programmed to deliver liquid volume increments corresponding to a theoretical hydraulic cylinder displacement Δx_p= 1 mm. Due to the stick slip effect, in this case it was not possible to observe the displacement of the rod in regular steps.

For both the mini and the micro sensor, the correspondence between simulation and experimental results were analyzed. It was investigated, whether the fringing effect is also negligible in reality and how mechanical tolerances affect the measurements.

5.2.2 Statistical analysis

The collected measurements were statistically analyzed using an ordinary least squares regression analysis (OLS) (Groß 2003).

The ordinary least square regression analysis is a statistical technique used to analyze, how a response variable, which is recorded in a desired interval, changes

in relation to an independent variable. The recorded data are modelled with a linear function, which can be used for data analysis and prediction of the system response. It can be applied under the assumptions of correct specifications, strict exogeneity, spherical error, and normality of error distribution (Groß 2003).

The method was chosen because it permits to model linear relations when the variables are continuous (Hutcheson et al. 1999), fitting the thesis case. It gives an estimation of the repeatability and allows to calculate easily the sensor precision (Taylor 1997), the desired value of which is specified in Table 1.More details about the calculation of the sensor precision can be found in the next subparagraph. One more reason for which the OLS method was preferred among the others is that by using the graphical method, it is possible to prove that the model assumptions such as linearity and constant variance are fulfilled (Hutcheson et al. 1999).

Given the independent variable x_p, which is the piston´s displacement in our case, and the response variable C, the capacitance, the first order polynomial $C = a \cdot x_p + b + \varepsilon$ was used to model the relationship between them, where ε is the error variable, which accounts for the discrepancy between the measured values and the predicted outcomes. b is the intercept and it is the predicted value of C when x_p is equal to 0. a is called the regression coefficient and is the slope of the curve. Its value corresponds to the sensitivity of the sensor.

The values of a and b were chosen such that the sum of squares of the difference between the measured data and the predicted responses by the linear function were minimized.

Two more relevant parameters were taken into account for the statistical analysis of the sensor performance: the Root Mean Square Error (RMSE) (Papoulis 1991) and the coefficient of determination R-squared (Groß 2003).

The RMSE is a measure of the accordance of measured and predicted values with the OLS model, indicating how well the model predicts the measurements. It can be calculated with the following formula

$$RMSE = \sqrt{\frac{\sum_{t=1}^{n}(\hat{C} - C)^2}{n}}, \tag{14}$$

where $\hat{C}$ is the model´s value of the capacitance, C the corresponding measured value and n the number of samples. The RMSE was used in this case to measure the deviation of the data from the model.

The coefficient of determination R-squared was also used to provide a measure of how well the model fits the measured data. It is defined as

$$R^2 = 1 - \frac{\sum_{t=1}^{n}\left(C - \hat{C}\right)^2}{\sum_{t=1}^{n}(C - \bar{C})^2}, \tag{15}$$

where $\hat{C}$ is the model´s value of the capacitance, C the measured value, $\bar{C}$ the average of the measured values and n the number of samples. It can take values between 0 and 1, where 1 indicates a perfect fit between model and measurements whereas 0 the opposite.

5.2.3 Sensor precision

From the measurement series, using the OLS parameters, the precision of the displacement sensor was deduced. The precision can be defined as the spread of measured values around the average measured value and it identifies the smallest interval that the sensor can measure (Pisani 1999).

For this estimation it was assumed that the displacement x_p is a function of the capacitance C and that the capacitance measurement is subjected to random fluctuations. It followed that the uncertainty on the displacement can be calculated according to Formula (16) (Taylor 1997).

$$\delta x_p = \left|\frac{dx_p}{dC}\right| \delta C, \tag{16}$$

where δC is the standard deviation of the capacitive value, hence the distance of the measured value from the average value of the measurements in the corresponding point and $\left|dx_p/dC\right|$ is the slope of the plot displacement against capacitance. Given that the statistical analysis was done under the assumption that the measurements are normally (or Gaussian) distributed, it followed that their average value corresponds to the best estimate.

5.2.4 The analysis of the mechanical hysteresis

During the measurement series, it was observed that the starting and stopping point of the piston changed every cycle and that the retraction and extension characteristic did not overlap, so a test was made to understand if this problem should be attributed to the mechanical hysteresis or to a sensor fault. In order to examine the problem, the optical encoder was used to measure the displacement of the cylinder, and the encoder embedded into the neMESYS pump was used to determine the volume of the liquid pumped into the hydraulic cylinder. The measurements of the liquid pumped in the cylinder against the displacement measurements were recorded and plotted. If the characteristic of the cylinder displacement showed the same behavior also when acquired with the two state of the art sensors, the fault of the coaxial cylindrical capacitive sensor could be excluded.

5.2.5 The wire length experimental test

The physical size of the laparoscopic instrument placed a limitation on the size of the chip used to transduce the capacitance value into a digital signal. The Texas Instruments´ FDC1004 has the smallest housing on the market, which is

nonetheless too big to be integrated on the instrument tip. It followed that the chip could only be integrated into the handle of the instrument and connected to the capacitive sensor by cables. Longer cables change the capacitance of the system. For this reason, an examination was necessary to estimate in which way the cable length affects the measurements. Therefore, the capacitive values and the corresponding displacements were recorded connecting the test rig and the FDC1004 with cables of various length. Experiments were made in which the length of the cables was increased by 165mm, 330 mm and 495 mm with respect to the 100 mm cable used for characterizing the sensor.

An increase of capacitance with the cable´s length was expected, as they can be considered as a form of transmission line (Ramo et al. 2005). When a voltage is applied, an electric field occurs between the conductors. They separate charges and, therefore, each length of a cable has a capacitance. Moreover, the flowing current generates a magnetic field around a conductor, hence cables also have an inductance. It follows that the cables can be modelled as a series of LC elements for each infinitesimally small section dz, as shown in Figure 5.9.

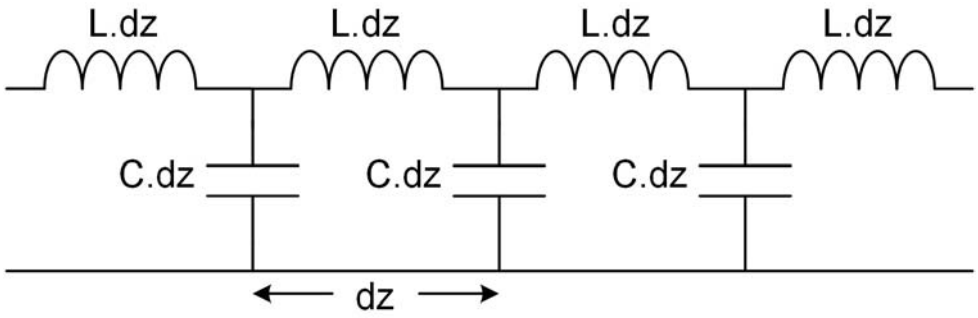

Figure 5.9: Cable represented as a series of inductors and capacitors

5.3 Results and discussion

5.3.1 Characterization of the sensor-actuator system

Figure 5.10 to Figure 5.13 show the characteristics of the coaxial cylindrical capacitive **sensor, integrated in the mini hydraulic cylinder**. The plots were obtained moving the rod in step increments of Δd = 1 mm, Δd = 0.5 mm, Δd = 0.05 mm, Δd = 0.025 mm respectively, and sampling the corresponding capacitance values.

For a good understanding of the graphs, it must be pointed out that the displacement´s range of the experiments shown in Figure 5.12 and Figure 5.13 is smaller in comparison to the one used for the experiments in Figure 5.10 and Figure 5.11. That is the reason why the standard deviation appears bigger in the last two graphs, even though it is the same for all the experiments.

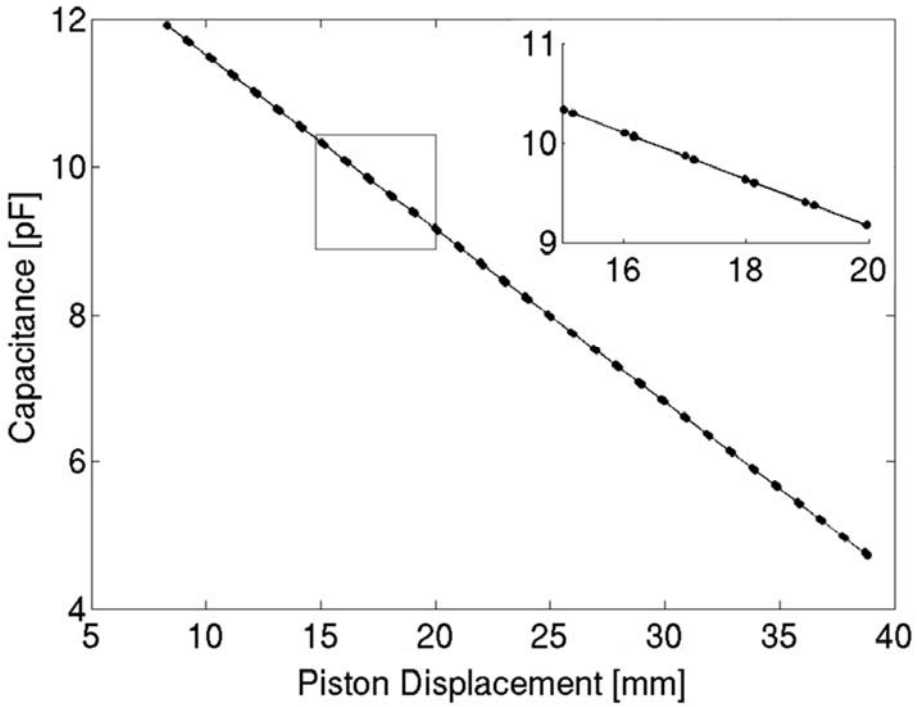

Figure 5.10: Capacitance against displacement of the mini hydraulic cylinder for 1 mm position´s increments taken over ten motion cycles Top right: detailed view of the part highlighted with the square

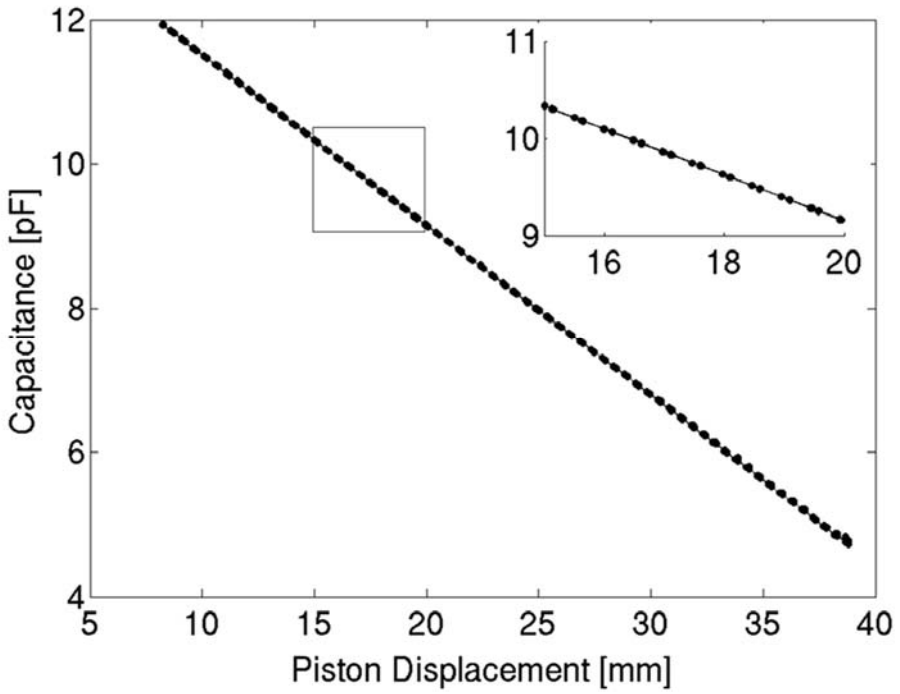

Figure 5.11: Capacitance against displacement of the mini hydraulic cylinder for 0.5 mm position´s increments taken over ten motion cycles **Top right:** detailed view of the part highlighted with the square

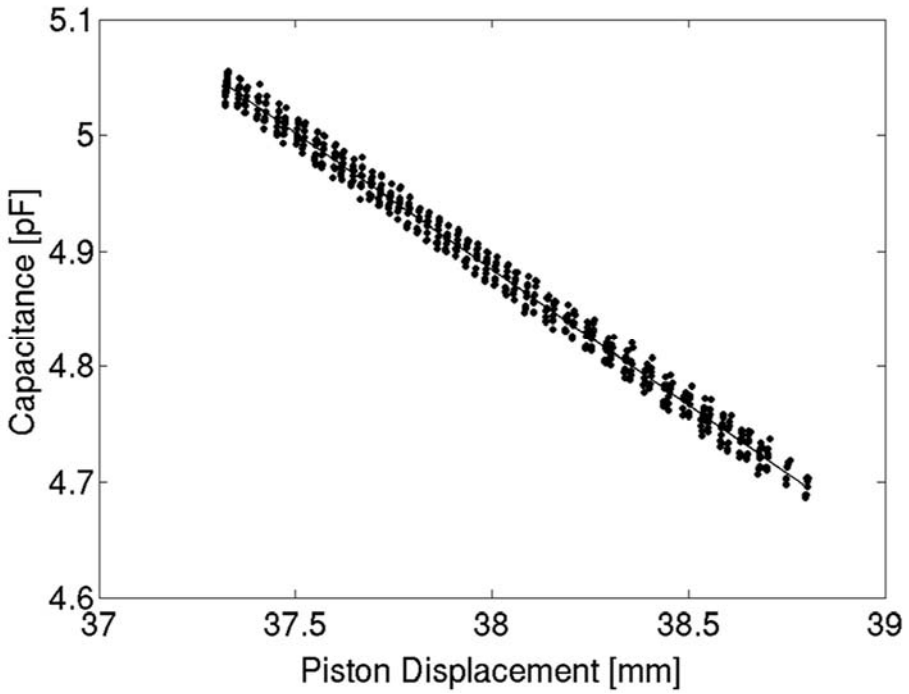

Figure 5.12: Capacitance against displacement of the mini hydraulic cylinder for 0.05 mm position´s increments taken over ten motion cycles

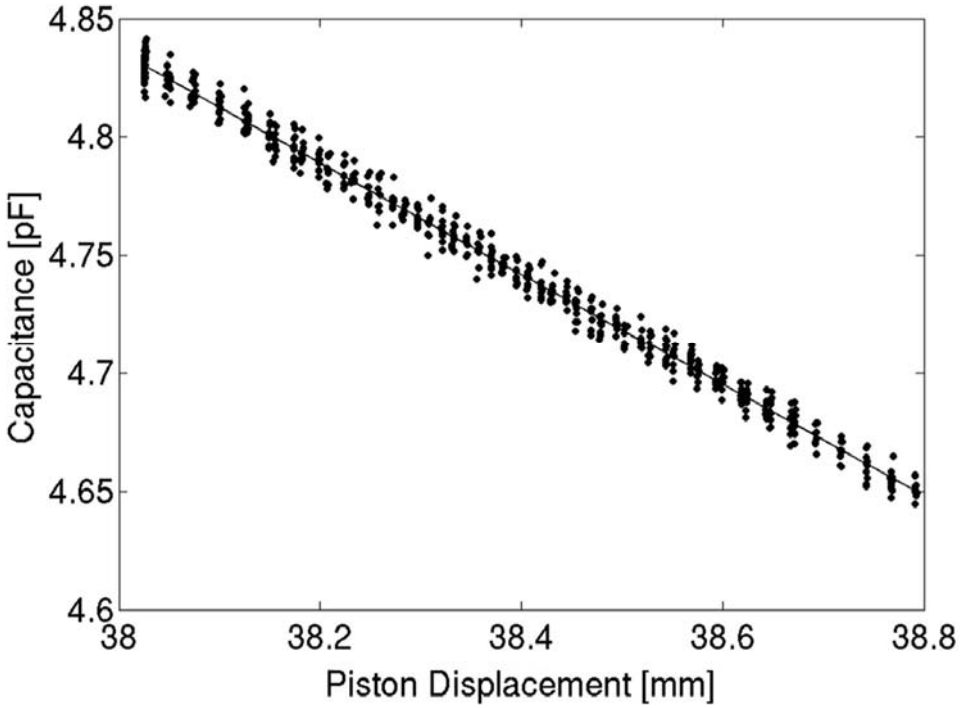

Figure 5.13: Capacitance against displacement of the mini hydraulic cylinder for 0.025 mm position´s increments taken over ten motion cycles

It can be observed that all the characteristics show a linear behavior. Moreover, in the top right of Figure 5.10 and Figure 5.11 the part of the characteristic enclosed into a rectangle is zoomed in. The zoomed graph shows that the measurements for each designated position are concentrated into two clouds of points which almost overlap. This is not observed for the characteristic in Figure 5.12 and Figure 5.13. It was hypothesized that a mechanical hysteresis caused this behavior. More details about this aspect follow in chapter 5.3.5.

One further observed aspect is that for the measurement test in Figure 5.13 a step of precisely 0.025 mm was never obtained. Moreover, the piston did not move for several steps when, in the beginning of the test, it had to leave its static position and when it changed its direction of movement. The reason for this behavior was that for a step of 0.025 mm the system was not rigid enough.

Therefore, the pressure built to move the cylinder of this distance was partially absorbed by the flexibility of the system, e.g., extension of tubes.

Figure 5.14 shows the characteristic of the coaxial cylindrical capacitive **sensor, integrated into the micro hydraulic cylinder**.

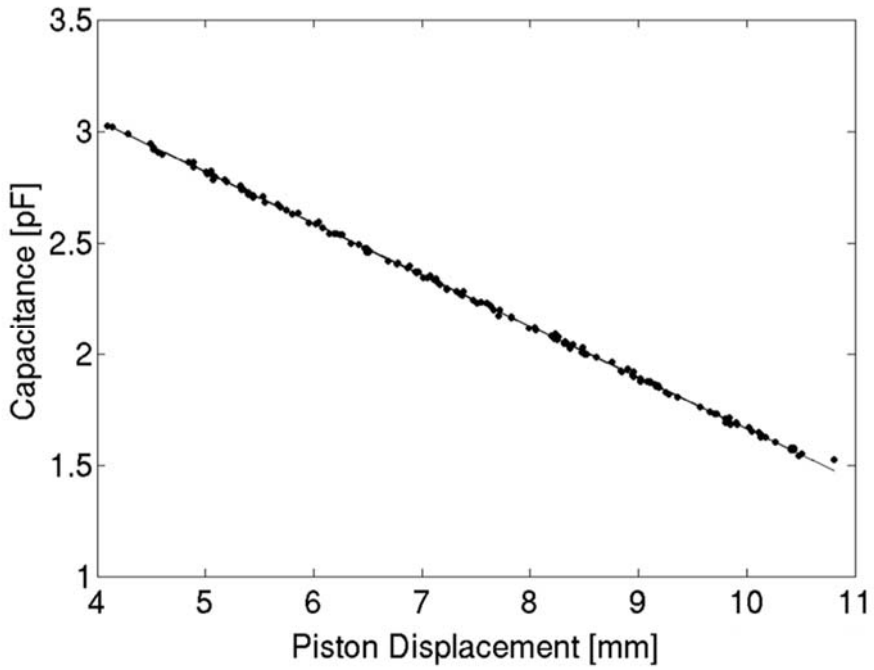

Figure 5.14: Plot of capacitance against displacement of the micro hydraulic cylinder

It can be observed that the behavior of the characteristic is linear like in the experiments run with the coaxial cylindrical capacitive sensor integrated on the mini hydraulic cylinder. Other than in the latter case, the distribution of the measurements is not homogenous along the curve. In both experiments, with the micro and the mini hydraulic cylinder, the setup in Figure 5.2 was programmed to obtain piston steps of 1 mm. The movement of the micro hydraulic cylinder, however, varied for every step because of the stick slip effect.

5.3.2 Statistical analysis

The ordinary least square regression analysis (OLS) was used to analyze the experimental results statistically. Linear regression models were calculated for the

experimental data shown in Figure 5.10 to Figure 5.13, and the corresponding OLS parameters are shown in Table 4.

Table 4: Results of the Ordinary Least Square regression analysis for the tests run on the mini hydraulic cylinder

Increment [mm]	b [pF]	a [pF/mm]	R-squared	RMSE [pF]
1	13.8730	-0.2356	1.0000	0.0044
0.5	13.8685	-0.2358	1.0000	0.0076
0.05	13.8406	-0.2357	0.9922	0.0091
0.025	13.7778	-0.2353	0.9921	0.0047

The least square regression analysis confirmed the linear behavior of the characteristics, as the calculated linear regression models matched the measured data with an R-squared of circa 1 and an RMSE of 0.00645 pF on average.

The parameter a, which is the slope of the linear regression model and corresponds to the sensor sensitivity, has the same value in all the four tests. The values of the parameter b are close to each other as well. It follows that the correspondence among the linear regression models of the experiments is good, and consequently that the measurements´ results are repeatable.

Table 5 shows the OLS parameters calculated from the experimental data in Figure 5.14. The OLS analysis confirmed also in this case the linear behavior of the characteristic as the parameter R-squared is approximately 1, indicating a good fitting between OLS model and measured data.

Table 5: Results of the statistical analysis for the micro hydraulic cylinder

Increment [mm]	b [pF]	a [pF/mm]	R-squared	RMSE [pF]
1	3.9738	-0.2311	0.9995	0.0091

Comparing the results of the OLS analysis in Table 4 and Table 5, it can be observed that the sensor´s behavior is not affected by the miniaturization. Both the sensor integrated on the mini hydraulic cylinder and the one integrated on the micro hydraulic cylinder present a linear behavior and the slope of the fitting curve *a* is the same for both of them. Therefore, it can be concluded that the sensitivity of the coaxial cylindrical capacitive sensor is not affected by the radial rescaling of the cylinder. This means the sensing method can be integrated on cylinders of different sizes. For this reason, it can be adapted to all the hydraulically driven laparoscopic instruments, not depending on their dimensions.

5.3.3 Sensor precision

The sensor precision was calculated using formula (16). For the sensor integrated on the mini hydraulic cylinder the data in Table 4 was used. $\left|dx_p/dC\right|$ was substituted with the inverse of the parameter a, and δC with the average of the RMSE of the capacitance measurements. For the sensor, integrated on the micro hydraulic cylinder, the data in Table 5 was used. $\left|dx_p/dC\right|$ was substituted with the inverse of the parameter a and δC with the RMSE.

The RMSE measures the difference between the value predicted by a model or an estimator and the value actually observed. The reason why the RMSE was used in place of the standard deviation is that the two values correspond under the assumption that no systematic error occurs. In this case, the model value provides the best estimate.

From the calculation it followed that the sensor system, integrated on the mini hydraulic cylinder, is able to measure with an average precision of ±27 µm, while a precision of ±38 µm was estimated for the sensor, integrated on the micro hydraulic cylinder. The lower precision in the second case was due to increased

leakage of the micro hydraulic cylinder. This aspect can be improved by changing the mechanical design of the cylinder, which is not the purpose of this thesis.

5.3.4 Comparison of experimental and simulation results

Figure 5.15 and Figure 5.16 show in one graph the characteristics measured on the mini and the micro hydraulic cylinder, obtained with the experimental measurements, the FEA simulations and formula (12). In both cases, all the curves have a linear behavior along the stroke of interest and a good correspondence is observable between the sensor characteristic calculated with the FEA simulation and the curve of the measured data. The linearity confirms that the effect of the fringing effect is negligible over the simulated stroke, also for the experimental measurements. The difference between the two curves´ slopes can be addressed by the mechanical tolerances resulting from the manufacturing of the test rig, because of which the alignment between the two electrodes is not perfect. This behavior matches the forecast of the FEA simulation shown in Figure 4.13.

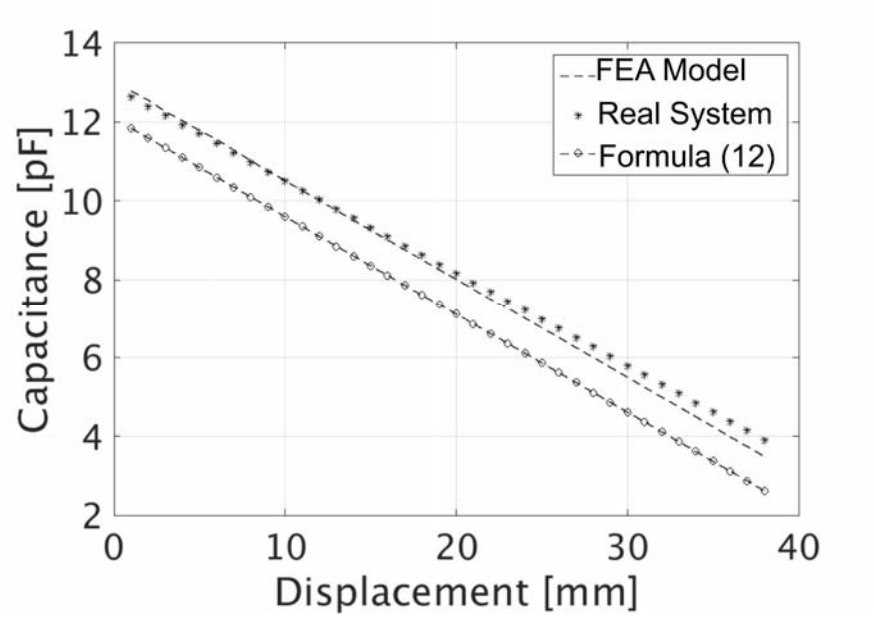

Figure 5.15: Comparison between the experimental results, the FEA model, and the analytic model in formula (12) for the mini hydraulic sensor.

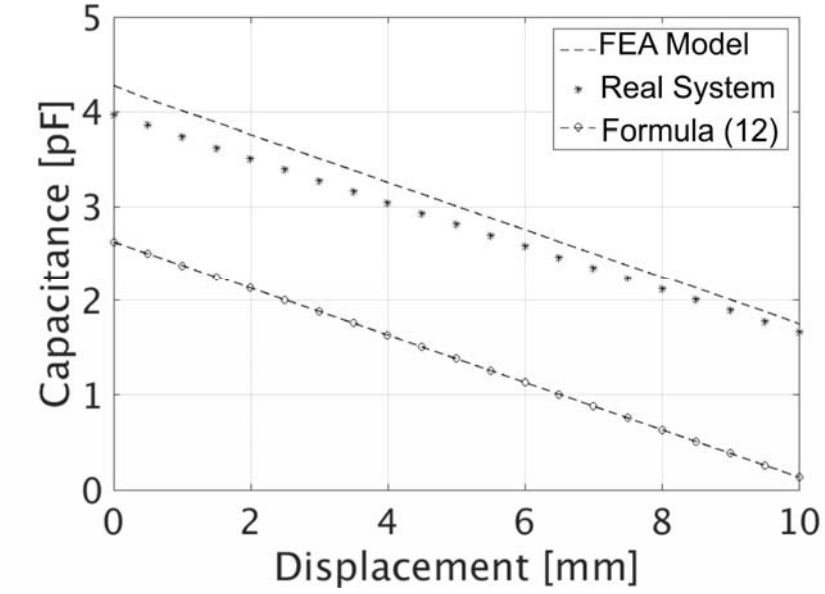

Figure 5.16: Comparison between the experimental results, the FEA model, and the simplified formula (12) for the micro hydraulic sensor

Furthermore, the experimental characteristic of the sensor and the FEA simulation curve have higher values than those predicted by formula (12). This simplified equation, showing the relationship between capacitance and displacement in the coaxial cylindrical capacitive sensor, was used in chapter 4 for a first analysis of the sensor solution concept. The formula was obtained by neglecting both the boundary effects of the electric field and the material characteristics of the electrodes. This is the reason for the lower capacitive values of this curve in comparison to the results obtained with experimental tests and FEA simulations.

5.3.5 Analysis of the mechanical hysteresis

It was hypothesized that a mechanical hysteresis is the cause of the aggregation of the measurements into two clouds of points in Figure 5.10 and Figure 5.11. Moreover, it is observed that all the measurements in the upper clouds correspond to the retraction movements and the measurements in the lower clouds correspond to the extension movements.

In order to get a better understanding of this phenomenon and to prove that it was caused by a mechanical hysteresis and not by a malfunctioning of the sensor system, a further experiment was executed.

For the experiment, the piston was moved over a period of four motion cycles, each consisting of an extension and a retraction movement. During these cycles, the piston´s displacements against the volumes of liquid pumped into the hydraulic cylinder were recorded. The displacement of the hydraulic cylinder was measured by using the optical encoder described in chapter 5.1. The measurement of the volume of the liquid, pumped into the hydraulic cylinder, was performed by the encoder embedded into the neMESYS pump. The data collected in those experiments is plotted in Figure 5.17 and Figure 5.18, which shows a zoomed-in view of Figure 5.17.

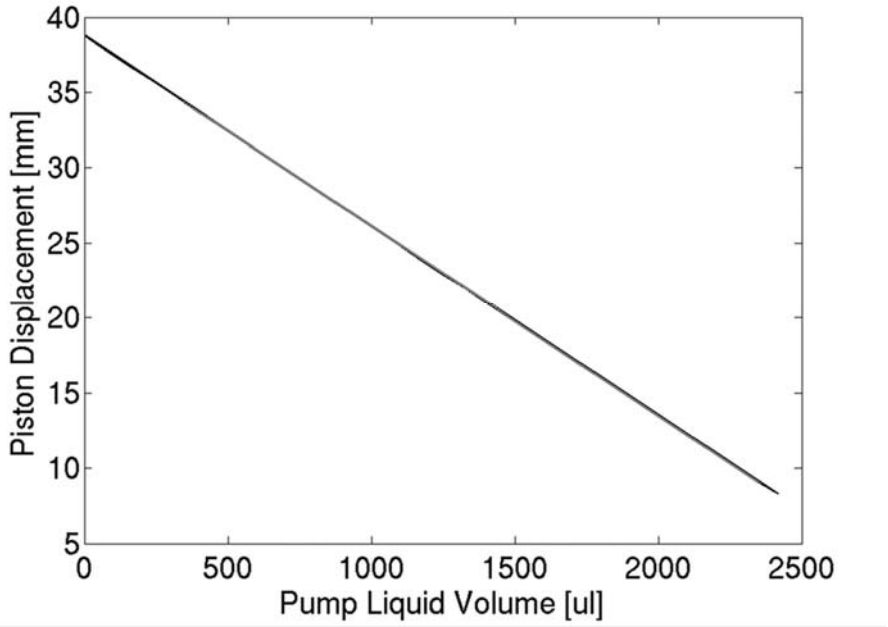

Figure 5.17: Displacement of the mini hydraulic cylinder against syringe pump volume

The experimental results in Figure 5.18 show two groups of curves. The upper group contains the measurements taken during the cylinder extension, the lower group shows the measurements taken during the retraction.

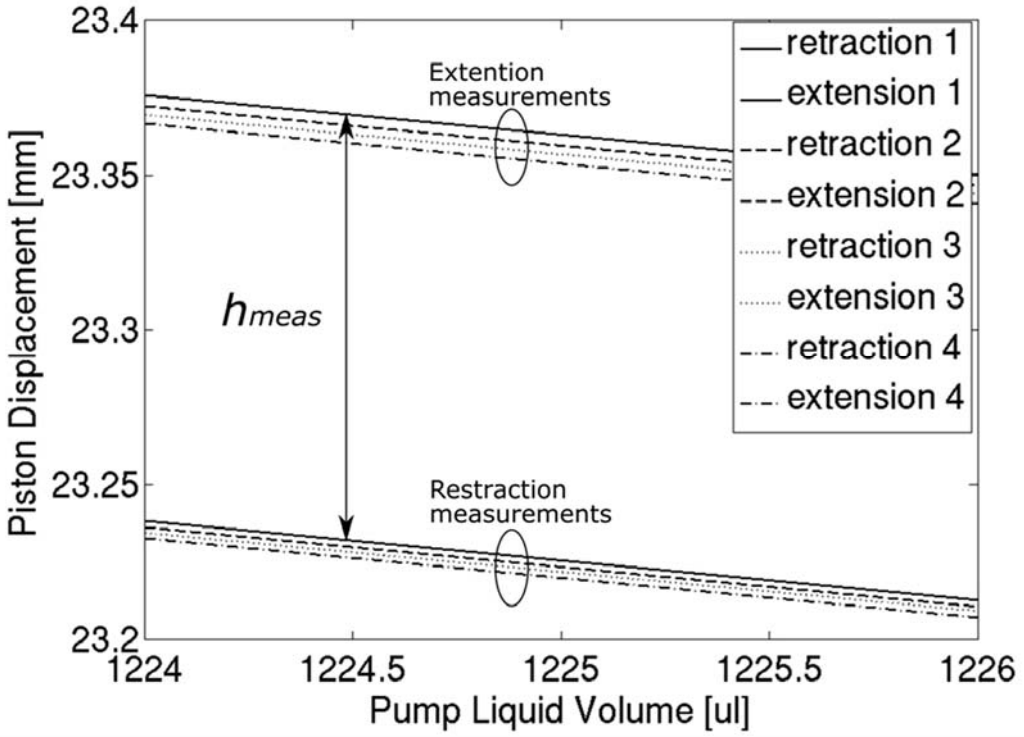

Figure 5.18: Magnified view of Figure 5.17 for consecutive extension and retraction movements of the cylinder

Moreover, the distance between the extension and retraction curve in every cycle is constant and its value is h_{meas} = 0.132 mm. Additionally, it can be observed that the displacement of both the extension and the retraction curve shifts downward each cycle.

The continuous reduction of displacement was explained as a small leakage, whereas the difference of displacement between extension and retraction movement was investigated and its cause identified.

The mechanical design of the piston and the play of the seal were identified as the cause of the mechanical hysteresis.

For a better understanding, a cross-section of the piston together with its sealing and their dimensions are shown in Figure 5.19.

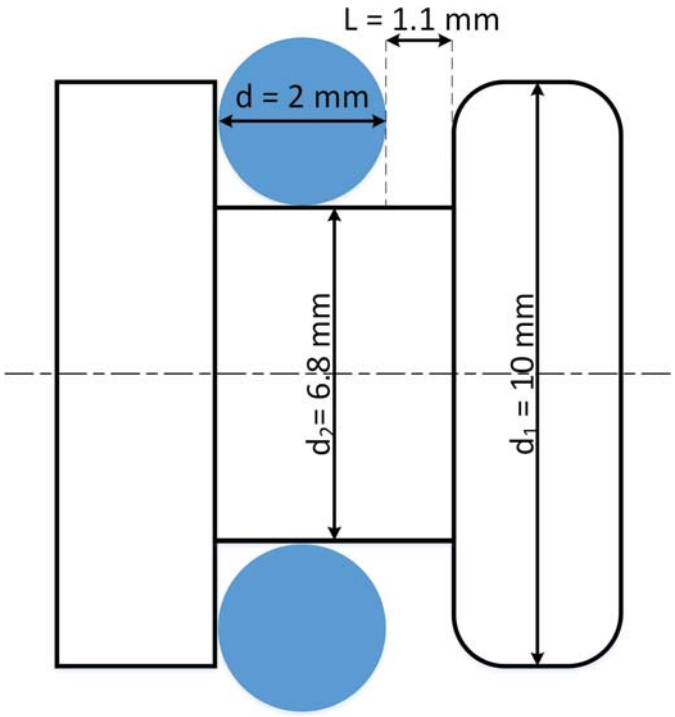

Figure 5.19: Cross-section of piston to show its design and its dimensions

Figure 5.19 shows that the seal´s slot is wider than the seal itself. This is necessary to assure the proper function of the O-Ring sealing (Parker Seals 2007). Because of the space available and the friction force applied by the cylinder barrel, the sealing moves in the slot during extension and retraction. During the extension, the seal is pushed toward the right side of the slot, whereas during the retraction it is pulled toward the left. This means that during retraction part of the liquid flows from the piston chamber toward the seal´s slot, whereas during extension, the liquid in the seal´s slot flows back into the cylinder chamber. Therefore, the liquid volume in the piston chamber is bigger during extension than during retraction, explaining why the piston´s displacement measured during extension is bigger.

In order to prove this hypothesis, the volume of the liquid moved by the seal´s shift was calculated. This value was used to estimate the cylinder displacement that this liquid can cause. The estimated cylinder displacement and the measured

offset h_{meas} were compared. The volume of liquid moved by the seal´s shift is

$$\mathrm{V_{gap}} = \pi \mathrm{L}\left[\left(\frac{d_1}{2}\right)^2 - \left(\frac{d_2}{2}\right)^2\right] = 46{,}44\ \mathrm{mm}^3, \tag{17}$$

and the cylinder displacement that the movement of this liquid can cause is

$$\mathrm{h} = \frac{\mathrm{V_{gap}}}{\pi\left(\frac{d_1}{2}\right)^2} = \frac{46{,}44}{\pi\, 5^2} = 0{,}591\ \mathrm{mm}, \tag{18}$$

where $\mathrm{V_{gap}}$ is the liquid volume in the piston chamber, L is the height of the piston chamber, d_1 is the diameter of the piston and d_2 is the diameter of the sealing holder.

The value of h calculated in equation (18) has the same order of magnitude as the measured offset h_{meas}, but is approximately 4.5 times bigger. The reason for this difference is that the volume of the seal´s slot is partially filled with lubricant grease, leaving a smaller volume than the theoretically expected value.

No hysteresis in form of two clouds of points can be observed in Figure 5.12 and Figure 5.13. The reason is that in these cases the step is smaller than the measured offset h_{meas}.

5.3.6 Wire length experimental tests

In the following, an experiment will be described, the purpose of which was to estimate how the connecting cables´ length affects the sensor measurements. Figure 5.20 shows the experimental test set-up. Cables of different lengths were connected between the capacitive sensor and the capacitance to digital converter.

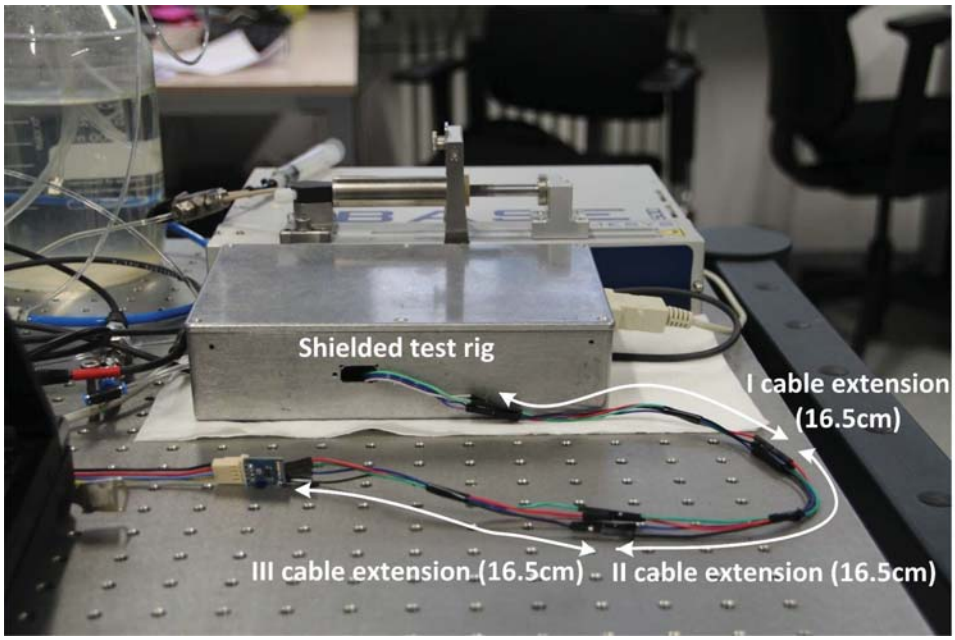

Figure 5.20: Measurement set-up for estimating how the wire length affects the sensor measurements

The results plotted in Figure 5.21 show that each time the cables are lengthened the characteristic is offset towards bigger capacitance values. Additionally, it was demonstrated that the characteristic preserves its linearity and precision if the cables are not twisted and run parallel.

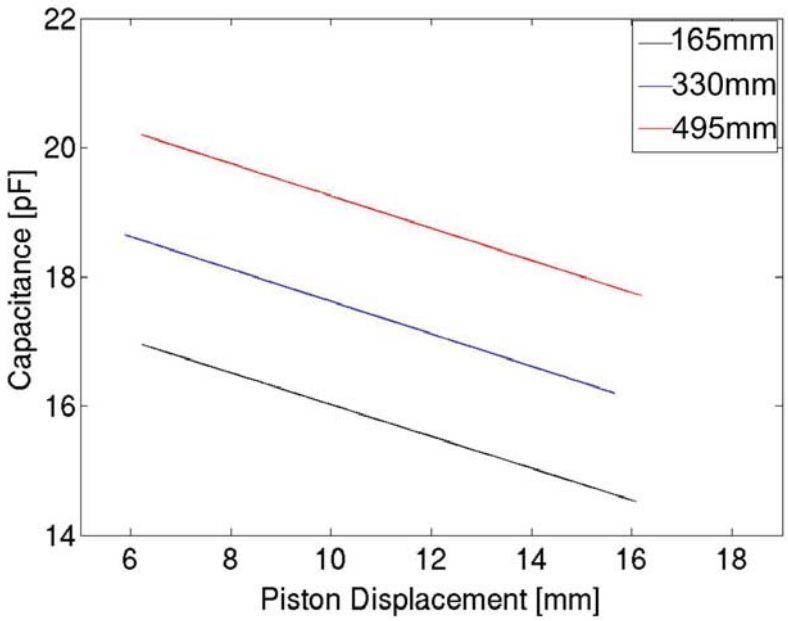

Figure 5.21: Plot of capacitance against displacement with lengthened wires

From the obtained results it was concluded that the cables´ length does not affect the sensor´s performance and that the offset caused by it can be excluded from the measurement with an initial calibration.

6 Sensor integration in closed loop

The aim of this chapter is to prove that the coaxial cylindrical capacitive sensor is able to control the movement of a laparoscopic instrument tip in closed loop. To do this, a hydraulic drive which permits the movement of the instrument tip is designed together with a PI (Proportional Integral) closed loop control. The PI control uses the position measured with the coaxial cylindrical capacitive sensor as feedback to generate the control signal. In order to tune the parameters of the PI control, we need the transfer function of the hydraulic drive, which will be calculated in the following paragraphs starting from the hydraulic drive´s model.
The chapter will be closed with an experimental test in which the designed PI control, the hydraulic drive and the coaxial cylindrical capacitive sensor will be integrated, and the suitability of the developed sensor to control the instrument tip position will be tested.
It must be noted that the scope of this study is not to provide the optimal control method, but to test the sensor in a classic closed loop system. Further investigation on the identification of the best control method is part of future work.

6.1 Hydraulic drive design

In the following, the hydraulic drive designed to control the movement of the instrument tip is presented. Figure 6.1 shows all the elements that constitute it and how they are connected. In addition, the figure shows the parameters that will be later used for the model and the positive direction of this corresponding vectors.

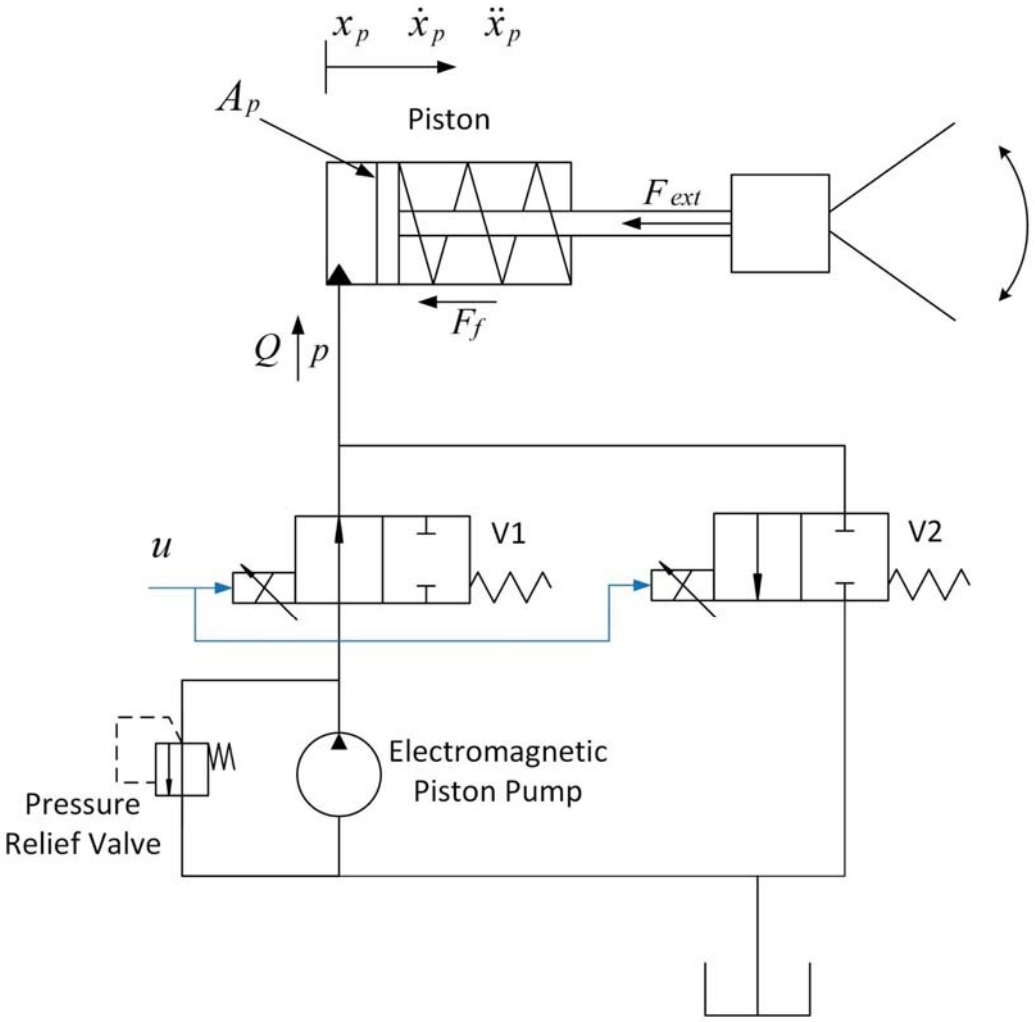

x_p $\dot{x}_p$ $\ddot{x}_p$	displacement, velocity and acceleration of the piston
A_p	piston surface
p	pressure
Q	flow rate
F_{ext}	external force
F_f	friction force
u	control signal
V1	valve 1
V2	valve 2

Figure 6.1: Schematic of the hydraulic drive to control the piston´s movement. The variables used in the model and the forces acting on the cylinder are defined together with their directions

The piston movement is regulated by the liquid flow in and out of the cylinder´s chamber, thereby generating the necessary pressure to move the cylinder´s load. Two 2/2 proportional Bürkert valves (model 2822 G1/8), V1 and V2, are used to control the flow rate by adjusting their opening. V1 controls the flow rate to drive the extension movement of the cylinder, V2 allows the control of the retraction movement. When both valves are closed, the piston´s position remains unchanged. The electric signal u, which can take values between 1 and 5 V, controls the valves´ opening.

The liquid is supplied by an electromagnetic piston pump from GOTEC (model ETG100) that provides constant pressure, while the return flow through V2 is fed to a tank at atmospheric pressure.

The circuit also contains a pressure relief valve from LO-Com (model 00615001), which is used to guarantee that the pressure in the system does not exceed 10 bar. Higher pressure values would damage the valves.

6.2 PI closed loop control

For the purpose of this work a PI closed loop control was selected to control the position of the instrument tip. It was chosen because it is an easily tunable compensator, and combines the fast response of a P controller and the exact compensation of an I controller.

The PI controller is widely used in industrial applications (Åström 2002). Its algorithm can be described by the following time domain equation

$$u(t) = K_p e(t) + K_i \int_{t_0}^{t} e(\tau)\, d\tau, \tag{19}$$

or the complex domain equation

$$U(s) = \frac{K_p s + K_i}{s} E(s), \tag{20}$$

where u is the control signal, e is the error signal measuring the difference between the actual and the desired position, K_p is the proportional gain parameter, K_i the integral gain parameter, and $U(s)$ and $E(s)$ are the Laplace transforms of $u(t)$ and $e(t)$ respectively. The schematic of this control method in the time domain is shown in Figure 6.2.

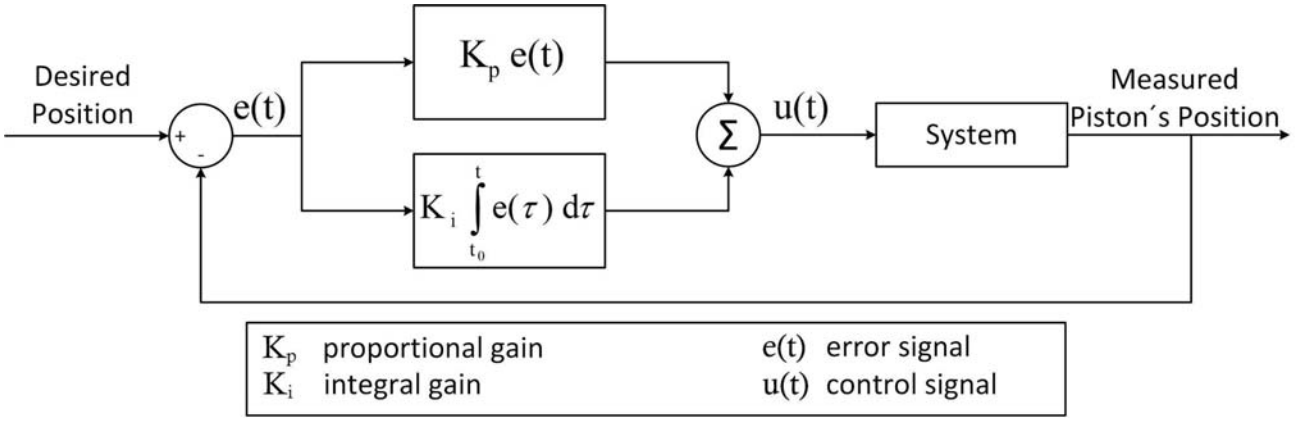

Figure 6.2: Schematic of the PI control

As shown in the schematic, the signal $e(t)$ in this specific case is the difference between the desired position of the piston and the actual position measured with the coaxial cylindrical capacitive sensor. This signal is fed into the PI controller, which computes a signal $u(t)$ to minimize the error $e(t)$. In our case the signal $u(t)$ drives the opening and closing of the proportional valves to bring the piston in the desired position.

The PI control tuning was done with the help of the Matlab PID tuner, an application that automatically tunes the gains of a PID controller for a SISO plant to achieve a balance between performance and robustness. To run the Matlab application, the transfer function of the hydraulic drive is necessary and will be calculated in the next two subchapters step by step, starting with the model of the hydraulic drive components.

6.3 Elementary model of the hydraulic drive components

The hydraulic drive in Figure 6.1 will be described in this chapter with a mathematical model that takes relevant dynamic and non-linear effects into account.

The model is a mathematical description of the elements in the system. Therefore, actuators, transductors, and variables of interconnection are described with mathematical relationships.

This subchapter is the first step towards the calculation of the mathematical model of the overall system. It will be focused on identifying the parts that constitute it and on defining a mathematical description of these elements.

The system can be divided into subsystems as shown in Figure 6.3.

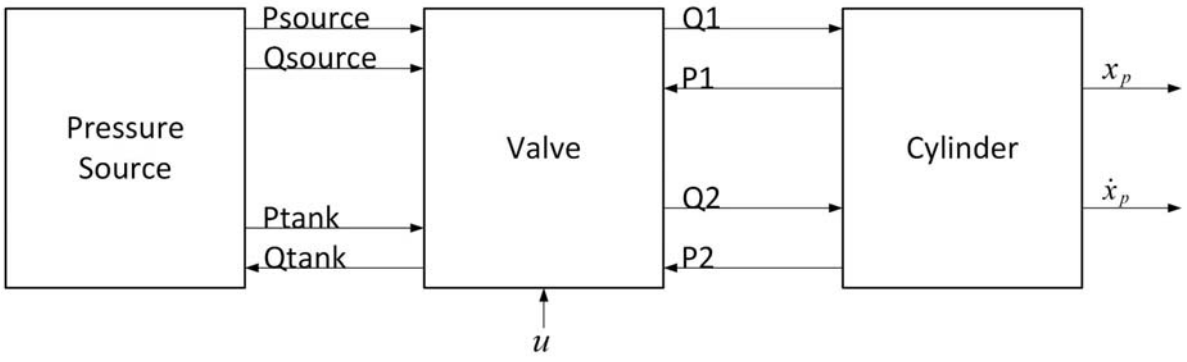

Psource	pump pressure	Q1	flow rate (cylinder extention)	u	control signal
Qsource	pump flow rate	P1	pressure (cylinder extention)	x_p	piston´s displacement
Ptank	tank pressure	Q2	flow rate (cylinder retraction)	$\dot{x}_p$	piston´s velocity
Qtank	tank flow rate	P2	pressure (cylinder retraction)		

Figure 6.3: Block diagram of the hydraulic drive´s model

The pressure source supplies the system with a constant pressure Psource and a flow Qsource during the cylinder´s extension. During the retraction the liquid goes back to the tank at a flow Qtank and a pressure Ptank. The valves define the cylinder input and output flow rate Q1 and Q2, depending on the control signal u and on the cylinder pressure.

The cylinder transfers the flow rate into mechanical movement. It takes the inputs Q1 and Q2 and gives out pressures P1 and P2, displacement x_p and velocity $\dot{x}_p$. In the following subchapters every block in Figure 6.3 will be analyzed in detail.

6.3.1 Valve model

The flow through a valve can be defined according to equation (21) (Jelali et al. 2003), if the spool position of the valve is linearly related to the flow area:

$$Q = C_V x_V \sqrt{\Delta p}\,, \tag{21}$$

where C_V is the valve flow coefficient, x_V the valve spool position and Δp the pressure difference between the valve output and the valve input. Equation (21) can also be formulated in terms of the applied voltage to the valve actuator

$$Q = C_V x_{vmax} \frac{u}{u_{max}} \sqrt{\Delta p}, \tag{22}$$

where x_{vmax} is the maximum aperture of the valve orifice and can be normalized to 1, u is the valve´s control voltage, u_{max} the valve´s maximum control voltage. The valve flow coefficient can be calculated as

$$C_V = \pi d_v \alpha_d \sqrt{\frac{2}{\rho}}. \tag{23}$$

C_V depends on the diameter d_V of the valve spool, the spool discharge coefficient α_d and the fluid mass density ρ. If the parameters in the formula are unknown, C_V can be calculated with the catalogue data of the manufacturer using the following equation

$$C_v = \frac{Q_N}{\sqrt{\frac{\Delta p_N}{2}}}, \tag{24}$$

where Q_N is the normal flowrate and Δp_N the pressure difference.

Equations (22) and (24) are used to calculate the characteristic of the valve´s flow

shown in red in Figure 6.5. To check if this characteristic approximates the valve´s behavior satisfactorily, an experimental test was carried out. Figure 6.4 shows the test setup, which consists of a continuous flow pump with a fixed output pressure of 10 bar, the solenoid proportional valve used in the hydraulic drive, a flow rate sensor and a tank at atmospheric pressure.

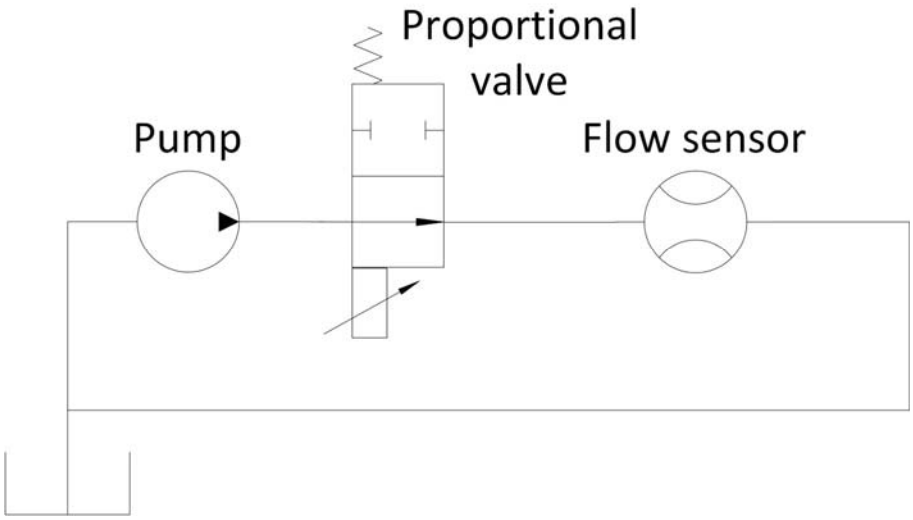

Figure 6.4: Hydraulic circuit for the characterization of the proportional valve

With constant pressure from the pump, the control input of the valve u was varied between 0 V and 5 V and the corresponding flow rate values were measured. The obtained characteristic is shown in blue in Figure 6.5. As the linear model (red line in Figure 6.5) does not approximate the observed behavior of the valve in an acceptable way, the adjusted nonlinear characteristic in Figure 6.6 was used for the model.

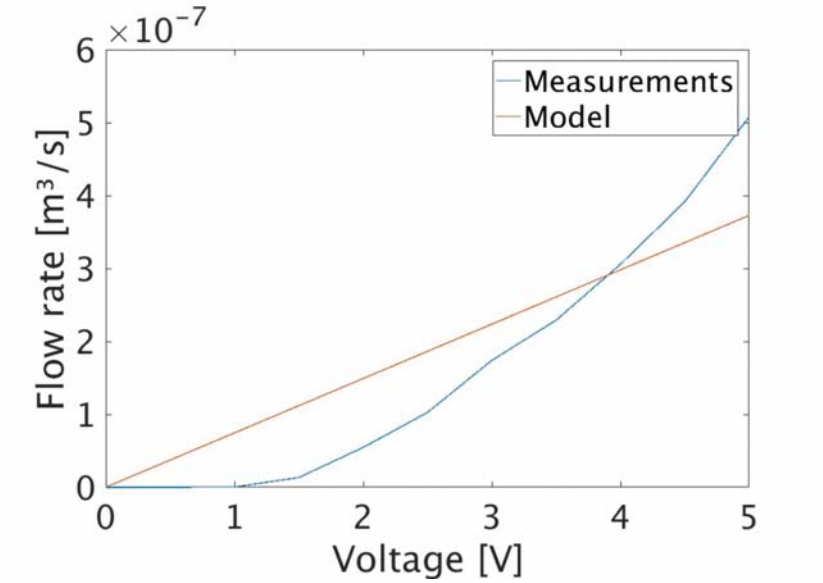

Figure 6.5: Characteristic of the proportional valve calculated with equation (22) in red and the results of the experimental characterization in blue

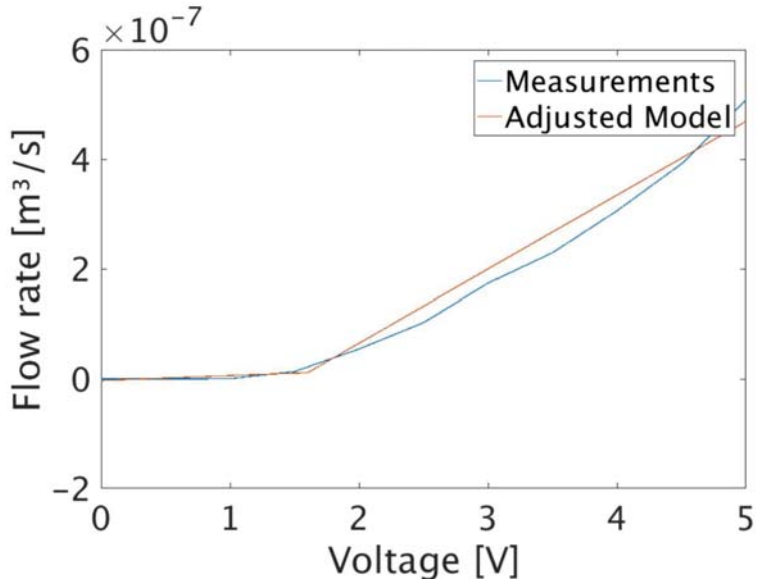

Figure 6.6: Measured valve´s characteristic in blue and the curve used to approximate it in the system´s model in red

The dynamic behavior of the valve was approximated as a first-order system, which is characterized by a delay between the moment in which the control voltage u is applied and the moment in which the valve´s aperture reaches the desired value.

6.3.2 Hydraulic cylinder model

The model of the cylinder can be divided into two subsystems: one describing the pressure in the cylinder´s chamber and one describing the piston´s movement. Figure 6.7 shows the two subsystems and how they are connected. The piston chamber pressure block takes the valve´s flow rate, the piston´s displacement and velocity as inputs, and calculates the pressure in the piston chamber which is afterwards used by the cylinder motion block to calculate the displacement and the velocity of the piston.

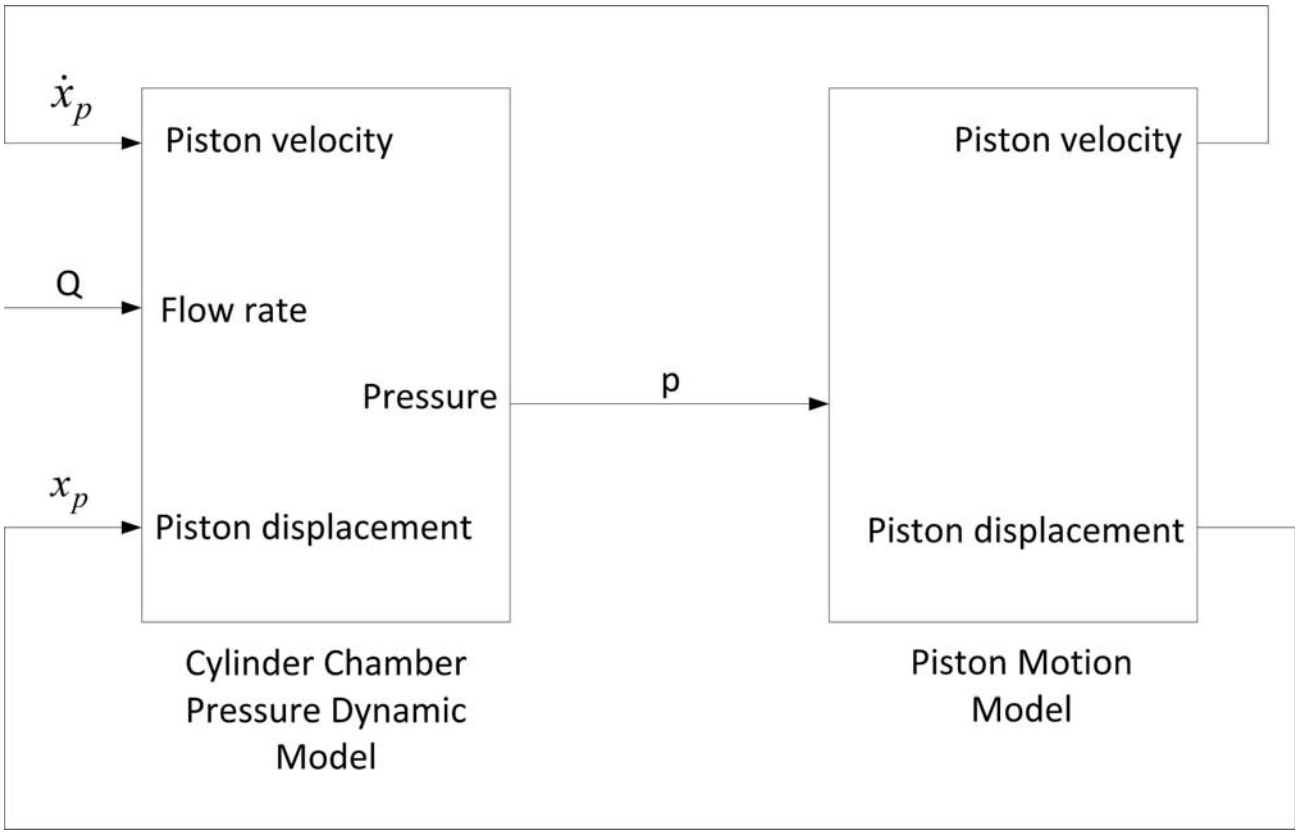

Figure 6.7: Block diagram of the cylinder´s model

6.3.3 Model of the pressure dynamics in the cylinder chamber

The mathematical relationship between the input flow rate of the cylinder and the chamber´s pressure is retrieved from the continuity equation

$$\dot{p} = \frac{E}{V}\left(\sum Q_{in} - \sum Q_{out} - \dot{V}\right), \tag{25}$$

where $\dot{p}$ is the derivative of pressure with respect to time, E is the fluid´s bulk modulus, V is the fluid volume, Q_{in} is the input flow rate, and Q_{out} is the output flow rate.

The continuity equation applied to the cylinder´s chamber yields the following equation

$$Q - Q_{Le} = \dot{V} - \frac{V}{E}\dot{p}, \tag{26}$$

where Q is the flow rate towards the cylinder´s chamber, V is the volume of the piston´s chamber, and Q_{Le} is the external leakage. The other parameters were already defined for equation (25).

The volume of the chamber is calculated as

$$V = V_0 + x_p A_p, \tag{27}$$

and its derivative is

$$\dot{V} = \dot{x}_p A_p, \tag{28}$$

where V_0 is the volume of the tube between the cylinder and the valve, and x_p and A_p are the position and the surface of the piston respectively.

6.3.4 Piston motion equation

The relationship between position and pressure, needed to model the piston motion sub-block in Figure 6.7, is obtained using Newton's second law

$$m_t a_p = p A_p - F_{ext} - F_f, \tag{29}$$

where m_t consists of the piston mass, the rod mass, and the mass of the metal block pushed by the rod (see Figure 5.6 and Figure 5.7). a_p is the piston acceleration, p the pressure on the piston, A_p the piston surface, F_{ext} the external force and F_f the cylinder friction force.

As shown in Figure 5.6 and Figure 5.7 the rod´s movement pushes a block, which slides on a rail, against a spring. F_{ext} is considered as the force exerted by the spring

$$F_{ext} = kx_p, \tag{30}$$

where k is the spring´s stiffness and x_p the spring´s displacement, which corresponds to the piston´s movement. The damping force

$$F_d = b\dot{x}_p, \tag{31}$$

where b is the damping factor caused by the slide of the block on the rail, is taken into account in the cylinder friction force F_f together with the friction due to contact between moving parts in the cylinder.

6.3.5 Pressure source model

The pressure source in the system is obtained by the combination of a pump and a pressure relief valve (see Figure 6.1). The relief valve ensures that in case of overpressure part of the liquid is returned to the reservoir and guarantees a constant pressure in the system. Hence the approximation of a constant output from the pressure source is sufficient for our model.

6.3.6 Tubing model

At high frequencies the tubing can introduce resonances in the system, playing an important role in its input-output behavior.

The tubes´ dynamics can be neglected as long as the length of the pipelines l stays under a threshold defined by c, the sonic velocity in oil, and f_{max}, the maximum frequency of the system, according to the following formula (Jelali et al. 2003)

$$l < \frac{c}{10 f_{max}}. \tag{32}$$

The analyzed system was designed for the control of the laparoscopic instrument tip. A period of 0.5 s was estimated as the minimum time for a full movement of the instrument tip, corresponding to a frequency of 2 Hz. Substituting this value in the equation, it results $l < 73m$. Relationship (32) is fulfilled, therefore the tubes´ dynamics can be neglected and their volume can be modelled as ineffective and added to the chamber´s volume of the cylinder.

6.3.7 Friction model of the cylinder

The friction of the hydraulic cylinder is modelled according to the Stribeck curve. This is a common method which describes friction as a combination of viscous friction $F_v(\dot{x}_p)$, Coulomb friction $F_c(\dot{x}_p)$ and static friction $F_s(\dot{x}_p)$ according to the formula (Jelali et al. 2003)

$$F_f = F_v(\dot{x}_p) + F_c(\dot{x}_p) + F_s(\dot{x}_p) \tag{33}$$

$$= sign(\dot{x}_p)\left[F_{c0} + F_{s0}\exp\left(-\frac{\dot{x}_p}{c_s}\right)\right] + d_z\dot{x}_p,$$

where F_{c0} is the parameter for the Coulomb friction, F_{s0} and c_s (known as Stribeck velocity) are the parameters for the static friction, and d_z is the coefficient of viscosity.

6.4 Simulation model

6.4.1 State space representation

In this subchapter all the equations derived in chapter 6.3 which mathematically describe the elements of the hydraulic drive are combined in an overall model in the state space representation form, given in equations (34) and (35). The state space representation provides a mathematical model of a physical system. This representation was chosen as it describes the system in a compact way. In case

the of a linear system it permits the estimation of the system observability and controllability, as well as the calculation of the transfer function. It is composed of first order differential equations which express the relationship between the system input $\boldsymbol{u}$, the output $\boldsymbol{y}$ and the state variables $\boldsymbol{x}$ in the following form

$$\dot{\boldsymbol{x}} = f\big(\boldsymbol{x}(t), \boldsymbol{u}(\boldsymbol{t})\big), \tag{34}$$

$$\boldsymbol{y} = g\big(\boldsymbol{x}(\boldsymbol{t}), \boldsymbol{u}(\boldsymbol{t})\big). \tag{35}$$

In equations (34) and (35) input, output and state variables are expressed as vectors in order to also model systems with multiple inputs and outputs in a compact way.

For the description of our system, two state space representations will be calculated: one for positive input values of the control signal of the valve $u \geq 0$, hence for the cylinder extension, and one for negative values of the control input of the valve, hence for the cylinder retraction.

The state space representation for $u \geq 0$ is first calculated, starting with the following definitions respectively for displacement, acceleration, and chamber pressure (whose positive directions are shown in Figure 6.1):

$$x_p = x_1, \tag{36}$$

$$\dot{x}_p = x_2, \tag{37}$$

$$p = x_3. \tag{38}$$

According to these definitions the cylinder´s dynamics equation

$$m_t a_p = p A_p - F_{ext} - F_f \tag{39}$$

can be rewritten in the following form

$$\begin{bmatrix} \dot{x}_1 \\ \dot{x}_2 \end{bmatrix} = \begin{bmatrix} x_2 \\ \frac{1}{m_t}\left(x_3 A_p - F_{ext} - F_f(x_2)\right) \end{bmatrix}. \tag{40}$$

The third equation of the state space representation is obtained by manipulating the equation of the chamber´s pressure (26), which is rearranged as follows.

$$\dot{x}_3 = \dot{p} = \frac{E}{V}\left(Q - Q_{Le} - A_p \dot{x}_p\right). \tag{41}$$

Its final form, in equation (42), is obtained substituting V with equation (27) and Q with equation (22). For the cylinder extension Δp in equation (22) is $p_{pump} - p_{cylinder}$.

From equations (40) and (41) the following state space representation for the system is obtained

$$\begin{bmatrix} \dot{x}_1 \\ \dot{x}_2 \\ \dot{x}_3 \end{bmatrix} = \begin{bmatrix} x_2 \\ \frac{1}{m_t}\left(x_3 A_p - k x_1 - F_f(x_2)\right) \\ \frac{E}{V_0 + x_1 A_p}\left(\frac{C_V x_{vmax}}{u_{max}}\sqrt{p_{pump} - x_3}\,u - Q_{Le} - A_p x_2\right) \end{bmatrix}, \tag{42}$$

$$y = x_1. \tag{43}$$

The input of the system is the voltage that controls the proportional valves u. The output is the piston´s displacement x_1. The state variables are the pressure of the piston´s chamber $\dot{x}_3$, the piston´s velocity $\dot{x}_1$ and its acceleration $\dot{x}_2$.

The state space representation for $u < 0$ can be obtained by following the same steps. The difference is that in this case in equation (22) $\Delta p = p_{cylinder} - p_{atm}$, which leads to the following first equation of the state space representation

$$\begin{bmatrix} \dot{x}_1 \\ \dot{x}_2 \\ \dot{x}_3 \end{bmatrix} = \begin{bmatrix} x_2 \\ \frac{1}{m_t}\left(x_3 A_p - k x_1 - F_f(x_2)\right) \\ \frac{E}{V_0 + x_1 A_p}\left(\frac{C_V x_{vmax}}{u_{max}}\sqrt{x_3 - p_{atm}}\,u - Q_{Le} - A_p x_2\right) \end{bmatrix}. \tag{44}$$

6.4.2 Model linearization and controllability

The next step towards the calculation of the hydraulic drive transfer function is the linearization of the model. The linearization procedure consists of describing the non-linear system with a linear model around an operating point. Linearization gives an approximation of the real system which is valid in a range around the operating point. It is valuable to analyze the system´s behavior and to design the control system using classical techniques, such as Bode plot and root locus design.

For the linearization some simplifications of the non-linear model have been done. The friction force, discussed in chapters 6.3.4 and 6.3.7, is modelled as a combination of the viscous force and the damping force, due to the sliding of the block on the rail and the contact between the moving parts of the cylinder $c_f \dot{x}_p = (d_z + b)\dot{x}_p$. The case in which the piston is in position $x_1 = x_{10} = 0{,}009$ m (middle point of the cylinder´s stroke), $x_2 = 0$, $x_3 = x_{30} = 7\text{e}5$ Pa, and the valve is totally closed ($u = 0$) is chosen as the operation point.

With the mentioned simplification the state space representations are

$$\dot{\boldsymbol{x}} = \begin{bmatrix} 0 & 1 & 0 \\ -\frac{k}{m_t} & -\frac{c_f}{m_t} & \frac{A_p}{m_t} \\ 0 & -\frac{EA_p}{V_0 + x_{10}A_p} & 0 \end{bmatrix} \boldsymbol{x} + \begin{bmatrix} 0 \\ 0 \\ -\frac{EC_V x_{vmax}\sqrt{p_{pump} - x_{30}}}{u_{max}(V_{10} + x_{10}A_p)} \end{bmatrix} \boldsymbol{u}, \tag{45}$$

$$\boldsymbol{y} = [1 \quad 0 \quad 0]^T \boldsymbol{x}, \tag{46}$$

$$\dot{\boldsymbol{x}} = \begin{bmatrix} 0 & 1 & 0 \\ -\frac{k}{m_t} & -\frac{c_f}{m_t} & \frac{A_p}{m_t} \\ 0 & -\frac{EA_p}{V_0 + x_{10}A_p} & 0 \end{bmatrix} \boldsymbol{x} + \begin{bmatrix} 0 \\ 0 \\ -\frac{EC_V x_{vmax}\sqrt{x_{30} - p_{atm}}}{u_{max}(V_{10} + x_{10}A_p)} \end{bmatrix} \boldsymbol{u}, \tag{47}$$

$$\boldsymbol{y} = [1 \quad 0 \quad 0]^T \boldsymbol{x}. \tag{48}$$

The values of the parameters in the model, used for the simulation, are shown in Table 6. k, C_v and u_{max} are derived from the manufacturer´s datasheet. The other variables in the table are characteristics of the real cylinder.

For the linearized models the controllability and the observability can be proven. A system is observable, if it is always possible to deduce the system states when knowing the system output. A linear time invariant system, the state vector of which has dimension n, is observable if the rank of the observability matrix is n (Bolzern et al. 2015).

Table 6: Values of the model´s parameters

Parameter	Description	Value	Unity
k	spring´s stiffness	3.516 1e3	$\left[\frac{N}{m}\right]$
m_t	piston mass	1e-3	$[kg]$
c_f	Friction coefficient combination of d_z and b	30	$\left[\frac{Ns}{m}\right]$
A_p	piston surface	7.85e-5	$[m^2]$
E	fluid´s bulk modulus	2.22e9	$\left[\frac{N}{m^2}\right]$
V_o	volume of the tube between cylinder and valve	5e-8	$[m^3]$
C_v	flow coefficient	3.9284e-10	$\left[\frac{m\sqrt{Pa}}{s}\right]$
u_{max}	valve´s maximum control voltage	5	$[V]$
P_{atm}	atmospheric pressure	1.013e5	$[Pa]$
x_{vmax}	Maximum aperture of the valve orifice	1	$[m]$

A system is defined as controllable, if the system input can move the system states from any initial state to any other final state in a finite time interval. A linear time invariant system, the state vector of which has dimension n, is controllable if the rank of the controllability matrix is n (Bolzern et al. 2015).

The system taken into consideration in this work is observable and controllable, as the observability and the controllability matrix have rank 3, which corresponds to the dimension of the state vector.

These two characteristics are relevant because, if the system is not controllable, it is not possible to move any initial state to any final state by changing the input signal. Whereas, if the system is not observable, the values of the state variables cannot always be measured with output sensors. In both cases the effect of control is limited, hence there is the possibility of instability.

Figure 6.8 shows the comparison of the simulation of the linear and the non-linear model.

It is assumed that the piston at t = 0 s is stationary in the 0 position. At t = 2.5 s a positive voltage is applied to the valve V1. V1 opens, leading to an extension of the cylinder. Afterwards, a 0 V signal is applied to the valves for five more seconds letting the cylinder stay in its position. Finally, a negative signal is applied which opens the valve V2 and allows the cylinder to retract. The figure shows that the curves of position, pressure and velocity calculated with the linear and the non-linear models almost overlap. This means that, for small variations of the input signal, the linear model sufficiently matches the non-linear one and it will be further used for the system analysis and the control design. Moreover, the figure shows that, due to the chosen spring´s constant, the extension movement is faster than the retraction.

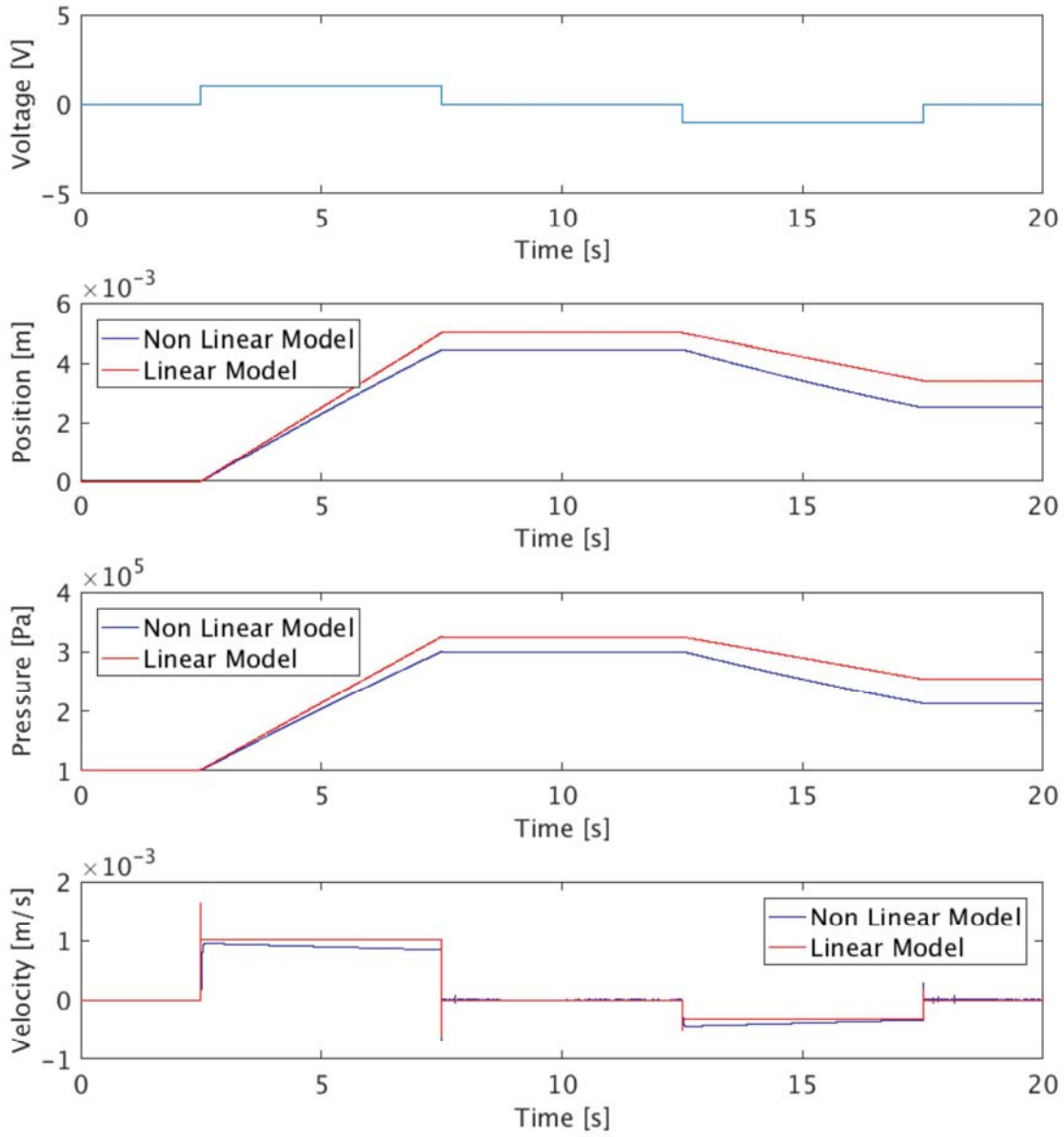

Figure 6.8: Simulation plots of voltage, Piston position, pressure and velocity over time, comparing the linear and non-linear model respectively in red and blue

6.4.3 Transfer function

From the linearized form of the state space representation it is possible to calculate the transfer function of the system.

The transfer function is a representation of the system in the Laplace space and describes the relationship between the Laplace transform of its input U and

output Y (Bolzern et al. 2015). It allows the study of the system using the classical techniques of systems and control theory. It facilitates the analysis of the system and the control design through graphic representations in the frequency domain, e.g., Bode Diagram and root locus. Moreover, the transfer function is used by the PID tuner for the definition of the PI control design.

The transfer function of the hydraulic drive when the cylinder extends is

$$\frac{Y(s)}{U(s)} = \frac{1.678\ 10^5}{s^3 + 16.39\ s^2 + 2.211\ 10^8\ s}\frac{m}{V}. \tag{49}$$

The transfer function when the cylinder retracts is

$$\frac{Y(s)}{U(s)} = \frac{1.258\ \ 10^5}{s^3 + 16.39\ s^2 + 2.211\ 10^8\ s}\frac{m}{V}. \tag{50}$$

Both the transfer functions of the hydraulic drive have a pole in the origin (integrating characteristic) and two complex conjugate poles with a negative real part in -8±14.869j s^{-1}. The pole distribution is shown in Figure 6.9. The pole distribution allows us to conclude that the response of the open loop system is not unstable, as there are no poles with a real positive part.

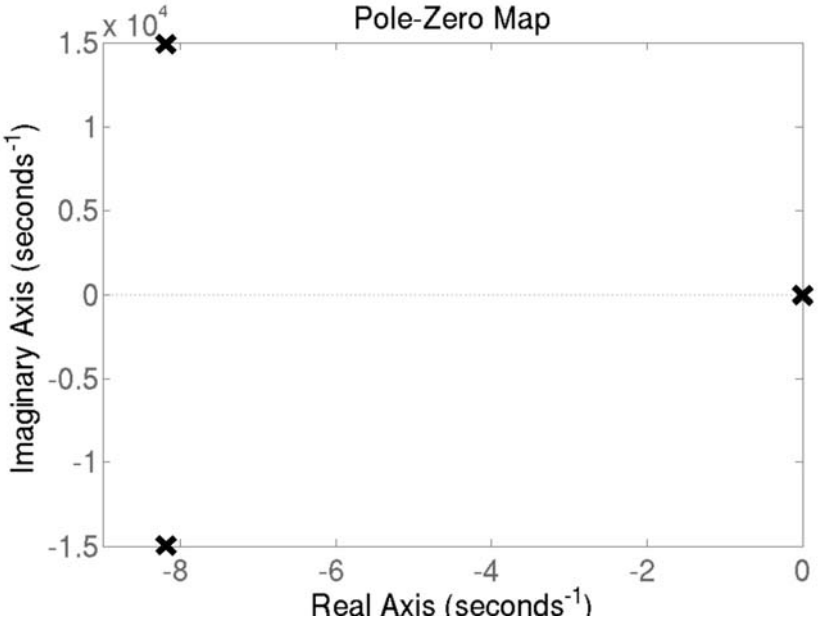

Figure 6.9: Graph showing the distribution of zeros and poles of the system

6.5 Experimental tests

Given the hydraulic drive transfer function, it is possible to proceed with the tuning of the PI control and the experimental tests of the coaxial cylindrical capacitive sensor in a closed loop system, as will be shown in this subchapter.

6.5.1 Measurement setup

The experimental setup for the test of the coaxial cylindrical capacitive sensor in closed loop is shown in Figure 6.10. Figure 6.11 shows the schematic of the test setup.

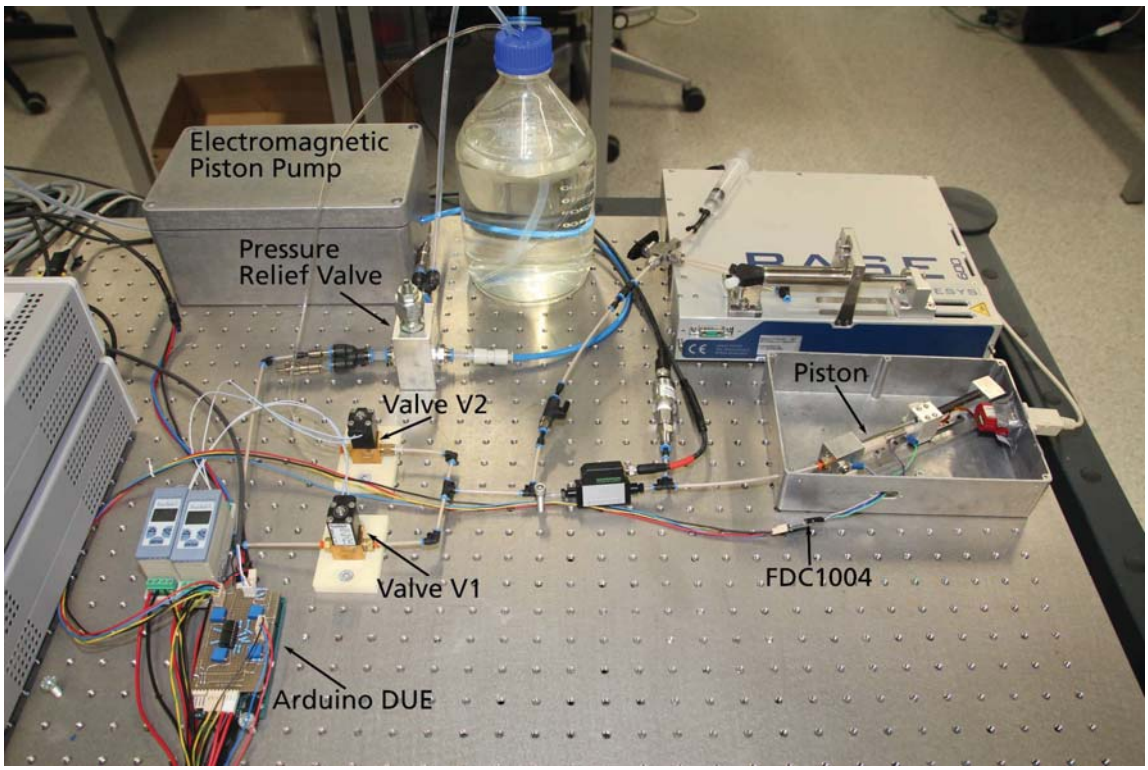

Figure 6.10: Experimental setup for the test of the coaxial cylindrical capacitive sensor into a closed loop system

The FDC1004 transduces the capacitance value into a digital signal. The Arduino DUE board acquires the signal and calculates the actual cylinder´s position. The control software determines the value of the valve´s control variable u to obtain

the correspondence between the measured and the desired cylinder´s position. If the desired position is smaller than the current position, V1 is opened, leading to an extension of the piston. If the desired position is bigger than the current one, V2 is opened to release liquid from the cylinder´s chamber to the tank. If the desired position and the current position coincide both the valves close.

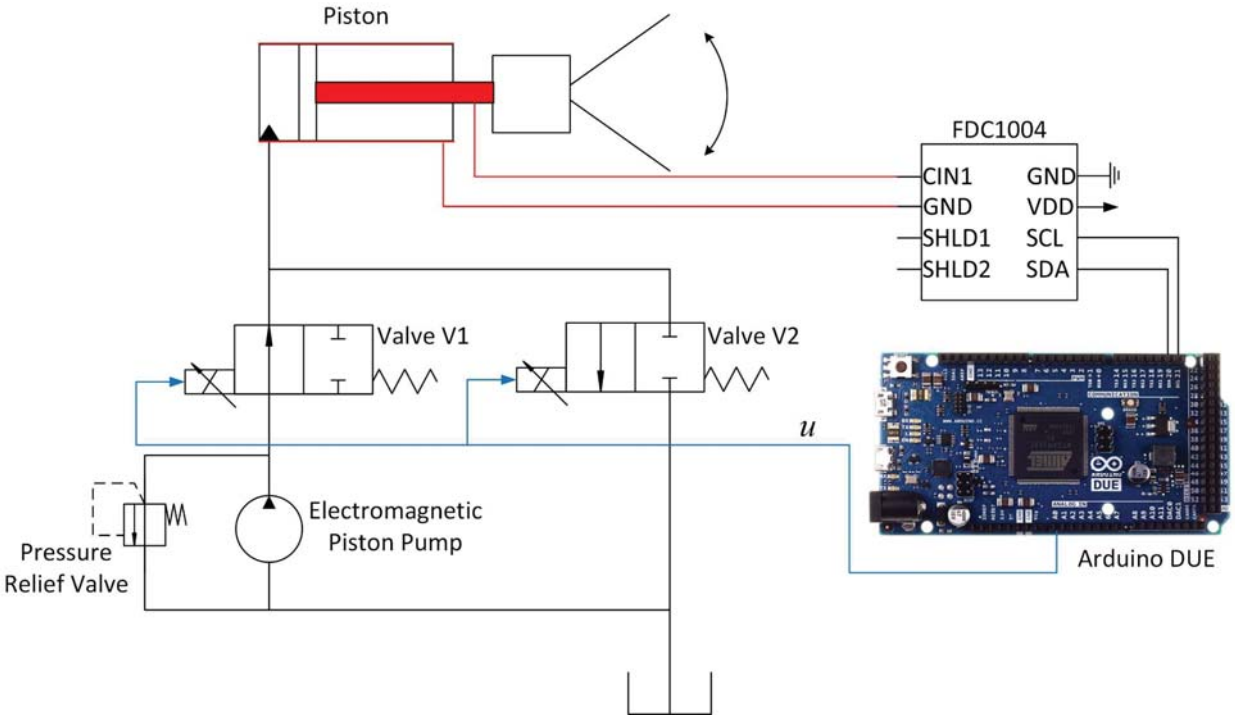

Figure 6.11: Schematic of the system setup for the test of the coaxial cylindrical capacitive sensor in closed loop

6.5.2 PI control tuning

Given the hydraulic drive transfer function, the PI control was tuned using the Matlab tool PID tuner, in order to identify the values of K_p and K_i that fulfill the requirements in chapter 2.5.

As a period of 0.5 s was estimated as the minimum time for the full movement of a laparoscopic instrument tip, which corresponds to a frequency of 2 Hz, a cut off frequency of 10 Hz was initially chosen as specification for the design, to guarantee the necessary dynamics of the instrument tip. With this specification

the Matlab tool was not able to find values of K_p and K_i which could make the designed hydraulic drive stable in the desired bandwidth. Therefore, it was chosen to reduce the bandwidth goal to 1 Hz, the closest value to the desired bandwidth for which the closed loop control was stable. This choice was made, since the purpose of this work is to test the sensor in a closed loop control and not to design the perfect control for this application.

With the help of the PID tuner it was identified that a proportional gain of K_p=12000 guarantees the desired bandwidth of 1 Hz without bringing the system to instability. The use of the proportional control caused a steady state error in the output, which was solved by the integral part of the controller. A simulation of the behavior of the system for K_p=12000 and growing values of K_i is shown in Figure 6.12. For increasing values of K_i, the settling time decreases but the overshoot increases, i.e. the pliers move beyond the desired position during both opening and closing. This is not desired, as the pliers could collide against parts which should not be reached or put stronger pressure on tissues.

However, it must be taken into account that the use of a square wave as input signal represents the worst-case scenario. In reality, the input signal originating from the doctor´s hand has a less steep front, hence the overshoot can be smaller. The investigation of this aspect will be the issue of future work, focused on the design of the control method which best suits the system. In order to evaluate the real entity of the overshoot, the input signal generated by the doctor´s hand can be recorded and, depending on the system´s answer to this signal, a suitable controller can be designed.

As already mentioned above, the PI control fulfills the purpose of this work, which is to test the sensor in a closed loop control, and it will be further developed and tested in the following paragraph.

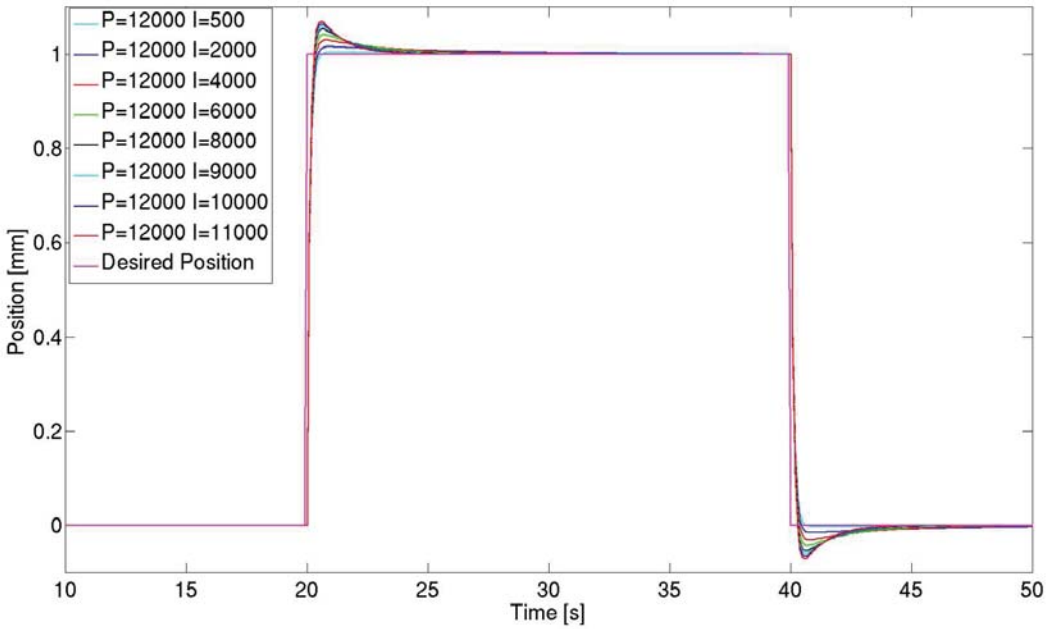

Figure 6.12: Simulated step response of the hydraulic drive controlled by a PI controller

Figure 6.13 and Figure 6.14, which gives a zoomed-in view of Figure 6.13, show the Bode diagram of the closed loop system, which according to the set specification has a bandwidth of 1 Hz.

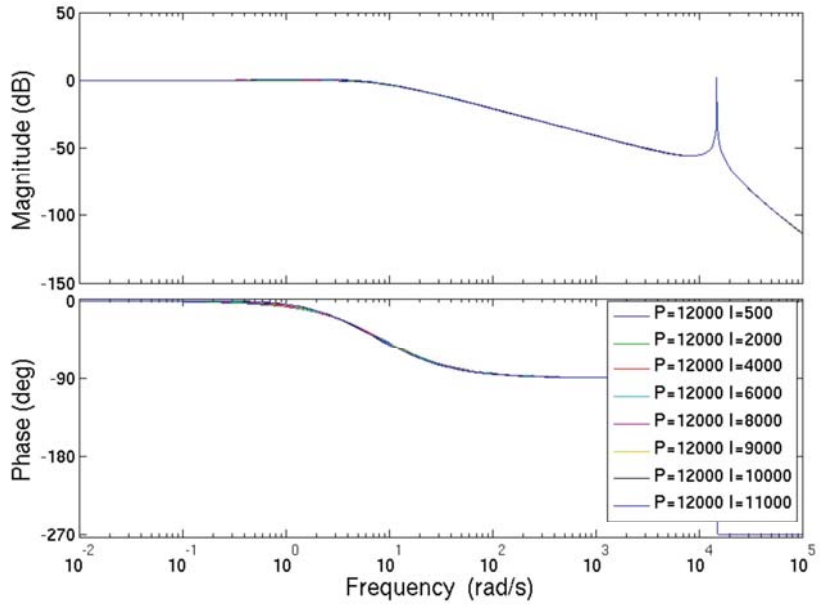

Figure 6.13: Closed loop Bode diagram of the hydraulic drive PI controlled

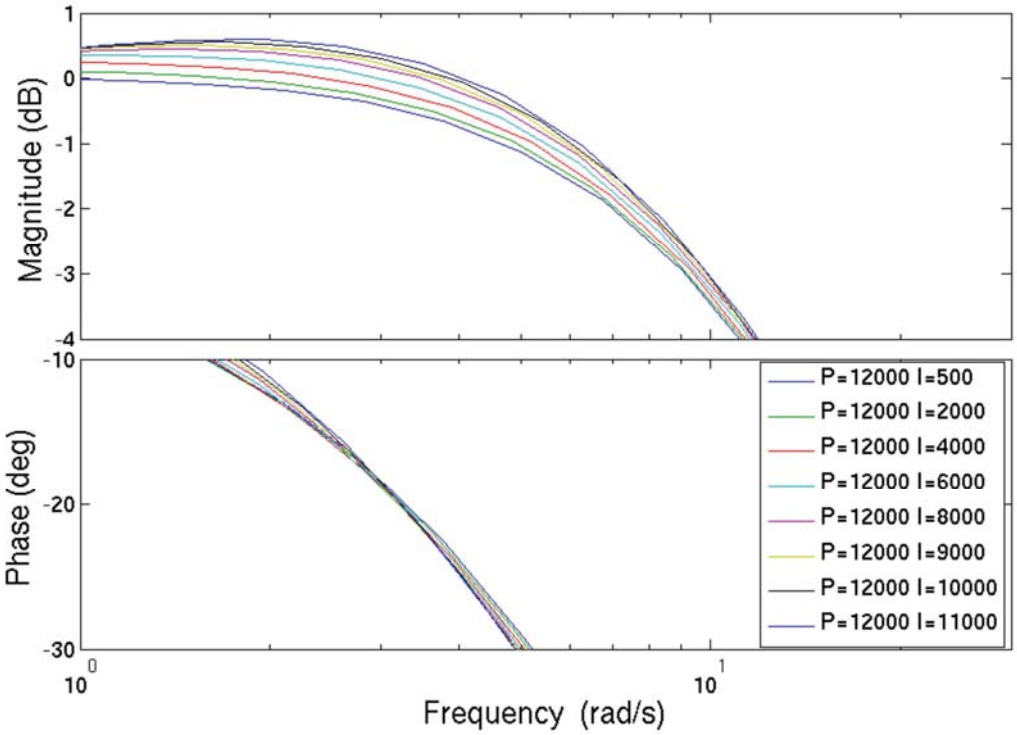

Figure 6.14: Zoomed in view of the Bode diagram in Figure 6.13

From the figures it can be asserted that a variation of K_i between 500 and 11000 causes changes in the Bode diagram, which are so small that the bandwidth is not significantly influenced.

The stability of the closed loop system is guaranteed by the fact that for the designed PI control the Bode criterion is satisfied. The Bode criterion states that:

1. if there are no poles in the right half plane, and
2. the magnitude of the open loop Bode diagram crosses the 0 dB axes only one time.

It follows that a necessary and sufficient condition for the asymptotic stability is that the gain of the system is bigger than 0 ($\mu > 0$) and the phase margin $\varphi_m > 0^{\circ}$, the latter being defined as $\varphi_m = 180° - |\varphi_c|$, where φ_c is the system phase when the module is 0 dB.

Figure 6.15 shows the open loop Bode diagram of the system for a fixed value of K_p and increasing values of K_I between 500 and 11000.

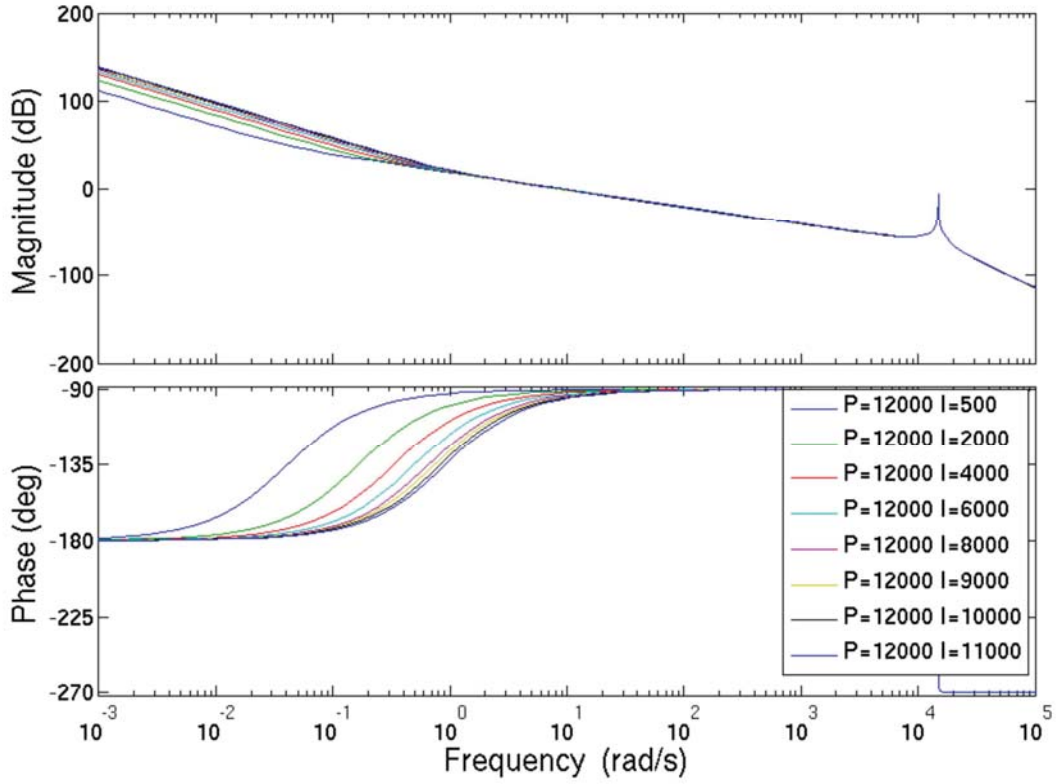

Figure 6.15: Open loop Bode diagram of the hydraulic drive with PI control

For all the cases condition 1 and 2 are fulfilled. The phase margin $\varphi_m = 90^{\circ}$, hence bigger than 0°. Moreover, given that the open loop transfer function for extension and retraction movement are

$$\frac{Y(s)}{W(s)} = 1.678\ 10^5\ \frac{K_p 1.678\ 10^5 s + K_I 1.678\ 10^5}{s^2(s^2 + 16.39s + 2.211\ 10^8)}\frac{m}{V} \qquad (51)$$

and

$$\frac{Y(s)}{W(s)} = 1.258\ \ 10^5\ \frac{K_p 1.258\ \ 10^5 s + K_I 1.258\ \ 10^5}{s^2(s^2 + 16.39s + 2.211\ 10^8)}\frac{m}{V}, \qquad (52)$$

the condition on the system´s gain is also fulfilled, in both cases ($\mu > 0$). Hence the asymptotic stability is guaranteed.

6.5.3 Measurements

Since approximations were made in order to linearize the model, the values of K_p and K_i identified on a simulation level were tested with an experimental test, to prove the validity of the model and the correspondence between the simulated and the real behavior of the system.

The experiment consisted in sending a signal to set the desired position of the cylinder, extending and retracting it for 1 mm. The response of the hydraulic drive was stored and the test results are shown in Figure 6.16. The experiment was repeated six times.

In order to reproduce the simulation in subchapter 6.5.2, K_p was set to 12000 while K_i increases from 500 to 6000. No bigger values of K_i were taken into consideration as the system was already unstable with $K_i = 3000$.

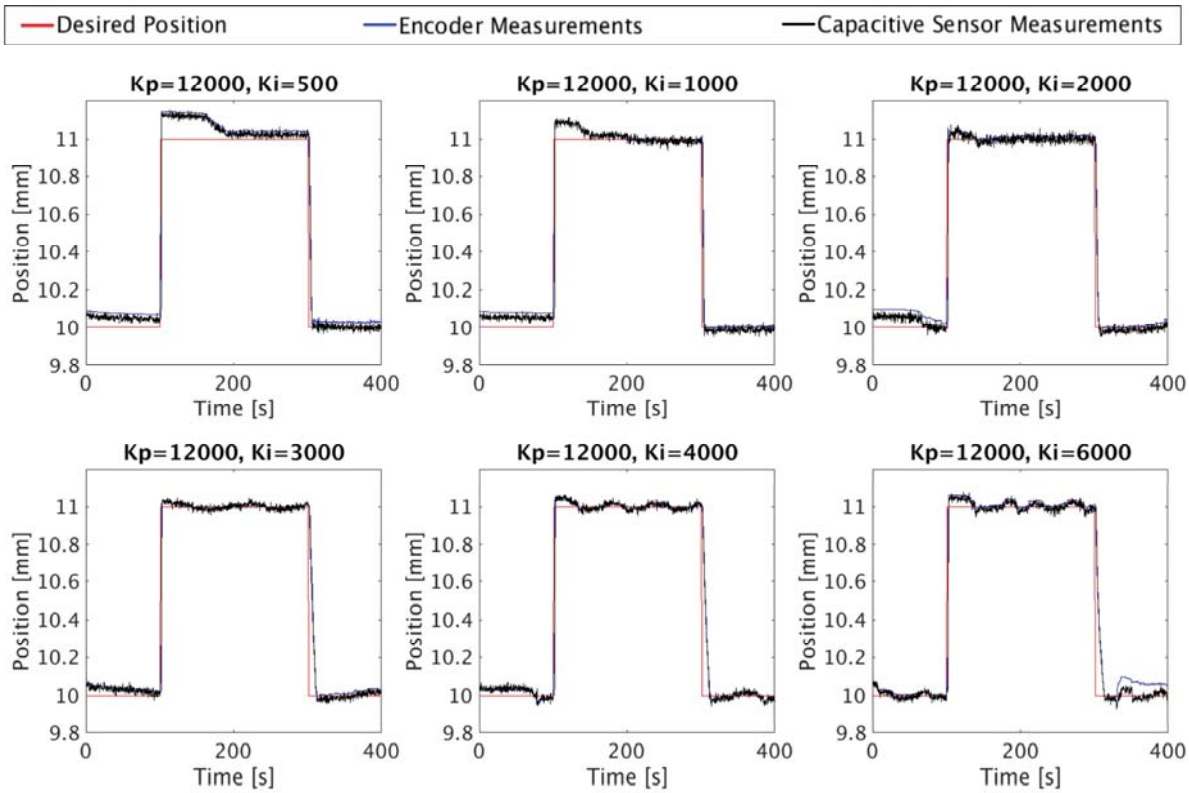

Figure 6.16: Measured step response of the hydraulic drive with proportional integral control

The experimental results confirm the simulations, showing that the increase of K_i reduces the steady state error and makes the hydraulic drive response faster. However, a value of K_i bigger than 3000 makes the system unstable. According to the experimental results, $K_p = 12000$ and $K_i = 2000$ were chosen. The experimental results show a good agreement with the simulations. This means that the model approximates the behavior of the real system in a suitable way. The differences observed between the experimental and simulation results are: the overshooting, smaller in the simulation, and the settling time, shorter in the simulation. Additionally, it can be observed that in the real system the instability of the hydraulic drive is reached for smaller values of K_i. These differences can be attributed to the approximation made on the friction force, which was modelled with the viscous component and the damping effect, due to the sliding of the block on the rail and the contact between the moving parts of the cylinder.

In Figure 6.16, three signals are shown: in red the desired position, in blue the encoder measurements and in black the measurements of the capacitive sensor. Both the encoder and the developed capacitive sensor measure the actual position of the cylinder, but only the capacitive sensor signal is used as a feedback to control its movement. The encoder measurements are only used to double-check the reading of the capacitive sensor and to prove that the measured actual position corresponds with the state of the art measurement of the encoder.

A second experiment was planned to test the ability of the sensor to control the opening and closing of the pincers of an instrument. This movement is obtained if the cylinder moves along a staircase-shape signal. For the test, the desired position of the cylinder changed by 1 mm every 50 s. For the first six steps the cylinder extended, for the next six steps it retracted. The output of the system in response to the input signal was stored and the results are plotted in Figure 6.17.

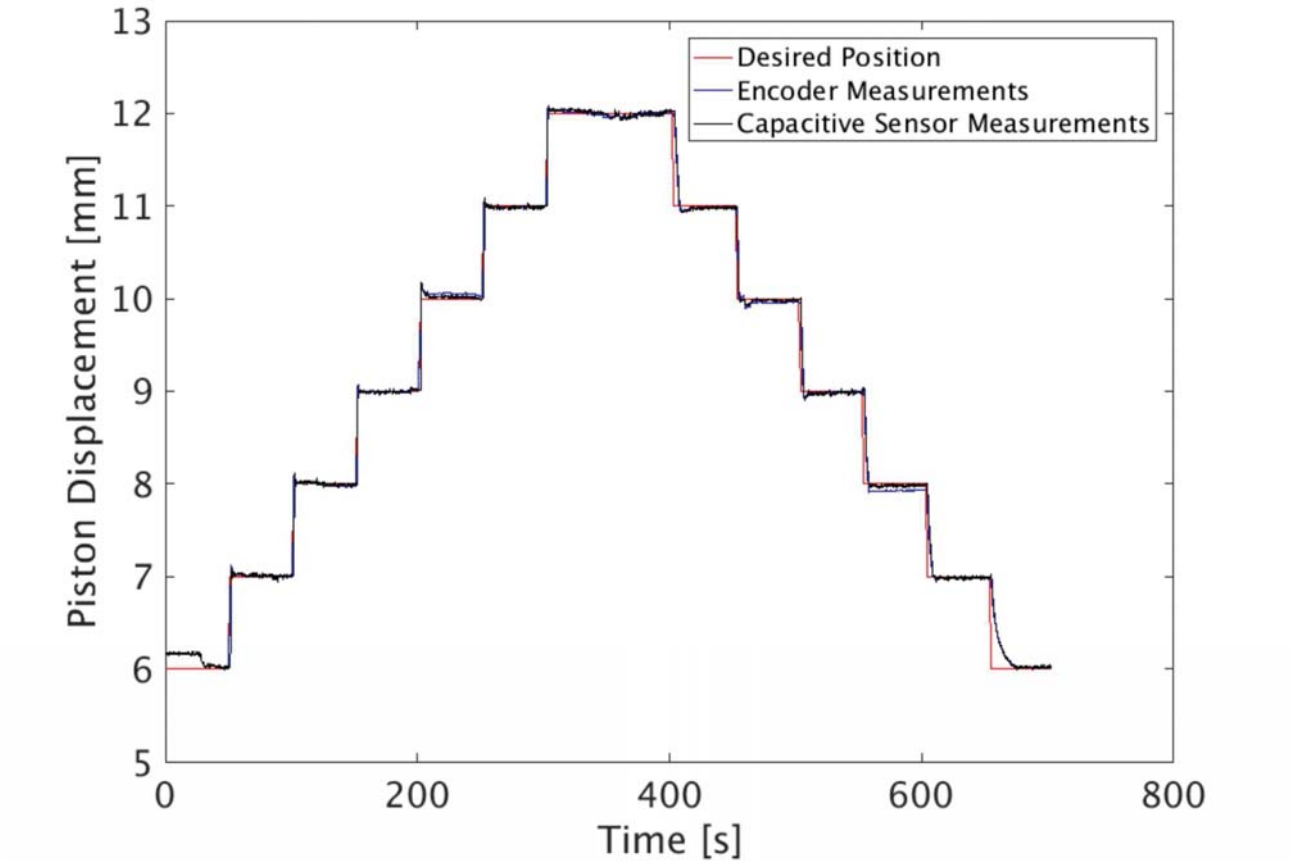

Figure 6.17: Plot of the staircase positioning test using the PI control with $\boldsymbol{K_p = 12000}$ and $\boldsymbol{K_i = 2000}$

As for the first experiment, shown in Figure 6.16, the coaxial cylindrical capacitive sensor was used to control the position, whereas the displacement acquired by an optical encoder served as a reference.

The average deviation of the measurements taken with the capacitive sensor from the ones taken with the encoder is 18 µm. This value is in compatible with the estimated precision (see chapter 5.3.3). The obtained results show a good correspondence between the measurements of the two sensors and prove that the designed sensing method is suitable to be used in a closed loop control system.

7 Conclusion

This chapter contains the conclusions of this thesis. In addition, an outlook on future work necessary for the mechanical integration of the sensor in the laparoscopic instrument is provided.

7.1 Critical discussion of the results

This work demonstrates that the coaxial cylindrical capacitive sensor is from today's point of view the most suitable solution for the discussed application. This sensing method offers the advantage that the integral structure of the hydraulic cylinder can be used as a sensor, without the need of additional elements and without alteration of its design.

An FEA simulation was used to validate the sensing concept before building the sensor up and to analyze first on a simulation level if the sensor concept fulfills the defined specification. The characteristic obtained through the experimental tests corresponds to the simulation results besides the curves´ slope. The difference between them can be addressed to the mechanical tolerances deriving from the manufacturing of the test rig, which causes a slight misalignment between the two electrodes. The mechanical tolerances don´t interfere with the linearity of the sensor, so its performance is not severely influenced. Nevertheless, this is an aspect that must be taken into account for the further optimization of the sensor performance. A study of the processes for the mechanical production of the cylinder is necessary to reduce the tolerances.

The experimental tests prove the linear behavior of the characteristic, confirmed by the match between regression model and measured data with an R-squared of circa 1. The measurements are repeatable, as proved by the comparability of

the linear regression model parameters in all the experiments. Moreover, the experimental tests confirm that the sensitivity of the coaxial cylindrical capacitive sensor is not affected by the radial rescaling of the cylinder as the slope of the fitting curve *a* is the same for the mini and the micro hydraulic cylinder.

The sensor integrated on the mini hydraulic cylinder has a precision of ±27 µm and a linear behavior within a stroke of 30 mm. A higher precision than the one set as a sensor specification was achieved. In the case of the sensor integrated on the micro hydraulic cylinder, a lower precision of ±38 µm was achieved, due to increased leakage of the cylinder. Although less precise, this still fulfills the specification on the sensitivity. However, for further development of the sensor adjustments in the design of the micro hydraulic cylinder will be necessary to reduce the leakage.

The experimental results show that the sensor is sensitive to noise from the environment. To preserve the repeatability and the precision of the measurements a Faraday cage is necessary, which screens the sensor from the environment and would therefore guarantee a sensor´s characteristic that better matches the simulation. This means that the sensor needs to be integrated together with a Faraday cage in the instrument in order to function correctly. Given the limited space available at the instrument tip, mechanical solutions must be investigated to solve this issue.

Because of the instrument size it was not possible to fulfill the specification in Table 1 according to which the sensor output digitalization should have been made at the tip of the instrument. The capacitance to digital converter can only be integrated in the handheld, where more space is available. This means that a cable must connect the sensor to the chip. Experimental results show that the cable introduces capacitance in the system, offsetting the sensor characteristic

towards bigger values of capacitance. An initial calibration is then necessary to exclude the offset from the measurements.

Due to the chosen material, both the electronics for the digital conversion and the capacitive sensor itself are able to withstand high temperatures. However, in order to be washable, disinfectable, and sterilizable, they must be resistant to liquids. This can only be achieved by encapsulating the system. This aspect was not deeply analyzed in this thesis, but as part of the sensor´s integration it belongs to future work.

The integration of the sensor in the hydraulic drive allowed the identification of two aspects that affect the mechanical behavior of the hydraulic cylinder: the stick slip effect and the hysteresis of the piston´s movement. The stick slip effect was observed in the experimental tests to characterize the mini hydraulic cylinder, in which a step of precisely 0.025 mm was never obtained. Additionally, it was observed that the piston needs several steps to leave its static position at the beginning of the test and when it has to change its movement direction. This behavior is due to the fact that the hydraulic drive is not rigid enough and must be improved in further work. The hysteresis causes a downward shift of the characteristic at every cycle and the missing overlap of the retraction and extension characteristics. The measurements´ results demonstrate that the shift is due to the leakage, whereas the missing overlap is due to the mechanical design of the piston and the movement of the seal into the sealing slot.

After the characterization, the performance of the sensor was evaluated when used to control the instrument tip with the PI method. The experimental tests match the results of the simulations, proving that the model matches adequately the system. The differences observed between experiments and simulation results are: the overshooting, smaller in the simulation, and the settling time, shorter in

the simulation. Additionally, it was observed that the instability of the system is reached for smaller values of K_i than in the simulation. These differences show the limits of the model and can be explained with the approximation made on the friction force.

The PI control is not the optimal method for this application, but it is enough for the main purpose addressed in this thesis, which is to test the coaxial cylindrical capacitive sensor in a closed loop system. It guarantees stability only within a bandwidth of 1 Hz, which is smaller than the required one of 2 Hz. Moreover, the system output is affected by overshoot, resulting in a further movement of the pliers beyond the desired position, during both opening and closing. This malfunction can cause the collision of the pliers against parts which should not be reached or can put stronger pressure on tissues than intended. The overshoot results from the PI control which in future work must be substituted with a control method more suitable for this particular application. The new control algorithm must be able to compensate friction forces and stick slip effect, and to cope with uncertainties and nonlinearities of the hydraulic cylinder, valves, and pump. Finally, the dynamic constraints are also given by the hydraulic system, which must be optimized in future work

7.2 Future work: integration of the sensor in the laparoscopic instrument

The mechanical integration of the sensor into the instrument tip is one of the main aspects to be investigated in future work.

To facilitate follow-up work towards this goal, the main mechanical specifications identified to successfully integrate the sensor in the instrument are listed. The first aspect to consider is that all measurements were executed with a shielded setup,

in order to reduce external interferences. For a final sensor-actuator design, a solution for the integration of both the sensor and the shield into the laparoscopic instrument must be found. This will require a conductive material surrounding the hydraulic cylinder, which could be the instrument´s shaft.

Electrical contact between the pincers and the sensor must be avoided, otherwise the capacitor would discharge every time the pincers touch the body.

The spring necessary for the cylinder retraction must be electrically isolated to avoid forming an LRC circuit, which would cause a sensor malfunction.

As the capacitance to digital converter must be placed on the instrument´s handle, the cables connected to the electrodes must be shielded.

A possible integration concept which addresses the mentioned aspects is shown in Figure 7.1.

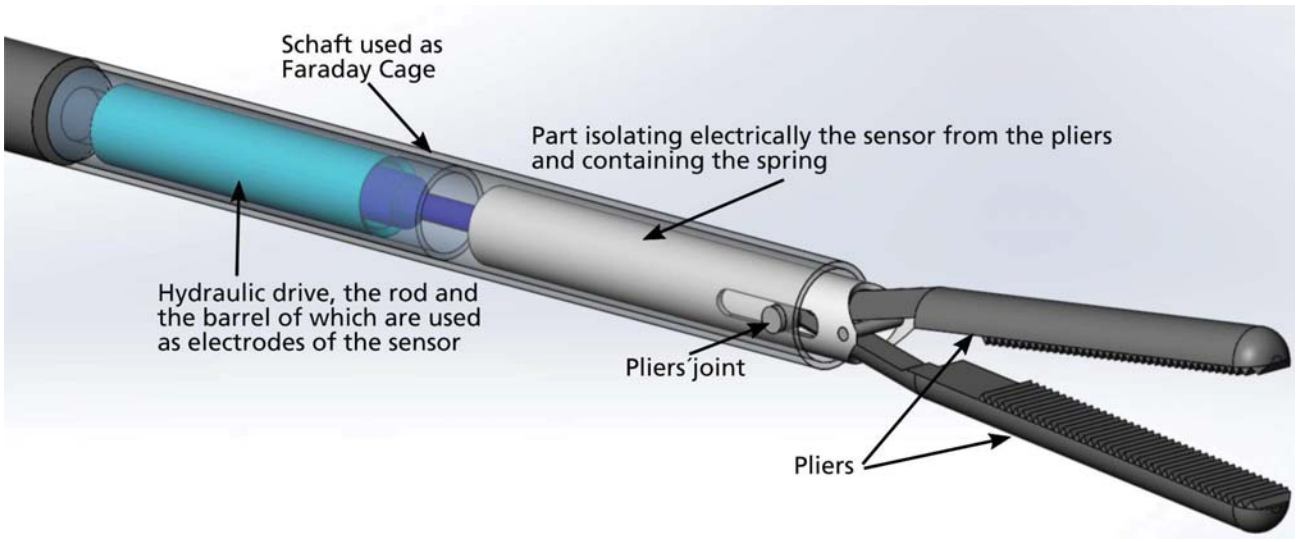

Figure 7.1: Conceptual design of the sensor integration in the laparoscopic instrument

In the drawing, the instrument´s shaft is used as a Faraday cage. The white cylinder, which connects the rod and the forceps, is made of an isolating material and provides electrical isolation between the sensor´s electrodes and the pliers. It contains the spring, which in this way is electrically isolated from the capacitive

sensor. The extension movement of the hydraulic cylinder pushes the white cylinder forward, which in turn presses the pliers together. During the retraction movement, the spring pulls the white cylinder backwards, letting the pliers open. To guarantee the complete isolation of the capacitive sensor from the environment, the pliers are electrically connected to the shaft via a conductive joint so that every source of disturbance coming in contact with the instrument tip is shielded as well.

8 Summary

Minimally invasive surgical techniques can be improved by intelligent micro manipulator instruments rather than simple manually-operated scissors. In former work, it was proved that hydraulic systems with their high force and power density are a good solution to drive this new generation of surgical tools. However, in order to make them suitable for automated instruments, a position sensor must be integrated which monitors and gives feedback on the cylinder´s movement. The integration of such sensor opens the scenario of a future in which automated hydraulically driven instruments are able to execute complex tasks. They would be capable to stitch tissues or cut complex geometries by moving automatically along pre-programmed trajectories. Moreover, hydraulic drives are influenced by trapped air, leakage, compressibility of the medium, and elasticity of the tubes in hydraulic circuits. Therefore, equipping them with a sensor would make the positioning more precise. This would guarantee a safer usage of the instrument, an aspect that is relevant in medical applications.

In this work, the scientific question was investigated, whether a sensor can be designed to monitor the displacement of micro hydraulic drives integrated in laparoscopic instruments, allowing the control of the movement of its tip. In order to answer this question, an analysis of the laparoscopic instruments on the market and of the newly developed hydraulically driven instruments was executed. From this analysis, the requirements for the sensor were identified. The space available on the instrument constitutes one of the major constraints. In fact, the sensor must be suitable to be miniaturized to fit into an instrument of 2.9 mm diameter and its integration must not alter neither the cylinder´s nor the instrument´s design. In order to be able to detect malfunctioning of the instrument, the sensor

must be integrated at the tip, where it can directly measure the displacement of the hydraulic cylinder. Moreover, in order to guarantee a good transmission of the sensor output, the signal digitization should be close to the sensor at the instrument tip. As the diameter of laparoscopic instruments varies according to their purpose, it is desirable that the sensor is adaptable to different cylinder sizes, so that it can be integrated into instruments with different dimensions. The sensor must guarantee a precision ≥50 µm, a measurement stroke ≤20 mm and a bandwidth ≥2 Hz. As it is meant for medical applications it also must be biocompatible, washable, disinfectable and sterilizable.

As there is no displacement sensor with the listed characteristics on the market, a sensing method was developed which can be miniaturized keeping the desired performance.

A review of the relevant literature led to the choice of the coaxial cylindrical capacitive method as the most suitable solution for the application discussed in this thesis.

This sensing method offers the advantage that the integral structure of the hydraulic cylinder can be used as a sensor, without the need of additional elements and without alteration of the cylinder´s design. This solves the problem of the lack of space at the tip of the instrument as the hydraulic cylinder itself is used as the sensor. The rod´s movement changes the overlap between the electrodes and its displacement can be measured in terms of capacitance variation.

The feasibility of the coaxial cylindrical capacitive sensor was theoretically analyzed, validated with an FEA simulation and an analytic model. The simulation showed that the sensor is expected to have a linear characteristic and that a radial rescaling of the cylinder would not affect the sensitivity of the sensor. This means

that it can be adapted to different cylinder sizes, hence can be integrated in instruments of different dimensions. Additionally, the simulation showed that mechanical imperfections due to manufacturing tolerances do not interfere with the sensor's linearity.

An experimental setup was developed for a mini hydraulic and a micro hydraulic cylinder to validate the analytical and simulation results. The experimental results matched, the simulations in both cases and confirmed the sensor´s behavior also on the experimental level.

The work was concluded with the design of a hydraulic drive to control the movement of the instrument tip. The full hydraulic drive was modelled and this model was used to design a feedback control which guarantees the stability within a bandwidth of 1 Hz. The hydraulic drive allowed the testing of the behavior of the sensor in a closed loop proving it suitability for the application.

9 Zusammenfassung

Das Hauptziel dieser Arbeit ist die Erforschung einer Sensormethode welche, integriert in laparoskopische Instrumente, die Regelung deren Instrumentenspitze ermöglicht und den Weg für eine neue Interpretation von chirurgischen Instrumenten ebnet. Der laparoskopische Eingriff bringt dem Patienten viele Vorteile. Die Komplexität der Ausführung kann jedoch für den Chirurgen ein Problem darstellen. Die Verbesserung der Instrumente welche bei diesen Eingriffen verwendet werden ist ein wesentlicher Schritt, um diese Komplexität zu überwinden und die vollständige Einführung dieser Operationsmethode zu ermöglichen. Die Vision ist, dass minimal-invasive Instrumente intelligente Mikromanipulatoren und keine manuell bedienten Zangen und Scheren sein werden. Die Entwicklung solcher automatisierten Instrumente, welche in einer komplexen Umgebung wie dem menschlichen Körper arbeiten, ist möglich wenn die Bewegung der Instrumentenspitze mittels Sensoren geregelt werden kann.
Angesichts der Größe der Instrumente, ist auf dem Markt kein Sensor verfügbar der für die beschriebene Anwendung geeignet wäre. Aus diesem Grund war die Identifizierung eines Sensorkonzeptes erforderlich, das sich in laparoskopische Instrumente integrieren lässt. Das Ziel dieser Arbeit welches sich daraus ergibt, kann mit der folgenden wissenschaftlichen Frage zusammengefasst werden: "Wie kann ein Sensorkonzept zur Bestimmung der Position der Spitze eines laparoskopischen Instruments so konzipiert werden, dass es genau genug für die Anwendung und kompakt genug ist, um in das laparoskopische Instrument integriert zu werden, ohne das mechanische Design des bestehenden Instruments wesentlich zu verändern?".

Um die Anforderungen an den Sensor zu identifizieren, werden die auf dem Markt befindlichen laparoskopischen Instrumente analysiert, dazu wird ihr Funktionsprinzip, ihrer Art der Anwendung und die nötige Wiederaufbereitung während ihres Lebenszyklus untersucht. Zudem werden ihre Abmessungen diskutiert, um den verfügbaren Platz für die Sensorintegration zu ermitteln. Darüber hinaus werden neu entwickelte Technologien, wie hydraulisch angetriebene Instrumente untersucht. Diese Antriebsart stellt nach Ansicht des Autors die neue Grenze des Möglichen bei der Optimierung laparoskopischer Instrumente dar. Aus diesem Grund wird der Sensor passend für diese Art von Antrieben entwickelt.

Um die beste Messmethode für die gegebenen Anforderungen zu finden wurde die einschlägige Literatur zu Wegmesssensoren analysiert. Bei dieser Analyse stellt sich das kapazitive Prinzip als das für die Anwendung am besten geeignete Verfahren heraus. Es kann miniaturisiert werden, um in die benötigten Dimensionen zu passen. Die Integration in das Instrument erfordert keine zusätzlichen Bauelemente. Darüber hinaus verfügt der Sensor über eine gute Leistung, Linearität und Präzision im erforderlichen Bereich.

Ein Vergleich der kapazitiven Sensorkonfigurationen führt zu dem Schluss, dass die koaxiale zylindrische kapazitive Methode die sinnvollste Lösung für die analysierte Anwendung darstellt. Diese Sensorkonfiguration kann direkt in den Hydraulikzylinder integriert werden indem man den Zylinder und die Kolbenstange jeweils als Außen- und Innenelektrode wählt. Die Machbarkeit des koaxialen zylindrischen kapazitiven Sensors wird im Anschluss theoretisch analysiert und mit einer FEA-Simulation und einem analytischen Modell validiert. Zusätzlich wird die Simulation zur Beurteilung des Einflusses mechanischer Toleranzen auf die Sensorleistung eingesetzt. Die Ergebnisse dieser Analyse

zeigen, dass die Miniaturisierung des Sensors die Sensitivität nicht beeinflusst, solange das Verhältnis zwischen innerem und äußerem Elektrodendurchmesser konstant bleibt. Die Sensorsensitivität kann maximiert werden, indem der Durchmesser der Kolbenstange möglichst weit an den Durchmessesser des Zylinders angenähert wird. Mechanische Toleranzen haben keinen großen Einfluss auf die Sensorleistung. Sie bewirken eine geringfügige Änderung der Steigung der Sensorkennlinie, ohne die Sensorlinearität zu beeinträchtigen. Diese Ergebnisse sind die Grundlage für die Definition der Sensorgeometrie und die Gestaltung der experimentellen Tests.

Zur Validierung des Sensorkonzepts wurde einen Versuchsaufbau entwickelt und die experimentellen Tests entsprechend definiert. Maßgeblich ist, dass die Tests mit zwei verschiedenen Hydraulikzylindern, einem Mini- (Zylinderdurchmesser 5mm) und einem Mikrohydraulikzylinder (Zylinderdurchmesser 2,7mm), durchgeführt wurden, um die Skalierbarkeit des Sensors und seine Integrierbarkeit in Instrumente unterschiedlicher Größe zu demonstrieren. Die experimentellen Ergebnisse, die in diesem Kapitel diskutiert werden, stimmen mit den Simulationen überein und bestätigen das Verhalten des Sensors auch auf experimenteller Ebene.

Schließlich wird der Sensor in ein geregeltes System integriert, um seine Eignung für die Regelung der Position der Instrumentenspitze in einem Szenario zu testen, welches dem realen Einsatz so nahe wie möglich kommt. Aus diesem Grund wird ein hydraulischer Antrieb betrachtet, der die Bewegung der Instrumentenspitze ermöglicht. Das hydraulische Antriebssystem wird modelliert und dieses Modell dient zur Auslegung einer Regelung, die die Stabilität des Systems in einer Bandbreite von 1 Hz gewährleistet. Die entworfene Regelung wird zuerst durch eine Simulation nachgewiesen. Anschließend wird sie mit Experimenten getestet,

um die Gültigkeit des Modells und die Übereinstimmung zwischen simuliertem und realem Verhalten des Systems nachzuweisen. Die Ergebnisse zeigen, dass sich die zuvor aufgestellte wissenschaftliche Frage positiv beantworten lässt. Es wurde ein Sensorsystem mit den erforderlichen Spezifikationen entwickelt und die Eignung des Sensors für die Anwendung nachgewiesen.

10 Literature

Aesculap 2012 Aesculap. 2012.
Laparoscopic Instruments Overview, viewed 13.11.2018.
From:https://www.aesculapusa.com/assets/base/doc/DOC960-Laparoscopic_Instruments_Overview_Brochure.pdf

Aesculap 2017 Aesculap. 2017.
Laparoscopic instruments: Product Catalog, viewed 03.12.2018.
From: https://www.aesculapusa.com/assets/base/doc/DOC465REV_M_Laparoscopic_Catalog.pdf

AKI Aufbereitung 2009 Arbeitskreis Instrumenten-Aufbereitung. 2009.
Instrumenten-Aufbereitung richtig gemacht.
9th ed.
Mörfelden-Walldorf : Arbeitskreis Instrumenten-Aufbereitung.
DOI: 10.4126/38m-004358746

ams AG 2013 ams AG. 2013.
AS5311 Datasheet: High Resolution Magnetic Linear Encoder, viewed 15.11.2018.
From: https://ams.com/documents/20143/36005/AS5311_

DS000200_2-00.pdf/856857e8-ca4a-31df-4c75-2fb9224bab8c

Ansys 2018 Ansys. 2018. *Funktionen von ANSYS Maxwell: Simulation niederfrequenter elektromagnetischer Felder*, viewed 19.11.2018. From: https://www.ansys.com/de-de/products/electronics/ansys-maxwell/maxwell-capabilities

Åström 2002 Åström, Karl Johan. 2002. *Control system design: lecture notes for ME 155A*. Santa Barbara : University of California Santa Barbara, viewed 26.02.2018. From: http://www.boti.oil.gov.iq/book/english%20ebooks/%D8%A7%D9%84%D9%83%D9%87%D8%B1%D8%A8%D8%A7%D8%A1/control%20sys/CSYS%20%203-Control%20System%20Design.pdf

Autorino et al. 2010 Autorino, Riccardo, Stein, Robert J., Lima, Estevão, Damiano, Rocco, Khanna, Rakesh, Haber, Georges-Pascal, White, Michael A. & Kaouk, Jihad H. 2010. Current status and future perspectives in laparoendoscopic single-site and natural orifice transluminal endoscopic urological surgery. *International journal of urology: official journal of*

the Japanese Urological Association **17** (5), pp. 410–431.
DOI: 10.1111/j.1442-2042.2010.02497.x

Beckmann 1777 Beckmann, Johann. 1777.
Anleitung zur Technologie, oder zur Kentniss der Handwerke, Fabriken und Manufacturen, vornehmlich derer, die mit der Landwirtschaft, Polizey und Cameralwissenschaft in nächster Verbindung stehn: Nebst Beiträgen zur Kunstgeschichte.
Göttingen : Vandenhoeck

Bell et al. 2005 Bell D.J., Lu T.J., Fleck N.A. & Spearing S.M. 2005.
MEMS actuators and sensors: observations on their performance and selection for purpose.
Journal of Micromechanics and Microengineering **15** (7), pp. 153.
DOI: 10.1088/0960-1317/15/7/022

Bensignor et al. 2016 Bensignor, Thierry, Morel, Guillaume, Reversat, David, Fuks, David & Gayet, Brice. 2016.
Evaluation of the effect of a laparoscopic robotized needle holder on ergonomics and skills.
Surgical Endoscopy **30** (2), pp. 446–454.
DOI: 10.1007/s00464-015-4217-7

Bentley 2005 Bentley, John P. 2005.
Principles of measurement systems.

4th ed.
Harlow, England : Pearson Prentice Hall.
ISBN 0130430285

Berguer et al. 1999 Berguer, R., Forkey, D. L. & Smith, W. D. 1999. Ergonomic problems associated with laparoscopic surgery.
Surgical Endoscopy **13** (5), pp. 466–468.
DOI: 10.1007/PL00009635

Berguer et al. 2009 Berguer, R., Remler, M. & Beckley, D. 2009. Laparoscopic instruments cause increased forearm fatigue: A subjective and objective comparison of open and laparoscopic techniques.
Minimally Invasive Therapy & Allied Technologies **6** (1), pp. 36–40.
DOI: 10.3109/13645709709152824

Bhayani et al. 2003 Bhayani, Sam B., Pavlovich, Christian P., Hsu, Thomas S., Sullivan, Wendy & Su, L.i-Ming. 2003. Prospective comparison of short-term convalescence: Laparoscopic radical prostatectomy versus open radical retropubic prostatectomy.
Urology **61** (3), pp. 612–616.
DOI: 10.1016/S0090-4295(02)02416-0

Bolzern et al. 2015 Bolzern, Paolo, Scattolini, Riccardo & Schiavoni, Nicola. 2015.
Fondamenti di controlli automatici.

4th ed.
Milano : McGraw-Hill Education.
ISBN 8838668825

Breedveld 1997 Breedveld, P. 1997.
Observation, Manipulation, and Eye-Hand Coordination Problems in Minimally Invasive Surgery.
In: *Proceedings of the XVI European annual conference on human decision making and manual control, 9.-11. December 1997, Kassel, Germany*

Breedveld et al. 2009 Breedveld, P., Stassen, H. G., Meijer, D. W. & Stassen, L. P. S. 2009.
Theoretical background and conceptual solution for depth perception and eye-hand coordination problems in laparoscopic surgery.
Minimally Invasive Therapy & Allied Technologies **8** (4), pp. 227–234.
DOI: 10.3109/13645709909153166

Canes et al. 2008 Canes, David, Desai, Mihir M., Aron, Monish, Haber, Georges-Pascal, Goel, Raj K., Stein, Robert J., Kaouk, Jihad H. & Gill, Inderbir S. 2008.
Transumbilical single-port surgery: Evolution and current status.
European urology **54** (5), pp. 1020–1030

Carus 2010 Carus, Thomas. 2010.
Operationsatlas laparoskopische Chirurgie.
2nd ed.
Heidelberg : Springer.
ISBN 364201707X

Colwell 2016 Colwell, Catharine H. 2016.
PhysicsLAB: Spherical, Parallel Plate, and Cylindrical Capacitors, viewed 12.12.2016.
From:
http://dev.physicslab.org/Document.aspx?doctype=3&filename=Electrostatics_CapacitorsParallelPlateCylindrical.xml

Comella et al. 2017 Comella, Laura M., Ayvazov, Krasimir, Cuntz, Timo, van Poelgeest, Auguste, Schachtele, Jonathan & Stallkamp, Jan. 2017.
Characterization of a Capacitive Position Sensor for a Miniaturized Hydraulic Actuator.
IEEE Sensors Journal **17** (1), pp. 113–120.
DOI: 10.1109/JSEN.2016.2620722

COMSOL® 2018 COMSOL®. 2018.
The COMSOL® Software Product Suite, viewed 19.11.2018.
From: https://www.comsol.com/products

Cuntz 2016 Cuntz, Timo. 2016.
Untersuchungen zur Eignung mikrohydraulischer Antriebe für die minimal invasive Chirurgie.
Stuttgart : Fraunhofer Verlag.
Stuttgarter Beiträge zur Produktionsforschung; 53.
Stuttgart, Univ., Diss., 2015
ISBN 9783839610237

Cuntz et al. 2013 Cuntz, Timo, James, Georgina, Valkov, Vladimir, Sanagoo, Arash & Kaltenbacher, Dominik. 2013.
Next Generation Surgical Instruments Powered by Hydraulics.
Biomedical Engineering / Biomedizinische Technik **58** (Suppl.1).
DOI: 10.1515/bmt-2013-4399

Cuntz et al. 2015 Cuntz, Timo & Comella, Laura. 2015.
Design and control of a 3-DOF hydraulic driven surgical instrument.
Current Directions in Biomedical Engineering **1** (1), pp. 140–144.
DOI: 10.1515/cdbme-2015-0036

Dyer 2004 Dyer, Stephen A. 2004.
Wiley Survey of Instrumentation and Measurement.
Hoboken : John Wiley & Sons Inc.
ISBN 9780471394846.

Feldman et al. 2012 Feldman, Liane, Fuchshuber, Pascal & Jones, Daniel B. 2012.
The SAGES manual on the fundamental use of surgical energy (FUSE).
New York, NY : Springer Science+Business Media.
ISBN 9781461420736.
DOI: 10.1007/978-1-4614-2074-3

Feußner et al. 2009 Feußner, Hubertus, Schneider, Armin & Meining, Alexander. 2009.
Endoskopie, minimal-invasive Chirurgie und navigierte Systeme.
In: Wintermantel, Erich & Ha, Suk-Woo (Hrsg.)*:* *Medizintechnik*.
5., überarbeitete und erw. Aufl.
Berlin : Springer, pp. 1121–1161.
ISBN 9783540939351

Fraden 2016 Fraden, Jacob. 2016.
Handbook of modern sensors: Physics, designs, and applications.
5th ed.
Cham, Heidelberg, New York, Dordrecht, London : Springer.
ISBN 9783319193021

Gadenne et al. 1999 Gadenne, Volker & Visintin, Aldo. 1999.
Wissenschaftsphilosophie.

1st ed.
Freiburg: Karl Alber.
Alber-Texte Philosophie; 5, pp. 99.
ISBN 9783495480052

Galilei 1974 Galilei, Galileo. 1974.
Two new sciences : Wisconsin UP.
ISBN 0299064042

Giddings 2013 Giddings, Dennis. 2013.
Surgical knots and suturing techniques.
4th ed.
Fort Collins, Colo. : Giddings Studio Publishing.
ISBN 1889326119

Groß 2003 Groß, Jürgen. 2003.
Linear Regression: Lectures Notes in Statistic.
Berlin, Heidelberg : Springer.
ISBN 364255864X

Haber et al. 2008 Haber, Georges-Pascal, Crouzet, Sebastien, Kamoi, Kazumi, Berger, Andre, Aron, Monish, Goel, Raj, Canes, David, Desai, Mihir, Gill, Inderbir S. & Kaouk, Jihad H. 2008.
Robotic NOTES (Natural Orifice Translumenal Endoscopic Surgery) in reconstructive urology: initial laboratory experience.
Urology **71** (6), pp. 996–1000.
DOI: 10.1016/j.urology.2008.03.023

Haber et al. 2010 Haber, Georges-Pascal, White, Michael A., Autorino, Riccardo, Escobar, Pedro F., Kroh, Matthew D., Chalikonda, Sricharan, Khanna, Rakesh, Forest, Sylvain, Yang, Bo, Altunrende, Fatih, Stein, Robert J. & Kaouk, Jihad H. 2010. Novel robotic da Vinci instruments for laparoendoscopic single-site surgery. *Urology* **76** (6), pp. 1279–1282. DOI: 10.1016/j.urology.2010.06.070

Hankinson et al. 2015 Hankinson, Matt & Luong, Robert. Date: 2015. Einsatz von Positionssensoren in Umgebungen mit hohen Temperaturen. *Newspaper: all-electronics.de.* Date: 22.09.2015, viewed 15.03.2017. From: http://www.all-electronics.de/einsatz-von-positionssensoren-in-umgebungen-mit-hohen-temperaturen/

Herr 2011 Herr, Norman. 2011. *Deductive Reasoning*. California State University, Northridge, viewed 26.01.2017. From: http://www.csun.edu/science/ref/reasoning/deductive_reasoning/index.html

Hodges 1993 Hodges, Bill. 1993.
Position Sensors for Hydraulic Cylinders.
In: *International Off-Highway and Powerplant Congress and Exposition, 13-15 September 1993, Milwaukee,* United States

Hoffmann+Krippner 2017 Hoffmann+Krippner GmbH. 2017.
Sensofoil wiper: Product Number 60300001, viewed 06.02.2017.
From:
https://shop.tastatur.de/de/Produkte/details/Artikel/20/Kategorie/9

Hutcheson et al. 1999 Hutcheson, Graeme. D. & Sofroniou, Nick. 1999.
The Multivariate Social Scientist: Introductory Statistics Using Generalized Linear Models : SAGE Publications.
ISBN 9781446229941.

iC-Haus GmbH 2012 iC-Haus GmbH. 2012.
Absolute Encoder Design: Magnetic or Optical?, viewed 15.11.2018.
From:
http://www.ichaus.de/upload/pdf/WP6en_Magnetic_vs_optical_17092012.pdf

Jelali et al. 2003 Jelali, Mohieddine & Kroll, Andreas. 2003.
Hydraulic servo-systems: Modelling, identification, and control.

London : Springer.
Advances in industrial control.
ISBN 9781852336929

Kano 1993 Kano, Nobuyasu. 1993.
Laparoscopic Surgeon's Thumb.
Archives of Surgery **128** (10), pp. 1172.
DOI: 10.1001/archsurg.1993.01420220092016

Karl Storz 2015 Karl Storz. 2015.
Urology, viewed 11.11.2018.
From:
https://www.karlstorz.com/cps/rde/xbcr/karlstorz_assets/ASSETS/3343855.pdf

Krivts et al. 2006 Krivts, Igor Lazar & Krejnin, German Vladimir. 2006.
Pneumatic actuating systems for automatic equipment: structure and design.
Boca Raton, FL : Crc Press.
ISBN 1420004468

Lazeroms et al. 1996 Lazeroms, M., La Haye, A., Sjoerdsma, W., Schreurs, W., Jongkind, W., Honderd, G. & Grimbergen, C. 1996.
A hydraulic forceps with force-feedback for use in minimally invasive surgery.
Mechatronics **6** (4), pp. 437–446.
DOI: 10.1016/0957-4158(96)00008-6

LORD Corporation 2014 LORD Corporation. 2014.
DVRT vs. LVDT: Comparison, viewed 15.11.2018.
From: http://files.microstrain.com/8401-0059-DVRT-vs-LVDT.pdf

Miniati et al. 2014 Miniati, R., Dori, F., Cecconi, G., Frosini, F., Saccà, F., Gentili, G. Biffi, Petrucci, F., Franchi, S. & Gusinu, R. 2014.
Hospital Based Economic Assessment of Robotic Surgery.
In: Roa Romero, Laura M. (Hrsg.)*: XIII Mediterranean conference on medical and biological engineering and computing 2013*, Vol. 41.
Cham : Springer, pp. 1144–1146.
ISBN 9783319008455.
DOI: 10.1007/978-3-319-00846-2_283

Mraz 2004 Mraz, Stephen. 2004.
Finding the right sensor for linear displacement.
Machine Design, viewed 12.12.2016.
From: http://machinedesign.com/sensors/finding-right-sensor-linear-displacement

MWK-BaWü 2015 Ministerium für Wissenschaft, Forschung und Kunst Baden-Württemberg. 2015.
Expertenkommission Ingenieurwissenschaften@BW2025:

Abschlussbericht. 21.12.2015, viewed 26.01.2017. From: https://mwk.baden-wuerttemberg.de/de/service/presse/pressemitteilung/pid/expertenkommission-ingenieurwissenschaftenbw2025-uebergibt-empfehlungen-an-wissenschaftsministerin/

Nakada et al. 2009 Nakada, Stephen Y. & Hedican, Sean. 2009. *Essential urologic laparoscopy: The complete clinical guide*

Luxemburg: Springer Science & Business Media. ISBN 1603278206

Norton et al. 2008 Norton, Jeffrey A. 2008. *Surgery: Basic science and clinical evidence.* 2. Aufl. New York : Springer. ISBN 9780387308005

Palep 2009 Palep, Jaydeep H. 2009. Robotic assisted minimally invasive surgery. *Journal of Minimal Access Surgery* **5** (1), pp. 1–7. DOI: 10.4103/0972-9941.51313

Papoulis 1991 Papoulis, Athanasios. 1991. *Probability, random variables, and stochastic processes.* 3rd ed.

New York : McGraw-Hill Education.
ISBN 0071008705

Pappas et al. 2008 Pappas, Theodore N. & Fecher, Alison M. 2008.
Principles of minimally invasive surgery.
In: Norton, Jeffrey A. (Hrsg.)*: Surgery*.
2nd ed.
New York : Springer, pp. 771–790.
ISBN 9780387308005

Parker Seals 2007 Parker Seals. 2007.
technisches Handbuch O-Ringe parker.
From:https://www.parker.com/literature/Praedifa/Catalogs/Catalog_O-Ring-Handbook_PTD5705-EN.pdf

Peirs et al. 1998 Peirs, Jan, Reynaerts, Dominiek & van Brussel, Hendrik. 1998.
A micro robotic arm for a self propelling colonoscope.
In: *Proc. Actuator 98, 6th International Conference on New Actuators, 17 - 19 June 1998, Bremen, Germany*

Pisani 1999 Pisani, Umberto. 1999.
Misure elettroniche: Strumentazione elettronica di misura.
Torino : Politeko.
ISBN 8887380147

Ramo et al. 2005 Ramo, Simon, Van_Duzer, Theodore, Whinnery, John R., Antognetti, Paolo, Chiabrera, Alessandro & Bianco, Bruno. 2005.
Campi e onde nell'elettronica per le comunicazioni.
Milano : F. Angeli.
ISBN 9788820473853

Rané et al. 2009 Rané, Abhay, Tan, Gerald Y. & Tewari, Ashutosh K. 2009.
Laparo-endoscopic single-site surgery in urology: is robotics the missing link?
BJU international **104** (8), pp. 1041–1043.
DOI: 10.1111/j.1464-410X.2009.08480.x

Renishaw 2016 Renishaw. 2016.
RESOLUTE™ with FANUC serial communications, viewed 10.12.2016.
From: http://www.renishaw.de/de/resolute-with-fanuc-serial-communications--14640

Robinson et al. 2003 Robinson, Ben C., Snow, Brent W., Cartwright, Patrick C., Vries, Catherine R. De, Hamilton, Blake D. & Anderson, Jeffrey B. 2003.
Comparison of Laparoscopic Versus Open Partial Nephrectomy in a Pediatric Series.
The Journal of Urology **169** (2), pp. 638–640.
DOI: 10.1016/S0022-5347(05)63980-8

Rosenblatt et al. 2008 Rosenblatt, Alberto, Bollens, Renaud & Espinoza Cohen, Baldo. 2008.
Manual of Laparoscopic Urology.
Berlin : Springer.
ISBN 3540747273

Santos et al. 2011 Santos, Byron F. & Hungness, Eric S. 2011.
Natural orifice translumenal endoscopic surgery: Progress in humans since white paper.
World journal of gastroenterology **17** (13), pp. 1655–1665.
DOI: 10.3748/wjg.v17.i13.1655

Sieber et al. 2017 Sieber, Marco Alain, Fellmann-Fischer, Bernhard & Mueller, Michael. 2017.
Performance of Kymerax© precision-drive articulating surgical system compared to conventional laparoscopic instruments in a pelvitrainer model.
Surgical endoscopy **31** (10), pp. 4298–4308.
DOI: 10.1007/s00464-017-5438-8

Spindler et al. 2013 Spindler, Christian, Kaltenbacher, Dominik & Schächtele, Jonathan. 2013.
Powerful Micro-Actuators for (Flexible) Surgical Instrument Tips.

Biomedizinische Technik. Biomedical engineering **58** (Suppl. 1).
DOI: 10.1515/bmt-2013-4397

Stoianovici 2000 Stoianovici, D. 2000.
Robotic surgery.
World Journal of Urology **18** (4), pp. 289–295.
DOI: 10.1007/PL00007078

Sumali et al. 2003 Sumali, Hartono, Bystrom, Eric P. & Krutz, Gary. W. 2003.
A displacement sensor for nonmetallic hydraulic cylinders.
IEEE Sensors Journal **3** (6), pp. 818–826.
DOI: 10.1109/JSEN.2003.820333

Sung et al. 2001 Sung, Gyung Tak & Gill, Inderbir S. 2001.
Robotic laparoscopic surgery: a comparison of the da Vinci and Zeus systems.
Urology **58** (6), pp. 893–898.
DOI: 10.1016/S0090-4295(01)01423-6

Supe et al. 2010 Supe, Avinash N., Kulkarni, Gaurav V. & Supe, Pradnya A. 2010.
Ergonomics in laparoscopic surgery.
Journal of Minimal Access Surgery **6** (2), pp. 31–36.
DOI: 10.4103/0972-9941.65161

Taylor 1997 Taylor, John R. 1997.
An introduction to error analysis: The study of uncertainties in physical measurements.
2nd ed.
Sausalito, Calif. : University Science.
ISBN 9780935702750

Terzic et al. 2012 Terzic, Edin, Terzic, Jenny, Nagarajah, Romesh & Alamgir, Muhammad. 2012.
Capacitive Sensing Technology.
In: Terzic, Edin, et al. (Hrsg.)*: A neural network approach to fluid quantity measurement in dynamic environments*.
London : Springer, pp. 11–37.
ISBN 9781447140603.
DOI: 10.1007/978-1-4471-4060-3_2

Texas Instruments 2015 Texas Instruments. 2015.
FDC1004 4-Channel Capacitance-to-Digital Converter for Capacitive Sensing Solutions, viewed 23.02.2018.
From: http://www.ti.com/lit/ds/symlink/fdc1004.pdf

Tjandra et al. 2006 Tjandra, J. J. & Chan, M. K. Y. 2006.
Systematic review on the short-term outcome of laparoscopic resection for colon and rectosigmoid cancer.
Colorectal disease : the official journal of the

Association of Coloproctology of Great Britain and Ireland **8** (5), pp. 375–388.
DOI: 10.1111/j.1463-1318.2006.00974.x

Tsoi et al. 1996 Tsoi, Edmund K. M. & Organ, Claude H. 1996. *Abdominal access in open and laparoscopic surgery*.
New York, Chichester : Wiley.
ISBN 0471133523

Uhrich et al. 2002 Uhrich, M. L., Underwood, R. A., Standeven, J. W., Soper, N. J. & Engsberg, J. R. 2002. Assessment of fatigue, monitor placement, and surgical experience during simulated laparoscopic surgery.
Surgical endoscopy **16** (4), pp. 635–639.
DOI: 10.1007/s00464-001-8151-5

Urologie Leipzig 2010 Klinik und Poliklinik für Urologie des Universitätsklinikums Leipzig. 2010. *Behandlungsmethoden - Klinik und Poliklinik für Urologie - Universitätsklinikum Leipzig*, viewed 05.07.2017.
From: http://urologie.uniklinikum-leipzig.de/urologie.site,postext,behandlungsmethoden,a_id,277.html

Volder 2008 Volder, Michaël de. 2008. Pneumatic and hydraulic microactuators a new

approach for achieving high force and power densities at microscale.
In: *Proceedings of the IEEE Vancouver EDS, 08.02.2008, Vancouver*

Volder et al. 2008 Volder, Michaël de, Coosemans, Johan, Puers, Robert & Reynaerts, Dominiek. 2008. Characterization and control of a pneumatic microactuator with an integrated inductive position sensor.
Sensors and Actuators A: Physical **141** (1), pp. 192–200.
DOI: 10.1016/j.sna.2007.07.012

Volder et al. 2010 Volder, Michaël de & Reynaerts, Dominiek. 2010. Pneumatic and hydraulic microactuators: a review.
Journal of Micromechanics and Microengineering **20** (4), pp. 43001.
DOI: 10.1088/0960-1317/20/4/043001

Webster 1999 Webster, John G. 1999.
The measurement, instrumentation, and sensors handbook.
Boca Raton, FL : CRC Press published in cooperation with IEEE Press.
The electrical engineering handbook series; 13.
ISBN 9780849383472

Wimmer-Schweingruber 2017 Wimmer-Schweingruber, Robert F. 2017. *Optische Instrumente: Das Auge*. Universität Kiel. From: http://www.ieap.uni-kiel.de/et/download/physik2/V13.pdf

Zahraee et al. 2010 Zahraee, Ali Hassan, Szewczyk, Jérome, Paik, Jamie Kyujin & Morel, Guillaume. 2010. Robotic Hand-Held Surgical Device. In: Jiang, Tianzi (Hrsg.)*: Medical image computing and computer-assisted intervention - MICCAI 2010: Evaluation of End-Effector's Kinematics and Development of Proof-of-Concept Prototypes*, Vol. 6363. Berlin : Springer, pp. 432–439. ISBN 978-3-642-15710-3. DOI: 10.1007/978-3-642-15711-0_54

Zdichavsky et al. 2015 Zdichavsky, Marty, Krautwald, Martina, Feilitzsch, Maximilian V., Wichmann, Dörte, Königsrainer, Alfred & Schurr, Marc Oliver. 2015. Laparoscopic gastro-jejunal anastomosis using novel r2 deflectable instruments in an ex vivo model. *Minimally Invasive Therapy & Allied Technologies* **25** (2), pp. 91–98. DOI: 10.3109/13645706.2015.1117494

Laparoscopy is a surgical technique performed in the abdomen through small incisions. At the current state of the art the surgeon is the one that controls constantly the movement of the instruments used for this procedure. His constant involvement implies the intensification of his fatigue.

To solve this problem and allow the further development of this surgical technique, in the vision of the author, instruments must become micro-manipulators, which allow the accomplishment of preprogrammed tasks. This would reduce the surgeon fatigue as the surgeon is not actively involved in the control of the instruments movement all the time.

To achieve this goal a sensor system was developed, which is able to monitor the movement of the tip of a laparoscopic instrument continuously. This work focuses specifically on the research and development of a capacitive sensor system concept which is accurate and compact enough to be integrated on the tip of a laparoscopic instrument without changing its design.

ISBN 978-3-8396-1550-8

9 783839 615508

FRAUNHOFER VERLAG